

# Toward Ultra-Resolution Biomolecular Mapping in Cells with Expansion Microscopy

By

Yixi Liu

S.B., University of Electronic Science and Technology of China (2013)

S. M., Tsinghua University (2016)

Submitted to the Department of Electrical Engineering and Computer Science in Partial  
Fulfillment of the Requirements for the Degree of

Doctor of Philosophy

at the

MASSACHUSETTS INSTITUTE OF TECHNOLOGY

May 2024

©2024 Yixi Liu. All rights reserved.

The author hereby grants to MIT a nonexclusive, worldwide, irrevocable, royalty-free license to exercise any and all rights under copyright, including to reproduce, preserve, distribute and publicly display copies of the thesis, or release the thesis under an open-access license.

Authored by: Yixi Liu  
Department of Electrical Engineering and Computer Science  
May 17, 2024

Certified by: Edward S. Boyden  
Y. Eva Tan Professor in Neurotechnology at MIT  
Thesis Supervisor

Accepted by: Leslie A. Kolodziejski  
Professor of Electrical Engineering and Computer Science  
Chair, Department Committee on Graduate Students



# Toward Ultra-Resolution Biomolecular Mapping in Cells with Expansion Microscopy

by  
Yixi Liu

Submitted to the Department of Electrical Engineering and Computer Science  
On May 17, 2024 in Partial Fulfillment of the  
Requirements for the Degree of Doctor of Philosophy in  
Electrical Engineering and Computer Science

## **Abstract**

To investigate the molecular and cellular foundations of biological functions, achieving nanoscale spatial resolution in biomolecular imaging is essential. Expansion microscopy (ExM)<sup>1</sup>, a new kind of super-resolution microscopy, enables this by physically enlarging preserved biological specimens. Thus allows the investigation of structure-function relationships at nanoscale resolution using conventional diffraction-limited microscopes. ExM involves a series of chemical processes, including anchoring, polymerization, softening, and expansion. Before biomolecules are secured to the gel network, there is a risk that fixation and these chemical steps may alter the integrity and organization of the biomolecules. As resolution increases, previously indiscernible structural changes become visible, highlighting the importance of preserving ultrastructure. In this thesis, we present several ultrastructure preservation methods that minimize perturbations during sample preparation and maintain the integrity and organization of biomolecules. We name the one strategy with better performance subzero temperature expansion microscopy (subExM), which showed improved structure preservation and fluorescent signal intensity. This method holds promise for broadening our understanding of biological systems and paves the way for elucidating how structural variations underpin functional differences across healthy and diseased states.

Thesis supervisor: Edward S. Boyden

Title: Y. Eva Tan Professor in Neurotechnology at MIT



## Acknowledgements

First, I would like to express my heartfelt gratitude to my advisor, Professor Ed Boyden, for his unwavering support and invaluable guidance throughout my PhD journey. Professor Boyden is not just a leader in science but also a dedicated advisor. His continuous encouragement and insightful advice have profoundly shaped my academic and professional growth. Under his mentorship, I have learned to think critically as a scientist, to identify and tackle significant research problems, and to approach challenges with strategic planning and innovative solutions.

I also thank my mentor, Chi Zhang, whose guidance has been indispensable in my journey as a PhD student. Chi Zhang has taught me a wide array of experimental techniques and has shown me not just how to design experiments but also how to deliver an effective scientific talk. His patience, expertise, and dedication have significantly contributed to my growth as a researcher. His extensive support with my project has been invaluable, and it could not have been done without his assistance.

I am also profoundly grateful to my thesis committee members, Professor Nir Shavit and Professor Sixian You. Their insightful feedback has been invaluable in refining my thesis. Their expertise has greatly enriched my academic experience.

My thanks also go to my academic advisor, Dr. Donnie Keathley from the EECS department, for his valuable advice throughout my PhD.

Additionally, I want to thank my academic advisor, Dr. Donnie Keathley from the EECS department. Dr. Keathley's encouragement and guidance have been a source of strength and inspiration, helping me to stay focused and motivated throughout my PhD.

A heartfelt thank you to all the members of the Boyden lab for their help and support. Learning from and being inspired by such brilliant minds has been a tremendous privilege. I am especially grateful to Jay Yu, Rui Gao, Orhan Celiker, Oz Wassie, Daniel Estandian, Alexi Choueiri, and Tay Shin for their invaluable assistance with my project and for the enriching discussions we've shared.

I am also deeply appreciative of the financial support provided by the MIT Presidential Fellowship, which granted me the freedom to choose my research field during my first year as a PhD student. Additionally, I extend my thanks to the Anala Fellowship for giving me the opportunity to deepen my understanding of the brain in the context of Down syndrome and to apply my techniques in the search for treatments for individuals with Down syndrome.

Last but not least, I want to express my profound gratitude to my parents, Zhijing Feng and Shubin Liu, for their unconditional love and support. Their unwavering belief in me has been my anchor, and I could not have achieved this milestone without them. Thank you for always standing by me and encouraging me.

# Table of Contents

<b>Abstract</b> .....	<b>3</b>
<b>Acknowledgements</b> .....	<b>5</b>
<b>Table of Contents</b> .....	<b>7</b>
<b>List of Figures</b> .....	<b>9</b>
<b>Chapter 1 Introduction</b> .....	<b>11</b>
1.1 Thesis Organization.....	11
1.2 Expansion Microscopy .....	11
1.3 General Chemistry Principles of Expansion Microscopy .....	13
1.4 ExM for Nanoscale Imaging of Proteins .....	17
1.4.1 Pre-expansion labeling ExM with ~4-5x linear expansion factor .....	18
1.4.2 Post-expansion labeling ExM with ~4-5x linear expansion factor.....	24
1.4.3 Increasing the linear expansion factor beyond ~4-5x for high-resolution protein imaging....	28
1.5 ExM for Nanoscale Imaging of RNAs .....	33
1.6 Applications of ExM .....	37
<b>Chapter 2 Cleavable Fixative for Improved Ultrastructure Preservation in ExM</b> .....	<b>45</b>
2.1 Introduction .....	45
2.2 Results .....	46
2.2.1 Strong fixative is needed for ultrastructure preservation in ExM .....	46
2.2.2 Designing and screening of new fixatives.....	50
2.2.3 Ultrastructure preservation of microtubules with new fixatives in new form of ExM.....	52
2.3 Discussion.....	56
2.4 Methods .....	57
2.5 Supplementary Information.....	62
<b>Chapter 3 Subzero Temperatures Expansion Microscopy for Ultrastructural Preservation</b> .....	<b>67</b>
3.1 Introduction .....	67
3.2 Results .....	69

3.2.1 Development of subzero expansion microscopy .....	69
3.2.2 subExM enables better ultrastructure preservation of microtubules .....	72
3.2.3 Enhanced protein retention of different cellular structures using subExM.....	74
3.3 Discussion.....	77
3.4 Methods .....	78
3.5 Supplementary Information.....	82
<b>Chapter 4 Conclusion and Future Directions.....</b>	<b>89</b>
<b>References .....</b>	<b>93</b>



# List of Figures

Figure 1 Principles and workflows of ExM.....	14
Figure 2 ExM-supported RNA imaging .....	37
Figure 3 Applications of ExM in cell biology .....	38
Figure 4 Applications of ExM in virology.....	40
Figure 5 Applications of ExM in microbiology.....	41
Figure 6 Applications of ExM in neurobiology.....	43
Figure 7 Strong fixative preserves ultrastructure but will prevent isotropic expansion .....	48
Figure 8 Mild softening methods using specific proteolytic enzymes cannot ensure the structure preservation and isotropic expansion when the strong fixative is applied.....	49
Figure 9 Design and screening of new fixatives .....	51
Figure 10 Ultrastructure preservation of the designed fixative using the new form of ExM. ....	53
Figure 11 The direct fixation of the proteins to the gel network by using acrolein.....	55
Figure 12 Subzero Temperature Expansion Microscopy (subExM) workflow for Cultured Cells .....	71
Figure 13 subExM enables better ultrastructure preservation of microtubules .....	73
Figure 14 Enhanced protein retention of different cellular structures using subExM.....	75



# **Chapter 1 Introduction**

## **1.1 Thesis Organization**

This thesis is composed of two main parts: the first part of the thesis focuses on ultrastructure preservation with cleavable fixative for expansion microscopy (ExM), and the second part of the thesis focuses on subzero temperatures expansion microscopy (subExM) where the key steps of structure preservation (fixation, anchoring, and gelation) are conducted at cold temperatures. The background, motivations, and applications of ExM are thoroughly discussed in Chapter 1. This chapter is adopted from an unpublished review paper written with Dr. Chi Zhang and Professor Ed Boyden, providing a comprehensive introduction to the ExM. The design, screening and performance improvements of cleavable fixative are described in Chapter 2. The motivation and design and performance improvements of subExM are described in Chapter 3. Finally, Chapter 4 concludes the thesis and outlines potential directions for future work, aiming to further refine and expand the methodologies developed in this thesis for broader applications in biomolecular imaging.

## **1.2 Expansion Microscopy**

Microscopy is a foundational tool widely used throughout biology because the components of biological systems, such as cells, organelles, and biomolecules, are all microscale to nanoscale and require microscopes to study their structures, organizations, and functions. Historically, many biology fields started with observations made under a microscope. Around the end of the seventeenth century, Antoine van Leeuwenhoek and Robert Hooke used their self-built microscopes to discover microorganisms, which commenced the field of microbiology. About two hundred years later, Santiago Ramón y Cajal made beautiful drawings of individual nerve cells by examining chemically stained brain tissues under a microscope, which laid the foundation of modern neuroscience.

To this day, microscopy has become the backbone of modern biological research and has been integrated into the day-to-day work of biologists; many biology research papers contain microscopy images of biomolecules, cells, or tissues. Particularly, optical microscopes, especially fluorescence optical microscopes, have been the primary tools to visualize biomolecules in cells and tissues, largely because of the development of many fluorescent

reagents, such as fluorescent proteins, fluorescent dye-conjugated antibodies, and fluorescent in situ hybridization probes, that selectively label biomolecules of interest. Such molecular contrast and specificity provided by fluorescent labels, together with the ability of the microscope to image multiple colors in the same specimen, enables researchers to study the spatial relationships amongst biomolecules and between biomolecules and their cellular and tissue environment, which are important for understanding biomolecular functions that change in response to alterations of biomolecular localizations and interactions.

However, due to the diffraction of light by lenses, conventional optical microscopes cannot resolve objects within a few hundred nanometers – a size far greater than a single biomolecule such as a protein. This means that, under conventional optical microscopes, nanoscale cellular structures and biomolecules will be shown as blurred images, making it difficult to discern accurate structures, spatial relationships, and localizations of biomolecules within small organelles, subcellular nanostructures, and microorganisms such as bacteria and viruses.

Through engineering the physical and optical mechanisms of the microscope, super-resolution microscopy has broken the diffraction limit and achieved imaging resolution down to nanometers, thus enabling imaging of single molecules and nanoscale biological structures (see references <sup>2,3</sup> for reviews on the principles and applications of super-resolution microscopy). Although powerful, super-resolution microscopy requires specialized hardware and software, has slow imaging speeds, and is difficult to use for imaging tissue volumes.

We recently showed that one could do nanoimaging on conventional diffraction-limited microscopes by chemically enlarging the preserved biological specimen in a process that we call expansion microscopy (ExM)<sup>1</sup>. Rather than optically breaking the diffraction limit, ExM physically magnifies preserved biological specimens, and evenly separates biomolecules within diffraction-limited volumes to resolve them under conventional diffraction-limited microscopes.

Over the last several years, variants of ExM have been developed to image biomolecules including proteins<sup>1,4-15</sup>, nucleic acids<sup>15-20</sup>, polysaccharides<sup>10</sup>, lipids<sup>11,14,21,22</sup>, and small molecules<sup>4,10</sup>, and have been applied to a diversity of species, tissue types, and cell types, for the nanoscale mapping of biomolecules in healthy and disease states. Previous ExM reviews from our group and others have primarily focused on the history and early technologies up to 2019<sup>23</sup>, applications to visualize protein-based cellular structures in cells and tissues<sup>24</sup>, or recent ExM anchoring and labeling chemistries for specific types of biomolecules<sup>25,26</sup>.

### 1.3 General Chemistry Principles of Expansion Microscopy

ExM builds on physical and chemical discoveries dating back decades, including the study of polymer physics of how polyelectrolyte hydrogel swell when immersed in water, such as the work of Toyochi Tanaka in the 1970s<sup>27</sup>, and the use of polyacrylamide hydrogel for tissue embedding to facilitate staining and imaging, such as the work of Peter Hausen and Christine Dreyer in the 1980s<sup>28</sup>. The polymer spacings within such hydrogels are as small as a few nanometers<sup>29</sup>, making us think that perhaps the spatial errors introduced from synthesizing such polymers throughout biological samples and the following expansion process could also be as small as a few nanometers, and that these polymers might be used in nanoimaging.

All forms of ExM follow the same fundamental chemistry principles (**Figure 1**) designed to ensure the isotropic 3D expansion of the biological specimen and the faithful preservation of the spatial information of biomolecules. Optionally, before the ExM process, one could apply labels to the biological specimen to equip biomolecules with reporters, such as fluorescent dyes, for detection after expansion. The ExM process starts with a first step in which biomolecules and/or their labels within the preserved biological specimen are modified with handles for crosslinking to the hydrogel network. Next, hydrogel monomers are uniformly diffused throughout the biological specimen and a polyelectrolyte hydrogel is evenly and densely synthesized within the specimen, with polymer chains going around and between biomolecules and/or their labels, so that the biomolecules and/or their labels are linked to the hydrogel network. Then, the sample is mechanically softened by enzymatic digestion or denaturation to disrupt interactions within and between biomolecules. Finally, water is added to the sample, causing the hydrogel and the specimen embedded within the hydrogel to isotopically expand in 3D, thus evenly separating the hydrogel-linked biomolecules and/or their labels in space. If no labels have been added to the biological specimen before expansion, one could label biomolecules after sample expansion. Adding labels before expansion might be more straightforward for many users because the labels are administered in a way similar to conventional sample labeling protocols. In comparison, adding labels after sample expansion, although less familiar to the users, may have the benefit of better labeling and higher imaging accuracy.

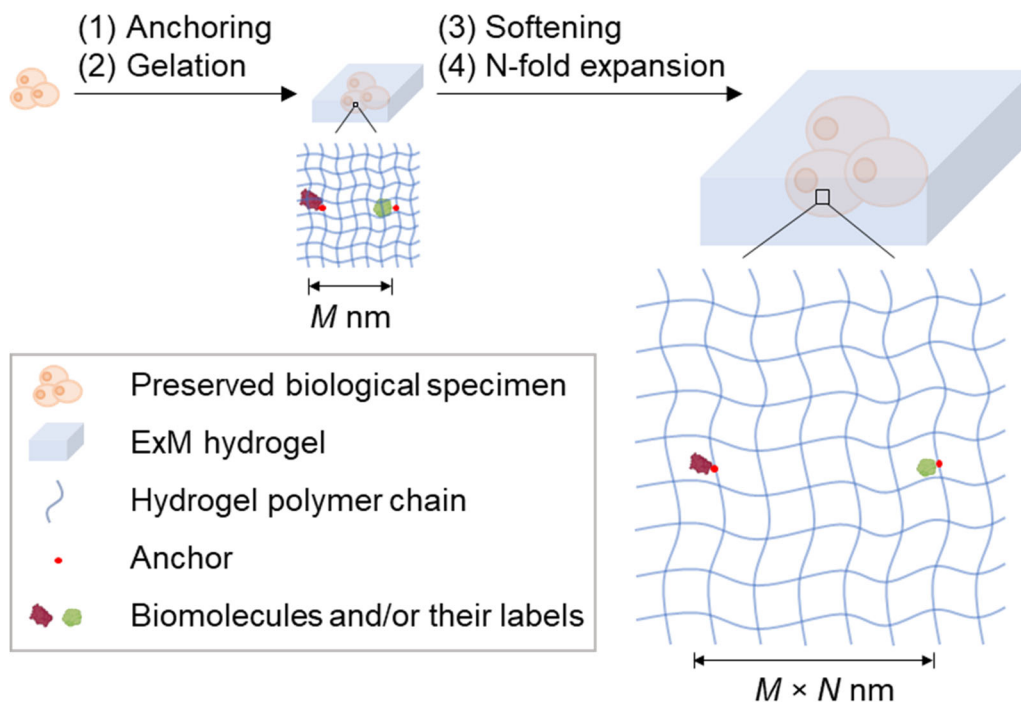


**Figure 1 Principles and workflows of ExM**

First, biomolecules and/or their labels in preserved biological specimens are conjugated with hydrogel anchors (step 1). Then, the ExM hydrogel is synthesized uniformly and densely throughout the biological specimen, which crosslinks biomolecules and/or their labels to the hydrogel polymer chains (step 2). Enzymatic digestion or denaturation is used to mechanically soften the hydrogel-embedded specimen (step 3). After treatment with water, the specimen expands in 3D (step 4). Expansion increases the distance between biomolecules and/or their labels ( $M$  nm) by the linear expansion factor  $N$ , resulting in a post-expansion distance of  $M \times N$  nm, and effectively improves the imaging resolution by  $N$ -fold. Imaging resolution is limited by the spatial errors introduced from the hydrogel synthesis and expansion process, which in principle could be as small as a few nanometers<sup>29</sup>.

Most ExM protocols expand the specimen by  $\sim 4$ - $5$ x in each linear dimension, resulting in  $\sim 4$ - $5$ -fold improvement of the imaging resolution of a microscope. For example, images of a  $\sim 4.5$ x linearly expanded sample acquired using a microscope with  $\sim 300$ -nm resolution will have an effective resolution of  $\sim 300/4.5 = \sim 70$  nm. By optimizing the ExM hydrogel system, one could expand the sample once beyond  $\sim 4.5$ x and up to  $\sim 10$ x to improve imaging resolution<sup>14,30,31</sup>. It is also possible to expand the sample twice in succession, resulting in  $\sim 4.5 \times 4.5 = \sim 20$ x expansion in each linear dimension, and an imaging resolution of  $\sim 25$  nm with a diffraction-limited

confocal microscope.<sup>7</sup> Such an imaging resolution is comparable to that of the best super-resolution imaging method applied to cells and tissues, but is slightly larger than  $\sim 300/20 = \sim 15$  nm, primarily owing to the spatial errors of the hydrogel synthesis and expansion process. Similar to super-resolution microscopy, ExM methods that apply labels (e.g., antibodies) before sample expansion will add additional spatial errors because the fluorophores (e.g., those attached to secondary antibodies) are displaced from the target biomolecules.<sup>7</sup> Such spatial errors from the labels can be reduced by applying the labels after sample expansion.

ExM has been validated by multiple labs, with many forms of ExM protocols, in diverse biological structures, cell types, and tissue types. Specifically, ExM protocols has been validated by two approaches, either by comparing images of the same region of interest acquired with ExM versus with traditional super-resolution microscopy methods, or by examining ExM images of biological structures that have well-known geometries and topologies. In the first validation approach, structured illumination microscopy, stochastic optical reconstruction microscopy, and stimulated emission depletion microscopy have been used to acquire images for registration with ExM images of the same region of interest.<sup>1,4,6,7,32,33</sup> These registration experiments showed that, compared to images acquired with super-resolution microscopy, ExM images exhibited distortions of a few percent of the measurement length around tens to hundreds of micrometers. Such small distortions are insignificant for most biological studies that interrogates the relative spatial relationships of, rather than the accurate distances between, biological structures and cells. In the second validation approach, protein structural features, such as microtubule width<sup>1,4,7</sup>, clathrin-coated pit radius<sup>1,4</sup>, centriole length, diameter, and chirality<sup>8</sup>, nuclear pore complex ring arrangements<sup>34</sup>, peroxisome membrane protein structures<sup>30</sup>, and virion spherical shapes<sup>35</sup>, have been analyzed in different ExM protocols to validate the resolution of imaging and the uniformity of expansion. Indeed, analysis of ExM images of these stereotyped structures showed structural measurements that were consistent with those from super-resolution imaging or electron microscopy. Overall, these extensive sets of validation experiments suggest that ExM is a reliable tool for testing biological hypotheses and making new discoveries.

From the users' perspective, for cell and tissue types that have validated ExM protocols, if the observed expansion factors are consistent with those reported in the literature and there are no obvious cracks or distortions of the sample after expansion, the users should be confident with the uniformity of expansion.<sup>36</sup> For cell and tissue types that have not been expanded before, and that have distinct mechanical properties compared with previous ExM-tested sample types,

validation experiments and optimization of the ExM protocol may be helpful to ensure the uniformity of expansion. For example, the ExM protocol that worked well for mouse brain slices in one mouse model could likely be applied to brain slices of similar brain regions and slice thickness in a different mouse model with minimal protocol optimization, because these brain slices are considered mechanically similar in the context of ExM.<sup>36</sup> However, different ExM protocols are required for cultured mammalian cells and bacteria as these sample types are considered mechanically different in the context of ExM, primarily because of the bacteria cell wall that requires optimized softening protocols for expansion<sup>37</sup>.

Expanded specimens can be imaged with any microscopes to improve the imaging resolution, provided that the labels used for imaging and the hardware setup of the microscope are compatible with ExM. In practice, fluorescence microscopes, in particular confocal fluorescence microscopes that are accessible to many biology labs, are popular for imaging diverse types of expanded cells and tissues. With confocal microscopes, various ExM protocols with linear expansion factors up to  $\sim 20x$ , attain imaging resolution that rivals the imaging resolution of the state-of-the-art optical super-resolution microscopy methods applied to cells and tissues. This means that one could use ExM and a confocal microscope to perform most of the experiments previously only possible with optical super-resolution microscopy. One exception is super-resolution live cell imaging, which is currently not possible with ExM because of the physical mechanisms of expansion. Optionally, one could image the expanded sample with super-resolution microscopy to further improve the imaging resolution.

Besides improving imaging resolution, the process of sample expansion by water treatment has the side product of optically clearing the biological specimen, enabling fast volumetric super-resolution imaging with fast volumetric microscopes. For instance, light sheet microscopes were used to image expanded samples such as virus-infected cells<sup>38</sup>, *Drosophila* brain tissues<sup>39</sup>, songbird brain tissues<sup>40</sup>, mouse kidney tissues<sup>41</sup>, mouse brain tissues<sup>42,43</sup>, and mouse spinal cord tissues<sup>39,44</sup>. Overall, combining expansion microscopy with fast 3D imaging techniques results in imaging resolution similar to optical super-resolution microscopy methods, but with significantly greater imaging speeds, volumes, and number of colors.



## 1.4 ExM for Nanoscale Imaging of Proteins

ExM protocols for protein imaging are categorized into two kinds based on whether the proteins are labeled before expansion (pre-expansion labeling) or after expansion (post-expansion labeling). In pre-expansion labeling ExM protocols<sup>1,4,6,45-47</sup>, proteins are labeled before expansion occurs. The protein labeling workflow of such pre-expansion labeling ExM protocols are the same as conventional protein labeling procedures such as fluorescent protein labeling or antibody staining, enabling the users to integrate ExM with their established sample labeling protocols. In post-expansion labeling ExM protocols<sup>4,5,8,9,48-51</sup>, proteins are physically separated away from each other by expansion, which facilitates later labeling. Before diving into the details of each protocol, we first discuss the pros and cons of each of these two, to help the users think about what protocols to use for their applications.

From the users' perspective, how to choose between pre- and post-labeling ExM formats? If the users have established sample labeling protocols, they might choose to try pre-labeling ExM protocols first, since these protocols are designed to work with conventionally labeled samples such as samples that are immunostained with primary antibody and dye-conjugated secondary antibody, or samples that contain fluorescent protein fused to the protein of interest. On the other hand, although post-expansion labeling ExM protocols are less familiar to users in terms of how the sample is labeled, they have several attractive features. Specifically, post-expansion labeling protocols can decrowd proteins in dense compartments for better labeling<sup>9,52</sup>, improve imaging accuracy by reducing the spatial errors introduced by antibodies<sup>9,50</sup>, and enable imaging of multiple (>4) proteins via cycles of antibody staining, imaging, and removal<sup>5,51</sup>. The first feature of protein decrowding by expansion is particularly important, because by doing so one might reveal otherwise invisible protein structures, as demonstrated in recent examples<sup>9,52</sup> of revealing new protein structures, and even entire invisible cells, in mouse brains and in human glioma tissues, as discussed in detail in Sections 1.4.2 and 1.4.3. If the users' application could benefit from the above-mentioned features, the users might consider applying post-expansion labeling ExM protocols to their samples.

Due to the distinct features offered by the two labeling formats and the varying imaging resolutions enabled by ExM protocols with different expansion factors, we present ExM protocols for protein imaging in three sub-sections. These are organized based on the labeling formats and the linear expansion factor. The first two sub-sections discuss the details of pre- and

post-expansion labeling ExM protocols that achieve approximately 4-5x linear expansion factors. The subsequent sub-section describes recently developed ExM variants that increase the linear expansion factor to approximately 10-20x for enhanced imaging resolution, accommodating both pre- and post-expansion labeling formats. For each ExM protocol, we detail its mechanism, expansion factor, and examples of sample types and protein labels that have been effectively tested with the protocol. This organization aims to assist users in selecting an ExM protocol that aligns with their sample type, labeling procedure, and required expansion factor.

### **1.4.1 Pre-expansion labeling ExM with ~4-5x linear expansion factor**

In pre-expansion labeling ExM, proteins are labeled before sample expansion. During ExM processing, the protein labels are crosslinked to the hydrogel network and expanded. The most popular ExM-compatible protein labels include standard antibodies introduced via immunostaining<sup>4</sup> and fluorescent proteins introduced perhaps via genetic fusion to the protein of interest<sup>4</sup>. As discussed later in this section, a large palette of fluorescent proteins and dyes (e.g., those conjugated to antibodies) are compatible with ExM chemistry and retain their fluorescence after expansion.<sup>4</sup> Standard antibodies and fluorescent proteins are most popular because many users might already have established protocols to label their proteins of interests with antibodies or fluorescent proteins, thus they only need to invest in cheap and commercial chemicals and use several simple chemical steps to do ExM on their samples for nanoimaging on a conventional microscope. In comparison to standard antibodies and fluorescent proteins, other fluorescent labels, such as fluorescent streptavidin added to stain biotin-labeled proteins<sup>4</sup>, or custom reagents such as DNA-conjugated antibodies<sup>1,45</sup>, have also been used in ExM contexts, but are less popular for day-to-day biological studies, primarily because they require custom reagents (i.e., biotin probes and DNA-conjugated antibodies), need development and validation for each protein target, and are less robust compared to commercial antibodies and fluorescent proteins, as discussed in more detail later in this section.

The expansion process will volumetrically dilute the protein labels applied before sample expansion. As a result, the expanded sample will have decreased fluorescent signal intensities compared to the labeled sample before expansion. It is therefore always helpful to enhance the fluorescent signals by staining the labels after expansion, by using antibodies against fluorescent proteins<sup>36</sup>, or by using fluorescent DNA labels against complementary DNA conjugated to antibodies applied before expansion<sup>1,7</sup>, or by using streptavidin against biotin-conjugated

antibodies added before expansion<sup>6,19</sup>. Note that these fluorescent labels are added after sample expansion solely for enhancing the fluorescent signals, which is conceptually different from post-expansion labeling ExM protocols, that decrowd protein complexes to reveal “hidden” protein structures.

Before diving into the popular forms of pre-expansion labeling ExM designed for standard antibodies and fluorescent proteins, we would like to discuss DNA-conjugated antibodies first, because several ExM variants have relied on DNA-conjugated antibodies to facilitate the expansion process<sup>1,7</sup>, signal amplification<sup>7,45,47</sup>, or multiplexed imaging<sup>47</sup>. The users need to be aware of two major limitations for DNA-conjugated antibodies when deciding whether to use standard antibodies (e.g., via ExM protocols described later in this section) or DNA-conjugated antibodies. First, and most importantly, attaching DNA to an antibody can alter its binding and create unwanted backgrounds, and as a result, each DNA-conjugated antibody will require extensive validation and might require optimization of staining conditions to reduce unwanted backgrounds.<sup>45,53</sup> Second, conjugating DNA to antibodies requires additional costs and/or end user labor compared to standard commercial primary and secondary antibodies. Nevertheless, the first version of ExM<sup>1</sup>, developed as a pre-expansion labeling ExM protocol, used custom DNA-conjugated antibodies for protein labeling and expansion. Specifically, the DNA on the antibody serves as a handle that links to the ExM hydrogel and are labeled with fluorophores and imaged after expansion. Later reports demonstrated that the DNA labels on the antibodies can be used to enable multiple rounds of expansion to increase expansion factors (discussed in more detail in Section 1.4.3)<sup>7</sup>, to improve fluorescence signals using DNA-based signal amplification chemistries<sup>7,45,47</sup>, and to support DNA-based multiplexing chemistries for imaging six protein targets in the same expanded mouse retina section.<sup>47</sup> Although these DNA-conjugated antibody-based ExM protocols have found applications in imaging proteins in cultured cells<sup>1,7</sup>, mouse brain<sup>1,7</sup> and retina<sup>47</sup> tissues, *Caenorhabditis elegans*<sup>54</sup>, and bacteria<sup>46</sup>, they are limited by the requirement of custom DNA-conjugated antibodies and concerns about unwanted backgrounds.

To overcome the limitations with DNA-conjugated antibodies, popular forms of pre-expansion labeling ExM for protein imaging, as discussed in detail below, have been designed and optimized to work with standard fluorescent proteins and commercial antibodies; these ExM protocols enable users to do nanoimaging without significant investments into custom reagents.

The first of such methods is protein-retention expansion microscopy (proExM)<sup>4</sup>, which has both pre- and post-labeling forms. In the pre-expansion labeling form of proExM, the preserved biological specimen, labeled with fluorescent proteins and/or antibodies, is first treated with a commercial reagent called AcX (succinimidyl ester of 6-((acryloyl)amino)hexanoic acid). AcX crosslinks proteins and/or their labels to the hydrogel network after hydrogel formation. Then, the hydrogel-embedded biological specimen is softened using enzymatic digestion by proteinase K (a nonspecific protease) to allow expansion by water treatment. Overall, proExM results in ~4.5x expansion and was initially demonstrated in ExM imaging of fluorescent protein-labeled and/or antibody-stained mammalian cultured cells, mouse brain, pancreas, spleen, and lung tissues, and macaque brain tissues.<sup>4</sup>

The fluorescence of most fluorescent proteins and commercial fluorescent secondary antibodies is retained after proExM processing<sup>4</sup> (although the signal intensity is decreased due to dilution by volumetric expansion), possibly because these fluorescent proteins and secondary antibodies are resistant to proteinase K digestion. Some labels such as cyanine dyes and bacteriophytochrome-based fluorescent proteins largely lose their fluorescence after gelation and proteinase K digestion.<sup>4</sup> For cyanine dyes, users should replace them with ExM-tested labels that have similar spectral properties (e.g., replace Cy3 with Alexa Fluor 546)<sup>4</sup>. For bacteriophytochromes-based fluorescent proteins, the users might consider using antibodies to stain such labels after expansion to enhance the fluorescent signal intensity. In addition to fluorescent proteins and antibodies, fluorescent streptavidin is also compatible with proExM and can be applied before expansion, as demonstrated in the visualization of post-translational modifications such as *S*-nitrosylation using a biotin probe.<sup>4</sup>

In a related and independently developed pre-expansion labeling ExM protocol<sup>6</sup>, MA-NHS (methacrylic acid *N*-hydroxysuccinimide ester) or glutaraldehyde was used to equip proteins with hydrogel anchors, followed by gelation, proteinase K digestion, and water treatment that are similar to those steps in the pre-expansion labeling proExM protocol. MA-NHS protocol was demonstrated in mammalian cultured cells and mouse brain tissues, while glutaraldehyde protocol was demonstrated in mammalian cultured cells.<sup>6</sup> The MA-NHS protocol has also been used to expand samples stained with biotin-borne secondary antibodies, with visualization by staining with fluorescent streptavidin post-expansion, which could be useful to allow imaging with fluorophores (e.g., cyanine dyes) incompatible with the ExM chemistry. MA-NHS is

functionally analogous to AcX in the context of ExM; both reagents are commercial and can be used interchangeably in expansion protocols.

ExM protocols based on proExM chemistry have been developed to work with sample types that have different mechanical properties and formats compared to mammalian cultured cells and mouse tissues. Below we discuss proExM-style ExM variants optimized for Gram-positive bacteria<sup>37,55</sup>, *Caenorhabditis elegans* (*C. elegans*)<sup>54</sup>, *Drosophila* tissues, whole larval zebrafish, whole mouse embryos, and human clinical tissues. In each of these sample types, the key optimization of the ExM protocol is to find ways to soften parts of the samples that are mechanically stiff and requires softening treatments in addition to the standard proteinase K conditions used in the proExM protocol<sup>4</sup> for cultured mammalian cells and soft tissues. As discussed in detail below, protocols have been optimized to digest the cell wall in bacteria and the cuticles in *C. elegans* and *Drosophila* samples, or to decalcify the bones in whole larval zebrafish or mouse embryos, or to break the dense protein crosslinks in human clinical tissues, to allow isotropic expansion of these samples. In addition to providing protocols for users that are interested in applying ExM to the sample types covered in this section, we hope these examples will help the users make informed decisions when optimizing ExM protocols for their own sample type.

In contrast to Gram-negative bacteria<sup>56–58</sup>, for which the standard proteinase K-based proExM protocol worked quite well, Gram-positive bacteria have thick cell walls composed of complex and stiff structures such as highly crosslinked peptidoglycans that are hard to be fully digested by proteinase K alone. To overcome this challenge, several enzymes have been used together with proteinase K in optimized ExM protocols for the expansion of Gram-positive bacteria. For example, lysozyme and lysostaphin (both are enzymes capable of digesting peptidoglycans) have been used together with proteinase K in the sample softening step of the proExM workflow to expand the Gram-positive bacteria *Staphylococcus aureus* (*S. aureus*) to ~4x, enabling nanoscale imaging of *S. aureus*-infected mammalian cells on a confocal microscope.<sup>55</sup> In another example, mutanolysin (a peptidoglycan-digesting enzyme) was used to digest bacterial cell walls, and then proceed to a series of standard proteinase K-based proExM steps to enable ~4x expansion of both Gram-positive and Gram-negative bacteria.<sup>37</sup> Overall, by optimizing the enzymatic digestion step for softening of the bacterial cell wall, the above-mentioned proExM-type ExM variants enables expansion of both Gram-negative and Gram-positive bacteria.

Similar to how expansion of Gram-positive bacteria is challenged by the thick cell wall that enclose the bacteria, the expansion of the nematode *Caenorhabditis elegans* (*C. elegans*) is challenged by its tough cuticle that enclose the animal and that predominantly composed of crosslinked collagens, lipids, and other proteins and peptidoglycans. To overcome this challenge, a set of protocols have been developed to enable expansion of fixed, intact, and cuticle-enclosed *C. elegans*, with both pre-expansion labeling and post-expansion labeling formats.<sup>54</sup> We discuss the pre-expansion labeling ExM protocol for *C. elegans* (referred to as expansion of *C. elegans*, or ExCel) here and describe the post-expansion labeling protocol for *C. elegans* (referred to as epitope-preserving ExCel) in Section 1.4.2. ExCel starts with a reduction step to permeabilize cuticle by breaking the disulfides between collagen fibers in the cuticle, which could facilitate diffusion of ExM reagent into the specimen. ExCel then uses modified AcX treatment, gelation, and proteinase K digestion steps, all aiming to ensure thorough diffusion of reagents throughout the entire *C. elegans*, and complete sample softening to allow isotropic expansion of the entire animal. Overall, ExCel enables the nanoscale visualization of fluorescent protein (e.g., GFP, mCherry, and TagRFP)-labeled structures by staining with antibodies against fluorescent proteins after expansion, and the animal anatomy by staining with general protein stains (*N*-hydroxysuccinimide ester dyes), in the entire ~4.5x expanded and intact *C. elegans*.<sup>54</sup>

Like *C. elegans*, another kind of organism, *Drosophila*, also has cuticles that must be softened to allow expansion of the cuticle-enclosed tissues. Standard proExM protocol has worked well for *Drosophila* tissues that are not cuticle-enclosed, such as *Drosophila* embryos and dissected *Drosophila* brain tissues<sup>59–61</sup>, but failed to isotopically expand *Drosophila* larval and adult body-wall specimens, which are cuticle-enclosed. For these cuticle-enclosed *Drosophila* tissues, a proExM-style protocol has been developed that used Chitinase (an enzyme that digests the polysaccharide Chitin, a major component of the *Drosophila* cuticle) in addition to proteinase K to digest the cuticle and completely soften the sample for ~4x expansion, enabling the nanoscale visualization of synaptic structures in expanded *Drosophila* tissues.<sup>61</sup>

proExM-style protocols have also been developed to expand whole vertebrates including larval zebrafish and mouse embryos. Standard proExM protocols have been shown to successfully expand the soft vertebrate body parts, such as mouse tissue sections<sup>4</sup>, or zebrafish embryos and dissected zebrafish brain tissues<sup>33</sup>. However, ExM of whole zebrafish larvae or mouse embryos is challenged by the hard body parts such as the bones. To overcome this challenge, whole-body ExM was developed as an proExM-style protocol to expand whole zebrafish larvae and mouse

embryos.<sup>62</sup> Compared to proExM, whole-body ExM used AcX treatment conditions with surfactant in the buffer to facilitate diffusing of AcX throughout the fixed and intact larval zebrafish or mouse embryos, modified ExM gelation conditions to ensure homogeneous gelation throughout the entire animal, prolonged and repeated proteinase K digestion, and post-digestion decalcification using ethylenediaminetetraacetic acid (EDTA) to remove bones, to allow ~4x expansion, and optimized total protein stains using a mixture of several *N*-hydroxysuccinimide ester dyes. Collectively, the above optimizations enabled the nanoscale visualization of anatomical structures and fluorescent proteins throughout the entire expanded larval zebrafish or mouse embryos.

As the last example of proExM-style protocol optimized for specific sample formats and types, expansion pathology (ExPath) has been developed as an optimized pre-expansion labeling proExM protocol for human clinical samples such as formalin-fixed, paraffin-embedded (FFPE), hematoxylin and eosin (H&E)-stained tissues, and fresh-frozen thin-sliced tissues.<sup>32</sup> Note that such clinical tissues can also be expanded with a post-expansion labeling ExM protocol called decrowding expansion pathology (dExPath)<sup>52</sup>, which we discuss in Section 1.4.2. ExPath starts with a series of steps, such as adding xylene to remove paraffin and antigen retrieval in hot citrate buffer, that convert clinical tissues to formats that are compatible with proExM. After AcX treatment and gelation, ExPath uses an optimized proteinase K-based softening condition that features elevated digestion temperature (60 °C, the optimal temperature for proteinase K) and increased concentration of EDTA in the digestion buffer. These optimizations of proteinase K digestion are necessary because formalin-fixed samples have higher extent of crosslinking compared to, for example, paraformaldehyde-fixed mouse brain tissues, and thus require stronger protease digestion for sample softening. For fresh-frozen tissues, the AcX treatment concentration needed to be reduced to enable consistent expansion without tissue cracks and/or distortions, possibly because fresh-frozen tissues have more protein sites available for AcX binding as compared to formalin-fixed samples. Overall, ExPath has been demonstrated to work well with clinical tissues including human skin, lung, liver, breast, prostate, pancreas, ovary, kidney, and colon in various preservation formats.<sup>32</sup>

## 1.4.2 Post-expansion labeling ExM with ~4-5x linear expansion factor

Post-expansion labeling ExM administers protein labels after sample expansion and has several important features. First, expansion physically separates protein epitopes in dense protein compartments so that antibodies can access these otherwise “hidden” protein structures for visualization post-expansion. For instance, decrowding expansion pathology (dExPath) was developed as a post-expansion labeling ExM protocol for human clinical specimens, which revealed new disease marker-positive cell populations in human glioma tissues.<sup>52</sup> Second, post-expansion labeling ExM improves imaging quality by increasing the labeling density and reducing the positional errors introduced by the size of the protein labels (e.g., tens of nanometers for primary and secondary antibody complexes), which could be essential for imaging protein ultrastructures, as demonstrated in post-expansion labeling and imaging of cellular ultrastructures such as centrioles, microtubules, and synapses.<sup>8,9,50</sup> At last, post-expansion labeling ExM enables multiplexed (>4) protein staining and imaging by iterative rounds of antibody staining, imaging, and antibody destaining (e.g., by treatment with heat and denaturant). For instance, a post-expansion labeling ExM protocol called magnified analysis of the proteome (MAP) was used to visualize eleven endogenous protein epitopes within the same expanded mouse brain tissue.<sup>5</sup>

Post-expansion labeling ExM protocols are categorized into two kinds based on different sample fixation and protein anchoring chemistry. The first kind of protocols are designed to work with regular paraformaldehyde-fixed cells and tissues, FFPE tissues, or fresh-frozen tissues by using the same type of protein anchoring (e.g., AcX treatment) and gelation chemistry as pre-expansion labeling proExM, with modifications to the softening chemistry by replacing proteinase K digestion with milder treatments that preserves protein epitopes. The second kind of protocols used a custom sample fixation protocol and protein anchoring chemistry based on formaldehyde and acrylamide, which are designed to reduce crosslinking between proteins to enable sample expansion with heat and denaturant while preserving protein epitopes for staining after expansion. We first discuss two key considerations to help the users think about and choose what kind of post-expansion labeling protocol to use and how to find and validate antibodies for their protein targets, then we discuss the above-mentioned two kinds of post-expansion labeling ExM protocols in detail.



From the users' perspective, the first key consideration is how to choose a post-expansion labeling protocol. Practically, the choice could be made first based on the preservation format and source of the sample. For example, if the users have limited control over how the sample is preserved (e.g., FFPE tissues), then we recommend the users to use the first kind of post-expansion labeling ExM protocols, because these protocols are designed to work with standard sample formats and preservation protocols. In comparison, if the users have complete control of how to preserve the sample (e.g., the user can perform custom mouse perfusion procedures), the users might try either kind of post-expansion labeling ExM protocols, and the choice of protocols will largely depends on whether there are established protocols for the users' sample types and whether there are ExM-validated antibodies (as discussed below) for the users' protein of interest. For new sample types and new protein targets that have never been tested in post-expansion labeling ExM protocols before, it might be helpful to try different protocols to see which one works best.

The second key consideration is how to choose and validate antibodies used for post-expansion labeling, because the protein epitopes are now in different states (i.e., preserved in expanded hydrogel) than in the unexpanded specimen. For protein targets that have validated antibodies used in reported post-expansion labeling protocols discussed in the rest of this section, we recommend the users to try the same antibodies and post-expansion labeling protocols. For new protein targets, we recommend the users to validate the antibodies first by checking whether the antibodies give expected staining patterns and compare the post-expansion staining outcomes to images of unexpanded samples stained with the same antibodies. The users should pay attention to cases where the post-expansion labeling revealed additional structures besides those stained before expansion, as these new structures might be "hidden" in crowded and dense protein compartments, as discussed in two examples in later parts of this section about revealing new structures in mouse brains<sup>9</sup> and human glioma tissues<sup>52</sup> via post-expansion labeling. Of course, the quality of antibodies might vary from different sources, so for post-expansion labeling experiments of new protein targets or new sample types, it might be helpful to try antibodies from several commercial vendors to find the best one for the users' experiments.

As an example of the first kind of post-expansion labeling ExM protocols that works for standard specimen preservation formats, post-expansion labeling variant of proExM was developed to expand paraformaldehyde-fixed mouse brain tissues to ~4-fold for post-expansion staining with commercial antibodies. This protocol used AcX anchoring and gelation conditions similar to pre-

expansion labeling proExM, but replaced proteinase K digestion with heat and denaturant treatment which preserves protein epitopes.<sup>4</sup> A related protocol called miriEx<sup>49</sup> uses a chemical named acrylic acid *N*-hydroxysuccinimide ester that performs similar chemistry as AcX to anchor proteins to the hydrogel, followed by similar heat and denaturant treatments to expand mouse brain tissues for antibody staining post-expansion. Besides heat and denaturant, mild and site-specific proteases such as LysC, which specifically cuts proteins at lysine sites, have also been used for sample softening to enable post-expansion antibody staining of the AcX-anchored protein fragments generated from LysC digestion.<sup>4</sup> While both of the LysC-based and the heat and denaturant-based post-expansion labeling proExM protocols have been used to visualize fluorescent proteins, cellular markers, and synaptic proteins in expanded mouse brain tissues<sup>4,49</sup>, the initial report<sup>4</sup> notes variability and inhomogeneity in terms of the expansion and antibody staining outcomes of different antibody and tissue identities, suggesting that further investigations are required to optimize the protocol for consistent antibody staining outcomes as well as validate the expansion isotropy at the nanoscale (e.g., by comparing images of the same region acquired pre- versus post-expansion).

Protocols based on post-expansion labeling proExM have been developed to work with sample types that have different mechanical properties than mouse tissues through optimizing the sample softening conditions. For example, decrowding expansion pathology (dExPath) has been developed to work with human clinical tissues.<sup>52</sup> dExPath uses strong denaturation conditions featuring high concentration of denaturant, autoclaving, reducing agent, and EDTA, all designed to disrupt the extensive inter- and intra-protein interactions in formalin-fixed human clinical tissues. As a result of such strong softening conditions, dExPath showed homogeneous ~4x expansion of clinical tissues, with nanoscale distortions of ~3-4% error over the measurement length of ~10  $\mu\text{m}$ <sup>52</sup> in expanded clinical tissues, which is consistent with previous proteinase K-based ExM protocols<sup>1,4,32</sup> applied to mouse tissues. dExPath has been applied to revealing new disease marker-positive cell populations in human glioma tissues.<sup>52</sup>

In another example of post-expansion labeling proExM-style protocol optimized for specific sample types, epitope-preserving expansion of *C. elegans* (epitope-preserving ExCel) has been developed to work with intact *C. elegans* that are enclosed by mechanically stiff and antibody-impermeable cuticles.<sup>54</sup> Epitope-preserving ExCel uses a heat denaturation treatment identified from screening a panel of softening conditions to optimize both linear expansion factor and epitope-preservation. The final epitope-preserving ExCel achieved antibody-staining of

endogenous protein epitopes in  $\sim 2.8$ x linearly expanded *C. elegans* with nanoscale distortions of  $\sim 8$ -25% error over the length of  $\sim 100\mu\text{m}$ . While further investigations might be needed to improve the expansion factor and isotropy, the current form of epitope-preserving ExCel has been applied to visualizing previously unreported localization of a protein at the cell junctions between developing cells, and resolving peri-active and active zone proteins in chemical pre-synapses.<sup>54</sup>

As an example of the second kind of post-expansion labeling ExM protocol, magnified analysis of the proteome (MAP) used acrylamide (a monomer used in ExM hydrogels) and formaldehyde (a chemical fixative) during sample fixation to equip proteins with hydrogel anchors and reduce formaldehyde-based crosslinking between proteins, thus enabling  $\sim 4$ x linear expansion of mouse tissues.<sup>5</sup> MAP showed a nanoscale distortion of  $\sim 2\%$  error over the measurement length of  $\sim 15\mu\text{m}$  for MAP processed cultured cells, and a microscale distortion of  $\sim 2\%$  error over the measurement length of  $\sim 2\text{mm}$  for MAP processed mouse brain tissues. MAP was demonstrated to expand entire mouse organs including heart, lung, spinal cord, liver, kidney, intestine, and brain, as well as cerebral organoids. Furthermore, the authors showed that more than 80% of  $>100$  antibodies tested successfully stained many protein targets, such as microtubules, neurofilaments, nuclear and membrane markers, and a diversity of neurotransmitters, neuromodulators, and synaptic proteins, in MAP-processed cells and tissues.

Based on the MAP-style ExM chemistry, ultrastructure expansion microscopy (U-ExM) has been developed to visualize ultrastructures in cultured cells and purified protein complexes.<sup>8</sup> Compared to MAP, U-ExM avoids chemical fixation and uses reduced concentration of acrylamide and formaldehyde in the protein anchoring step, which the authors found to be important for preserving the ultrastructure of centrioles. With such optimizations, U-ExM enabled the visualization of ultrastructural details such as the chirality of centriole protein arrangements. However, the authors noted that the lack of chemical fixation led to loss of some cellular components when applying U-ExM to cultured cells.<sup>63</sup> To overcome this limitation, U-ExM has been optimized and combined with cryofixation, in a method termed cryo-ExM, to enable preservation and visualization of a range of cellular structures, such as microtubule, actin, endoplasmic reticulum, mitochondria, lysosome, and autophagosome.<sup>64</sup> Taken together, U-ExM and cryo-ExM demonstrated developments and optimizations of ExM methods for ultrastructure preservation and visualization in cultured cells and isolated protein complexes, and points to the

next step of combining tissue cryofixation (e.g., using high-pressure freezing) with ExM to enable ultrastructure visualization in expanded tissues.

Recently, epitope-preserving magnified analysis of the proteome (eMAP) has been developed as a post-expansion labeling ExM protocol that does not use chemicals to anchor proteins to the hydrogel. The authors proposed that the protein epitopes were preserved and expanded via the physical entanglement between proteins and the hydrogel polymer chains. With eMAP, the authors showed 49 out of 51 and 46 out of 49 synaptic antibodies tested successfully stained their targets in expanded mouse and marmoset brain tissues, respectively. The nanoscale uniformity of expansion in eMAP has yet to be validated by comparing images acquired with super-resolution microscopy before expansion versus images of the same biological structure after eMAP expansion; it is thus an open question of whether the protein ultrastructures and nanoscale expansion isotropy are preserved in eMAP.

### **1.4.3 Increasing the linear expansion factor beyond ~4-5x for high-resolution protein imaging**

As previously discussed, the imaging resolution of ExM increases when expansion factor gets higher but is fundamentally limited by the error of the hydrogel synthesis process which in principle could be as small as a few nanometers<sup>29</sup>. In practice, multiple approaches<sup>7,9,14,30,35,48,51,54</sup> have been developed to increase the linear expansion factor to ~10-20x to improve the imaging resolution down to ~20nm. Unlike proExM<sup>4</sup> which has been applied to diverse sample types, these high-expansion-factor ExM protocols are relatively new and has not been extensively tested in diverse sample types. Therefore, in addition to describing how these high-expansion-factor ExM protocols work, and the sample types tested with these protocols, we emphasize the limitations and remaining challenges of these methods, which we hope could help the users make informed decisions regarding what protocol to use now and point to future optimizations required to make these protocols more robust.

Based on how many times the sample needs to be expanded to reach expansion factor higher than ~4-5x, we categorize the high-expansion-factor ExM protocols into two kinds. The first kind of protocols optimize the hydrogel recipe and composition to achieve up to ~10x expansion in a single round of expansion<sup>14,30,31</sup>. The benefit of the first kind of protocol is that it has a similar ExM gelation workflow as previous ~4-5x ExM methods (discussed in Sections 1.4.1 and

1.4.2), which is practically simpler than the second kind of protocols which expands the sample twice in succession. The second kind of protocol, although needs multiple gelation steps to expand the sample twice, can reach overall expansion factor of  $\sim 10\text{-}20\times$ <sup>7,9,35,48,51,54</sup>, which is higher than the expansion factor of the first kind of protocol and therefore provides improved imaging resolution. Because we have covered the features of pre- and post-expansion labeling protocols in previous Sections 1.4.1 and 1.4.2, here in this section, we focus on discussing the expansion factors, but we will mention whether each protocol is pre- or post-expansion labeling format, so that the users have an idea of what features the protocol could bring. Below we first discuss the one-round higher-expansion-factor protocols, and then dive into protocols that expand the sample twice.

Four ExM variants, TREx, ZOOM, X10, and MAGNIFY, have been reported to achieve  $\sim 8\text{-}11\times$  expansion in a single round either through optimizing polyacrylamide/polyacrylate hydrogel composition (TREx and ZOOM)<sup>14,31</sup>, or using alternative hydrogel monomers (X10 and MAGNIFY)<sup>30,65</sup>. Both TREx and X10 followed the pre-expansion labeling format similar to those ExM protocols discussed in Section 1.4.1 and used proteinase K for sample softening; ZOOM and MAGNIFY followed the post-expansion labeling format similar to those ExM protocols discussed in Section 1.4.2 and used heat and denaturant for sample softening. We describe each of these methods in detail below. We note that unlike the widely used proExM protocol developed in 2016 (as discussed in Section 1.4.1), these new one-shot  $\sim 8\text{-}11\times$  expansion protocols are relatively new and thus could benefit from validation in more biological samples and systems before robust deployment to wider biological contexts.

In TREx, a hydrogel recipe, using the same hydrogel crosslinkers and monomers as proExM<sup>4</sup>, has been systematically optimized to enable  $\sim 10\times$  linear expansion of cultured human cells and mouse brain tissues, primarily via decreasing the hydrogel crosslinker concentration. TREx has been shown to be compatible with antibody-stained samples and commercial small molecule total protein stains and membrane labels. The TREx authors note that the exact crosslinker concentrations that produce  $\sim 10\times$  expansion varied between different labs, so the authors recommend that a range of crosslinker concentrations should be tested when using TREx for  $\sim 10\times$  expansion with the end user's choice of specimen and experimental setups.

In ZOOM, alkaline buffers and heat have been used to convert polyacrylamide hydrogels to charged and expandable polyacrylate hydrogels to enable up to  $\sim 8\times$  linear expansion, in a fashion

similar to a protocol called high pH iterative ExM (hp-iExM, reported together with the iExM protocol<sup>7</sup> as discussed later in this section) that showed ~16x expansion of immunostained cultured mammalian cells. The ZOOM authors showed expansion of multiple types of biological specimens at different expansion factors, such as cultured human cells (6.3x expansion), mouse brain tissues (up to 8x expansion), human clinical brain tissues (3.7x expansion), and *Caenorhabditis elegans* (3.1x expansion), suggesting that further optimizations might be required for ZOOM to achieve consistent ~8x expansion for diverse sample types.

In X10, a hydrogel based on *N, N'*-dimethylacrylamide (DMAA) monomer<sup>66</sup> and sodium acrylate (same charged monomer as in the proExM hydrogel) was used to increase the expansion factor, enabling ~10x linear expansion of cultured mammalian cells and mouse brain tissues.<sup>14</sup> The X10 authors reported that the high expansion factor of X10 requires stronger proteinase K digestion than regular ~4.5x expansion protocols, which causes significant loss of the fluorescence of fluorescent proteins and requires immunostaining against fluorescent proteins to amplify signals for visualization.<sup>30,67</sup> Moreover, the X10 authors noted that because DMAA hydrogel formation is very sensitive to oxygen, the users are recommended to carefully purging oxygen from X10 gelation solutions to ensure successful gelation and ~10x expansion, which is laborious.<sup>67</sup>

In MAGNIFY, a hydrogel recipe involving DMAA and the same hydrogel monomers and crosslinkers used in proExM was developed to enable up to ~11x expansion of cultured mammalian cells, mouse brain tissues, human lung organoids, and human FFPE tissues. Unlike other ExM protocols that performs an anchoring step (e.g., AcX treatment to anchor proteins in proExM, as discussed in Section 1.4.1) before forming the expansion hydrogel, MAGNIFY used a chemical called methacrolein mixed in the gelation solution to perform the biomolecule anchoring and the hydrogel formation in a single step, enabling anchoring of multiple kinds of biomolecules including proteins, nucleic acids, and lipids in the MAGNIFY-expanded samples. MAGNIFY has been demonstrated to visualize nanoscale structures including synaptic proteins in mouse brain tissues, podocyte foot processes in human kidney tissues, and structural changes of cilia and basal bodies in human lung organoids treated with drugs.

The expanded samples have been expanded again in a process called iterative expansion microscopy, or iExM<sup>7</sup>. iExM is a pre-expansion labeling ExM method that uses DNA-linked antibodies to label protein structures, and a DNA hybridization-based scheme to preserve and

transfer the spatial information of biomolecules between rounds of hydrogel expansion. Specifically, the DNA-conjugated antibody-labeled sample is expanded with proteinase K-based softening with the first expansion hydrogel, then re-embedded in a neutral gel to keep the sample expanded during following treatments. The first expansion gel and the re-embedding gel used hydrogel crosslinkers that can be cleaved, so that these gels won't inhibit the second round of expansion. Because the first gel will be cleaved and discarded, iExM requires DNA labels complementary to those from the DNA-conjugated antibodies to preserve and transfer the spatial information of biomolecules from the first expansion hydrogel to the second expansion hydrogel. Then, after cleaving the first expansion gel and the re-embedding gel, the second gel can be expanded, resulting in overall  $\sim 4.5 \times 4.5 = \sim 20x$  linear expansion and thus could in theory attain  $\sim 300/20 = \sim 15$  nm resolution with a conventional diffraction-limited microscope. In practice,  $\sim 25$ -nm-resolution imaging of synaptic proteins and dendritic spine structures have been demonstrated in  $\sim 20x$  expanded cultured neurons and mouse brain tissues.<sup>7</sup> The imaging resolution of iExM is slightly larger than  $\sim 15$  nm, primarily owing to the spatial errors from the hydrogel synthesis and expansion processes.<sup>7</sup> Similar to iExM, iExCel<sup>54</sup>, a  $\sim 20x$  ExM protocol for imaging *C. elegans*, uses DNA-linked green fluorescent protein (GFP) antibodies to visualize GFP-labeled neurons in  $\sim 20x$  expanded intact *C. elegans* at  $\sim 25$ -nm resolution. In another iExM-style protocol<sup>35</sup>, virion envelope proteins in intact viruses were labeled with DNA and expanded in two rounds to  $\sim 10x$ , enabling the visualization of the shape of individual virions.

Although iExM and its variants have enabled high resolution imaging of protein nanostructures in cultured cells<sup>7,35</sup>, mouse brain tissues<sup>7</sup>, *C. elegans*<sup>54</sup>, and viruses<sup>35</sup>, the requirement of custom DNA reagents limits the deployment of iExM in day-to-day biological studies that uses commercial dyes and off-the-shelf antibodies. To address this limitation, three post-expansion labeling iterative expansion methods, pan-ExM ( $\sim 13$ - $24x$  expansion), expansion revealing (ExR,  $\sim 20x$  expansion), and eMAP ( $\sim 10x$  expansion) have been reported that work with commercial protein staining reagents in expanded cells (pan-ExM), mouse brain tissues (pan-ExM, ExR, and eMAP), and marmoset brain tissues (eMAP), as discussed in detail below. Note that all three of these iterative expansion methods used the post-expansion labeling ExM format (as discussed in Section 1.4.2) and relied on heat and denaturant treatments for sample softening, followed by labeling proteins with antibodies or small molecule total protein stains after sample expansion.

In pan-ExM, cultured cells were expanded to  $\sim 13$ - $21x$ , followed by labeling of proteins with small molecule dyes and/or antibodies, enabling the visualization of cellular ultrastructures such

as mitochondrial cristae and centrosomes.<sup>48</sup> Similar to the gelation steps in iExM described above, pan-ExM used a similar sequences of first gel expansion, re-embedding into a neutral gel to keep the first gel expanded, and then cast a second expansion gel, followed by cleavage of the first expansion gel and re-embedding gel, to enable overall ~13-21x expansion of the cells. Importantly, pan-ExM added an additional anchoring step after first expansion, so that the proteins could be anchored and retained in the second expansion. pan-ExM has recently been optimized to work with mouse brain tissues, in a protocol called pan-ExM-t<sup>68</sup>, which enables imaging brain ultrastructures, such as synapses, in ~24x expanded mouse brain tissues.

In ExR, mouse brain tissues are expanded twice in succession, resulting in overall ~20x expansion. Different from the iExM and pan-ExM gelation protocols which require cleaving the first expansion gel and the re-embedding gel, ExR does not require gel cleavage and thus retains the first expansion gel as well as the anchored proteins for expansion by the second expansion gel. ExR was used to systematically compare synaptic proteins labeled with antibodies applied before versus after expansion, demonstrating that protein decrowding via expansion and post-expansion antibody staining could reveal otherwise invisible protein structures in the mouse brain tissues. ExR was further demonstrated to reveal details of mouse brain structures such as the nanocolumns formed by the aligned pre- and post-synaptic protein machineries, and new amyloid-containing nanoclusters.<sup>9</sup>

In eMAP, mouse and marmoset brain tissues were expanded in four rounds of expansion to ~10x for nanoscale imaging of synaptic protein structures.<sup>51</sup> Similar to ~4x eMAP protocol discussed in Section 1.4.2, the current ~10x eMAP protocol also lacks validation of the nanoscale uniformity of expansion, which raises the question about whether nanoscale ultrastructures are expanded isotopically. Compared to the case of ~4x eMAP, it is even more important for ~10x eMAP to validate such nanoscale isotropy, because with a higher expansion factor (i.e., ~10x compared to ~4x) comes with the expectation of higher imaging resolution and thus require more careful validation and testing to ensure that uniform expansion is achieved at such a high imaging resolution.



## 1.5 ExM for Nanoscale Imaging of RNAs

The most popular forms of ExM for RNA imaging follow the post-expansion labeling format: endogenous RNAs are anchored to the ExM hydrogel first, then the sample is softened via proteinase K digestion, enabling post-expansion labeling and imaging of hydrogel-anchored RNAs. Importantly, expansion clears the space around RNAs and makes them more accessible, which facilitates labeling, multiplexing, and amplification chemistries for RNA imaging, as discussed later in this section.<sup>16,19,20,69</sup>

RNAs are anchored to the hydrogel using either one of three reagents (LabelX<sup>16</sup>, MelphaX<sup>20</sup>, or GMA<sup>15</sup>) in different ExM protocols described in this section. All three reagents and their associated protocols have been demonstrated in multiplexed RNA imaging experiments in expanded tissues: LabelX and GMA has been used in mouse brain tissues and human cancer tissues, while MelphaX has been used in mouse brain tissues.<sup>16,19,20,69</sup> These three reagents perform similar RNA anchoring chemistries and could likely be used interchangeably in the context of ExM for RNA imaging. The major difference between these three reagents, in the context of RNA anchoring for ExM imaging, is that LabelX and MelphaX need to be synthesized in-house using commercial building blocks and cost tens of dollars (MelphaX) or thousands of dollars (LabelX) per milligram, while GMA is a single commercial reagent that only cost less than a cent per milligram. Considering the simplicity and the vastly reduced cost of GMA compared to MelphaX and LabelX, we recommend the users to use GMA to anchor RNAs for ExM experiments.

We note that it is possible to do nanoimaging of RNAs via pre-expansion labeling: RNAs are labeled first, then the RNA labels are anchored to the ExM hydrogel, followed by sample softening via proteinase K digestion, enabling sample expansion and imaging of the physically separated RNA labels.<sup>17,18</sup> But such pre-expansion labeling protocols do not have the feature of clearing spaces around RNAs for better labeling, requires custom RNA probes bearing hydrogel anchors, and do not retain endogenous RNAs to support imaging more than four RNAs via rounds of probe administration, imaging, and removal. Considering the above limitations of pre-expansion labeling ExM for RNA imaging, below we focus on describing RNA imaging methods that follow the post-expansion labeling format.

The first ExM method developed for nanoscale RNA imaging is called ExFISH<sup>16</sup> (see examples in **Figure 2a-2f**), which uses fluorescence in situ hybridization (FISH) probes to label RNAs

anchored to the ExM hydrogel. In ExFISH, RNAs are anchored to the ExM hydrogel network using a reagent called LabelX, which is a reagent synthesized from two commercial building blocks: AcX, which labels amines with a hydrogel anchor (as discussed in Section 1.4.1), and Label-IT amine, which labels RNAs with an amine. LabelX equips the guanine bases in RNAs with hydrogel anchors, and crosslinks RNAs to the hydrogel network after polymerization. After proteinase K digestion and expansion, the hydrogel-linked RNAs are labeled with FISH probes and imaged.<sup>16</sup> In ExFISH, the expansion process physically separates RNAs and clears the space around them, which supports multiplexed RNA imaging via rounds of single-molecule FISH in expanded cultured cells and signal amplification chemistries such as hybridization chain reaction (an enzyme-free DNA amplification chemistry).<sup>16</sup> ExFISH has been used to determine subcellular localizations<sup>16,70,71</sup>, expression levels<sup>16</sup>, and structures<sup>(16)</sup> of RNAs, which enables the mapping of RNAs in nanoscale mouse brain structures such as synapses<sup>71</sup> and dendritic spines<sup>16</sup>.

Following the ExFISH concept and workflow, several protocols have been developed for multiplexed RNA mapping with nanoscale spatial resolution, by applying various multiplexed RNA imaging chemistries to expanded samples, as described below.

In expansion sequencing, or ExSeq<sup>19</sup>, LabelX-anchored and physically separated RNAs are mapped with in-situ sequencing chemistries. ExSeq has been demonstrated in mapping RNA transcripts in nanoscale compartments such as dendritic spines and branches in mouse brain tissues and determining cell types and states in the mouse visual cortex tissue as well as human breast cancer tissues (see examples in **Figure 2g-2j**). ExSeq has also been used with unified ExM (uniExM, an ExM protocol that used GMA to anchor biomolecules) to map GMA-anchored and physically separated RNAs. UniExM-supported ExSeq has been demonstrated in mapping a set of genes in expanded patient-derived xenografts.<sup>15</sup>

In expansion-assisted iterative fluorescence in situ hybridization, or EASI-FISH<sup>20</sup>, MelphaX-anchored and physically separated RNAs are labeled with FISH probes followed by hybridization chain reaction (HCR)-based signal amplification. MelphaX is a reagent synthesized using AcX and an RNA-labeling reagent Melphalan and performs similar RNA anchoring chemistry as LabelX. Compared to LabelX, MelphaX has been shown to produce enhanced FISH signals in expanded cultured mammalian cells. EASI-FISH has been

demonstrated in mapping cell types and spatial organizations in a specific brain region, the lateral hypothalamic area, in expanded mouse brain tissues.

Besides the above-mentioned in-situ sequencing chemistries used in ExSeq, or iterative FISH chemistries used in EASI-FISH, multiplexed error robust fluorescent in situ hybridization, or MERFISH, has also been applied to expanded samples. Different from the protocols described above that anchor RNAs using small molecule reagents (i.e., LabelX, MelphaX, or GMA), in ExM-supported MERFISH<sup>69</sup>, mRNAs are anchored to the ExM hydrogel using poly(dT) probes bearing hydrogel anchors and hybridized to the poly(A) tail of mRNAs. Because expansion physically separates RNAs and clears the space around them, ExM-supported MERFISH achieved ~100% detection efficiency for a ~130 RNA library, and more than 10-fold improvement in RNA detection density compared to previous MERFISH protocols without expansion.<sup>69</sup> ExM-supported MERFISH has been demonstrated in mapping mRNAs in subcellular compartments, the profiling of gene expression at stages of cell cycles, and the transcriptomic level mapping of ~10,000 genes in expanded cultured mammalian cells.<sup>72</sup>

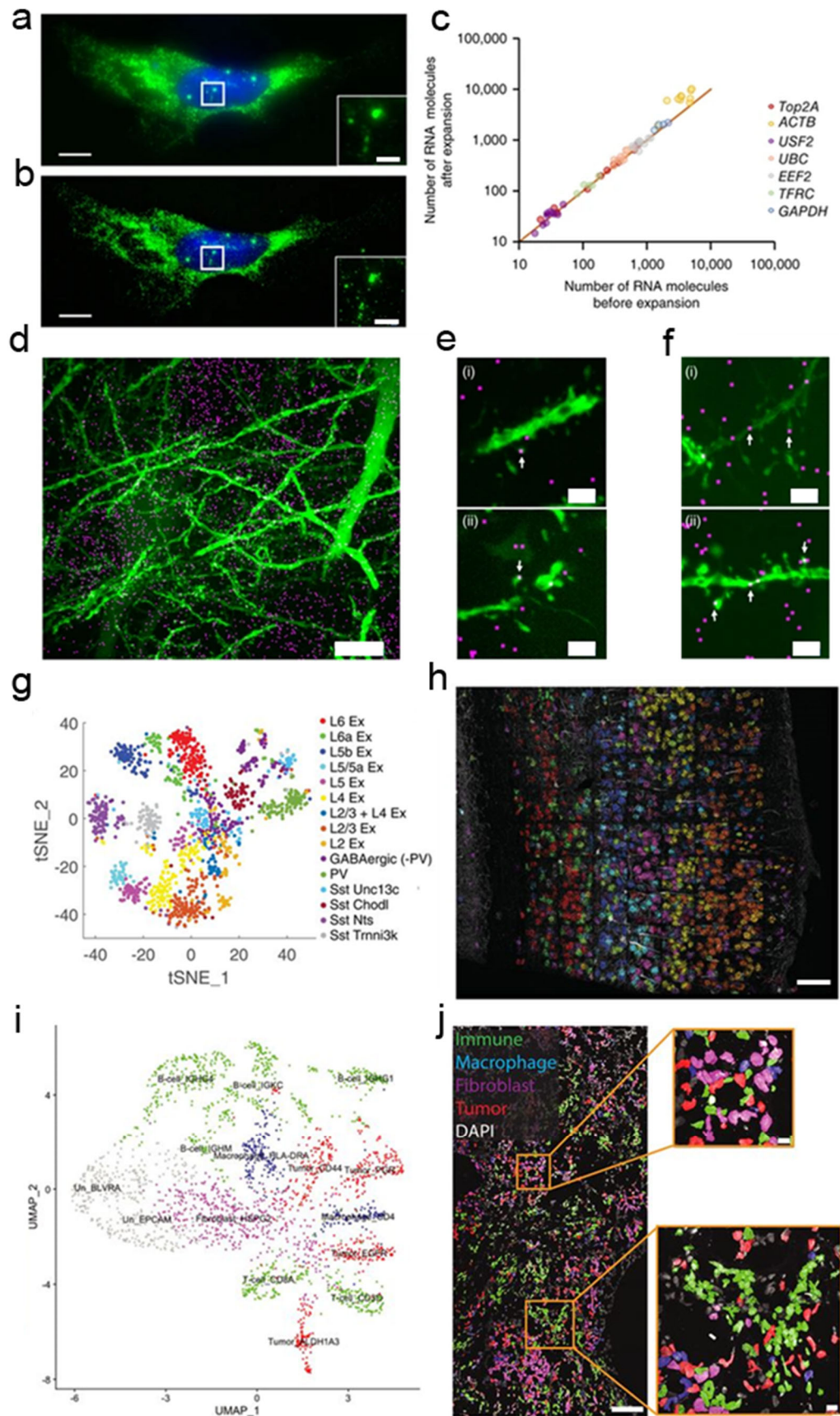


## Figure 2 ExM-supported RNA imaging

**(a-c) ExFISH quantification of RNAs in cultured cells.** (a) Single-molecule fluorescent in situ hybridization (smFISH) imaging of *ACTB* before expansion of a cultured HeLa cell. Inset zooms in on the boxed region that highlights transcription sites in the nucleus. (b) smFISH imaging of *ACTB* after expansion of the same HeLa cell in (a). (c) smFISH counts of genes before vs. after expansion (n = 59 cells; each symbol represents one cell). Scale bars in pre-expansion units that are calculated as the physical sizes of the scale bars of the image divided by the expansion factor: (a, b) 10  $\mu\text{m}$ , inset 2  $\mu\text{m}$ . Expansion factor:  $\sim 3\times$ . **(d-f) ExFISH visualization of transcripts in dendritic spines and processes in mouse hippocampal tissues.** (d) Confocal image of expanded Thy1-YFP mouse hippocampal tissues showing *Dlg4* transcripts (magenta, imaged with ExFISH followed by hybridization chain reaction) and YFP (Thy1-YFP). (e) Dendrites with *Dlg4* localized to spines (white arrows). (f) *Camk2a* transcripts (magenta, imaged with HCR-ExFISH) localized to dendritic spines and processes. Scale bars in pre-expansion units: (d) 10  $\mu\text{m}$ ; (e, f) 2  $\mu\text{m}$ . Expansion factor:  $\sim 3\times$ . Panels (a-f) adapted from ref. <sup>16</sup> **(g, h) ExSeq of 42 genes to map neuronal cell types in Thy1-YFP mouse primary visual cortex tissue.** (g) ExSeq gene expression profiles of 1,154 cells clustered into 15 cell types. (h) Spatial organizations of cell types identified in G, showing cells in the same color as in G, and YFP signals in white. Scale bar in pre-expansion units: 100  $\mu\text{m}$ . Expansion factor:  $\sim 4\times$ . **(i, j) ExSeq of 297 genes to map cell types and states in metastatic breast cancer tissues.** (i) Uniform manifold approximation and projection (UMAP) representation of principal components analysis (PCA)-based expression clustering reveals cell types and states indicated by different colors: green (T cells and B cells), red (tumor cells), blue (macrophages), magenta (fibroblasts), and gray (unannotated clusters) (j) Spatial organization of transcriptionally defined cell types identified and colored as in (i). Scale bars in pre-expansion units: (j) 100  $\mu\text{m}$ , inset 10  $\mu\text{m}$ . Expansion factor:  $4\times$ . Panels (g-j) adapted from ref. <sup>19</sup>

## 1.6 Applications of ExM

For cell biology applications (see examples in **Figure 3**), ExM has been used to explore the localization of proteins throughout organelles and cell biological protein assemblies, and how these organizations are altered by perturbations such as gene deletion or alterations in cell health, of mitochondria<sup>6,8,21,48,73–77</sup>, endoplasmic reticulum<sup>6,21,78</sup>, Golgi apparatus<sup>21,48</sup>, centrioles and centrosomes<sup>8,79–88</sup>, cilia<sup>84,89</sup>, synaptonemal complexes<sup>59,90–92</sup>, kinetochore<sup>93</sup>, mitotic spindles<sup>94–96</sup>, microtubule and actin networks<sup>1,4,7,97–103</sup>, nucleus<sup>104,105</sup>, chromosomes<sup>106,107</sup>, stress granules and other biological condensates<sup>108–111</sup>, glycocalyx<sup>112</sup>, endosomes<sup>113</sup>, microvilli<sup>114</sup>, intercellular tunneling nanotubes<sup>115</sup>, and membrane receptors<sup>116</sup> in diverse cell types such as human<sup>8,48,74,75,80–84,86,88,89,93,95,97,100,102,103,106–112,115</sup>, other mammalian<sup>6,7,73,78,85,98,101</sup>, and other animal cell lines in

culture<sup>79</sup>, isolated fly and mouse spermatocytes<sup>87,91,92</sup>, isolated mouse oocytes<sup>94</sup> and blood platelets<sup>116</sup>, primary human immune cells<sup>114</sup>, ciliates<sup>88</sup>, malaria parasites<sup>96</sup>, and green algae<sup>80</sup>, various tissue types such as human kidney<sup>117,118</sup>, mouse and rat brain<sup>21,119</sup> and kidney<sup>117,120–124</sup>, *Drosophila* larva<sup>99</sup> and ovary<sup>59,90</sup>, zebrafish embryonic brain<sup>113</sup>, plant ovule and seed<sup>125,126</sup>, and 3D cell cultures such as tumor spheroids and organoids<sup>127</sup>.

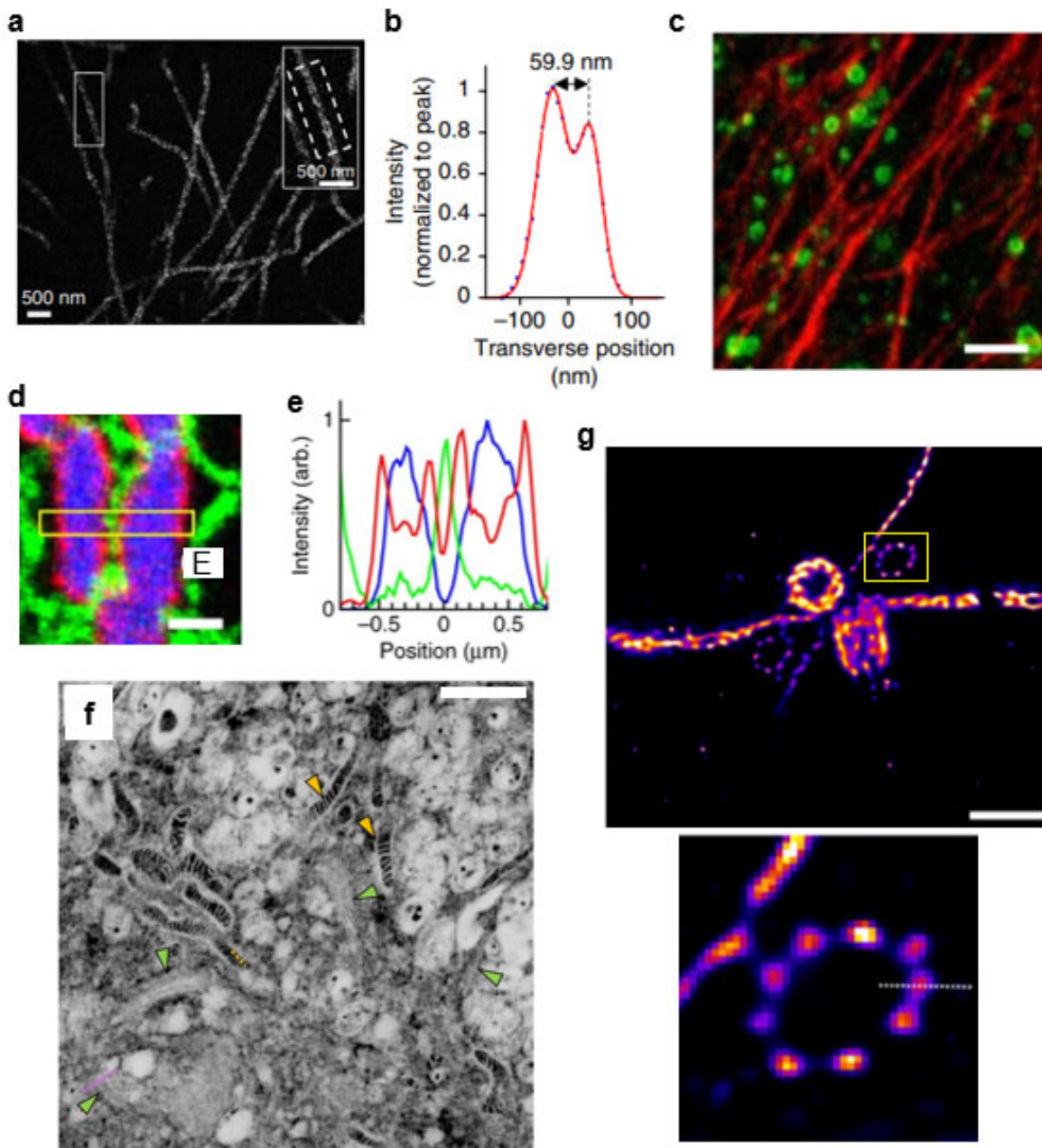


**Figure 3 Applications of ExM in cell biology**

**(a, b) iExM imaging of microtubules.** (a) Confocal image of iExM-processed cultured BS-C-1 cells with immunostained microtubules. The inset zooms in on the upper left white box. (b) Transverse profile of microtubules in the boxed region (dotted lines) of the inset in (a) after averaging down the long axis of the box and then normalizing to the peak value (blue dots), with superimposed fit with a sum of two Gaussians (red lines). Expansion factor:  $\sim 20\times$ . Panels (a, b) adapted from ref. <sup>7</sup>. **(c) Dual-color proExM imaging of clathrin and keratin.** Confocal image of proExM-processed HeLa cells expressing fluorescent protein-fused clathrin (mEmerald, green) and keratin (mRuby2, red). Scale bar in pre-expansion units: 1  $\mu\text{m}$ . Expansion factor:  $\sim 4\times$ . Adapted from ref. <sup>4</sup> **(d, e) Three-color ExM imaging of ER and mitochondria.** (d) Confocal image of ExM-processed BS-C-1 cells expressing ER tag $\beta$ Sec61-GFP (green) and mitochondrial inner membrane tag mito-DsRed (blue); mitochondrial outer membrane was immunolabeled with antibodies against mitochondrial outer membrane protein TOM20 (red). Scale bar in pre-expansion units: 500 nm. (e) Cross-sectional fluorescence intensity profile of the yellow boxed region in (d). arb.: arbitrary units. Expansion factor:  $\sim 4\times$ . Panels (d, e) adapted from ref. <sup>6</sup> **(f) pan-ExM imaging of cellular ultrastructures.** Confocal image of a region of a pan-ExM expanded HeLa cell stained with a succinimidyl ester dye, revealing cellular ultrastructures such as mitochondrial cristae (yellow arrows) and Golgi cisternae (green arrows). Scale bar in pre-expansion units : 2  $\mu\text{m}$ . Expansion factor:  $\sim 14\times$ . Adapted from ref. <sup>48</sup> **(g) U-ExM imaging of centriole.** Top: deconvoluted confocal image of an isolated centriole expanded with U-ExM. Bottom: zoomed-in view of the boxed region in the top image. Scale bar in post-expansion units: 1  $\mu\text{m}$ . Expansion factor:  $\sim 4\times$ . Adapted from ref. <sup>8</sup>.

In virology (see examples in **Figure 4**), ExM has been used to analyze how viruses such as herpes simplex virus <sup>135,128,129</sup>, hepatitis C virus<sup>130</sup>, influenza virus<sup>38</sup>, and rabies virus<sup>131</sup>, alter host cell structures, such as the cytoskeleton<sup>128,131</sup>, organelles<sup>128</sup>, members of signaling cascades<sup>128</sup>, and chromatin<sup>129</sup> during virus infection, and even to visualize the shapes of viruses themselves, and how the spatial distribution of viral proteins inside host cells changes in response to pharmacological perturbations<sup>130</sup>.

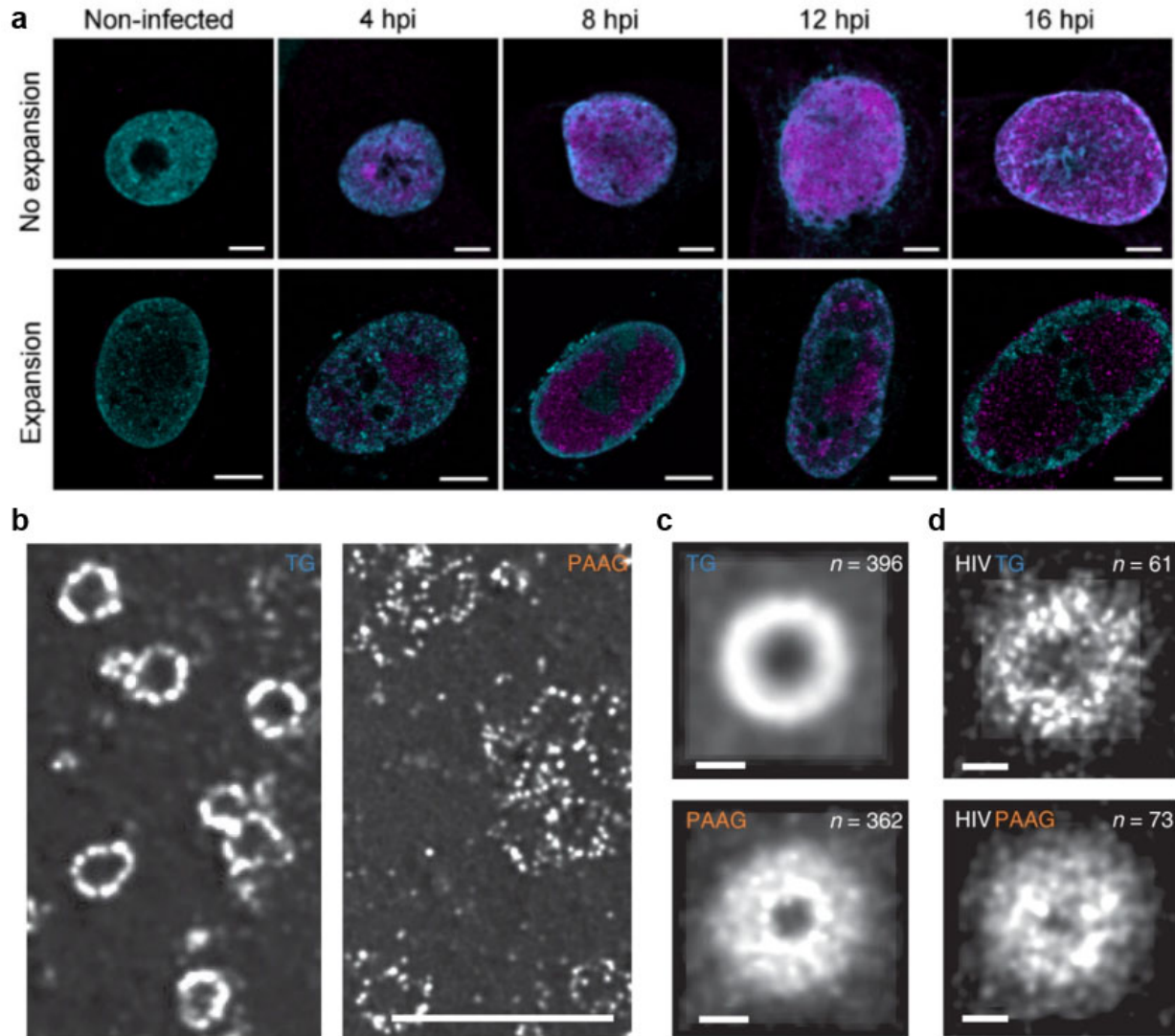


**Figure 4 Applications of ExM in virology**

**(a) ExM imaging of herpesvirus-infected cells.** Confocal images of unexpanded (top row) and expanded (bottom row) nuclei of non-infected and infected cultured Vero cells at 4, 8, 12, and 16 hours post infection (hpi). Chromatin was stained with a mixture of histone antibodies (H3K27ac, H3K9me3, H4K20me3; cyan); viruses were stained with an antibody against the viral capsid protein VP5 (magenta). Scale bars in pre-expansion units: 5  $\mu\text{m}$ . Expansion factor:  $\sim 4\times$ . Adapted from ref. <sup>129</sup> **(b-d) ExM imaging of virions.** **(b)** Herpes simplex virus 1 (HSV-1) virions imaged with tetragel (TG)-based iterative expansion microscopy. A representative image was shown. **(c)** Single-particle average image of TG-expanded HSV-1 virions ( $n = 396$  virions). **(d)** Single-particle average image of TG-expanded HIV virions ( $n = 61$  virions). Scale bars in pre-expansion units: **(b)** 1  $\mu\text{m}$ ; **(c, d)** 100 nm. Expansion factor:  $\sim 10\times$ . Panels **(b-d)** adapted from ref. <sup>35</sup>



In microbiology (see examples in **Figure 5**), ExM has been used to visualize the cytoskeleton<sup>132–139</sup>, organelles<sup>136,140</sup>, and protein complexes<sup>57,58,133,141–144</sup> of microbes such as *Toxoplasma*<sup>132,133</sup>, *Chlamydia*<sup>22,58</sup>, *Giardia*<sup>134,135</sup>, *Trypanosoma*<sup>136–138,140</sup>, *Escherichia coli*<sup>37,46,56,57,141</sup>, *Staphylococcus aureus*<sup>55</sup>, *Plasmodium*<sup>139</sup>, and several other fungal<sup>142,143</sup>, Gram-negative and Gram-positive bacterial<sup>22,37,55,144</sup> species, and how some of these microbial structures change at different developmental stages of the microbes<sup>58</sup>, and in response to gene deletions<sup>133</sup> and antibiotic treatments<sup>37</sup>. ExM has also shown promise for analyzing spatial relationships within microbial communities<sup>37</sup>, and between microbe and host cell structures<sup>22,55,58</sup>.

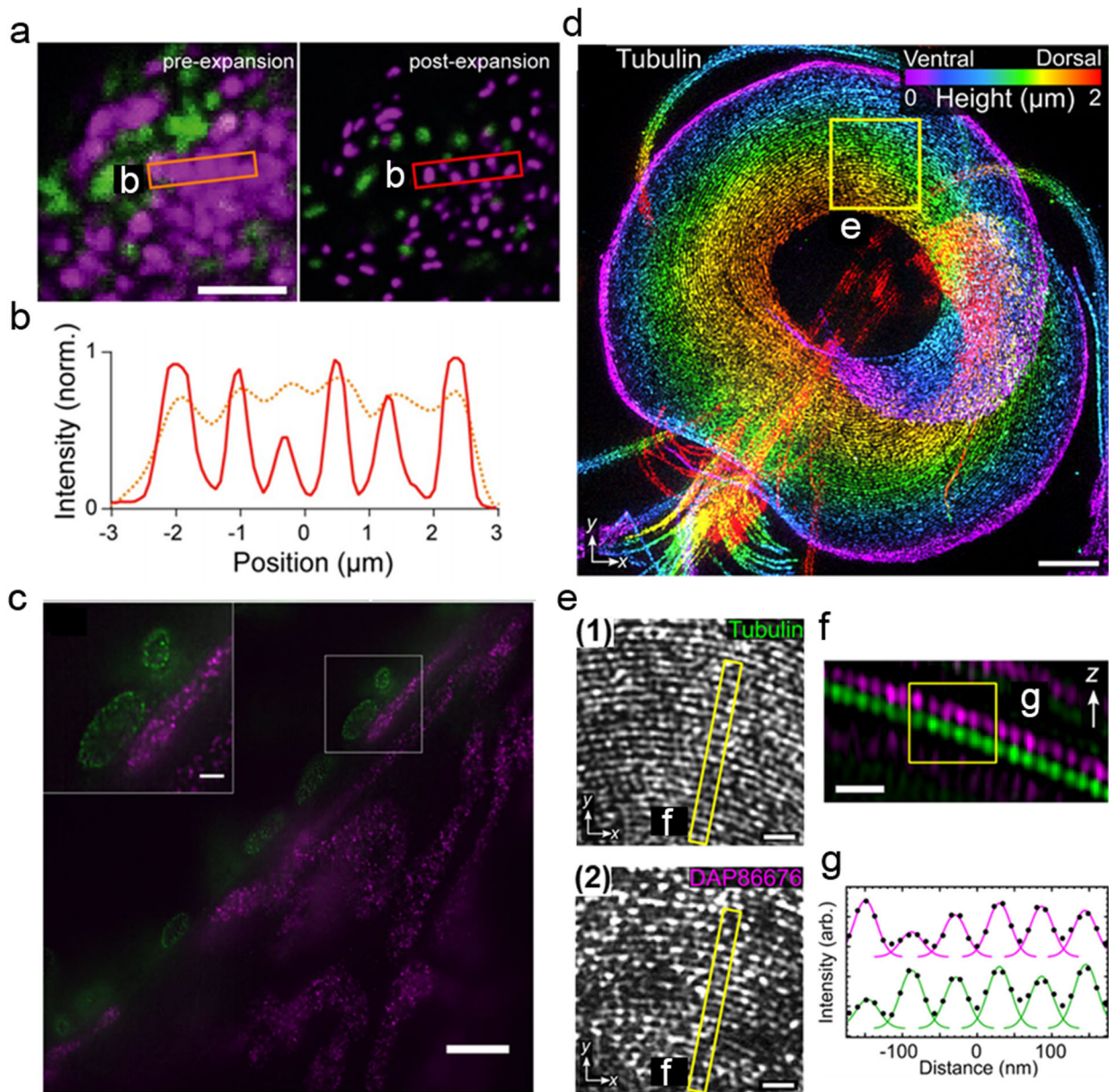


**Figure 5 Applications of ExM in microbiology**

**(a, b) ExM imaging of a bacteria mixture.** (a) Pre-expansion (left) and post-expansion (right) images of mCherry-tagged *Lactobacillus plantarum* (magenta) and GFP-tagged *Acetobacter tropicalis* (green). Scale bars in pre-expansion units: 5  $\mu\text{m}$ . Expansion factor:  $\sim 1.1\times$  for *Lactobacillus plantarum*;  $\sim 3.1\times$  for *Acetobacter tropicalis*. (b) Red solid and orange dotted lines correspond to the cross-sectional normalized fluorescence intensity profiles in the red and orange boxes in (a), respectively. Panels (a, b) adapted from ref. <sup>37</sup> **(c) ExM imaging of *Chlamydia*-infected cells.** Confocal image of expanded infected HeLa229 cells with immunolabeled mitochondrial marker protein Prx3 (magenta), and *Chlamydia* labeled with a membrane probe (green). Inset shows the zoomed-in view of the region in the upper right white box. Scale bars in pre-expansion units: 10  $\mu\text{m}$ , inset, 2  $\mu\text{m}$ . Expansion factor:  $\sim 10\times$ . Adapted from ref. <sup>22</sup> **(d-g) ExM imaging of the cytoskeleton structures of *Giardia*.** (d) Maximum intensity projection of structured illumination microscopy images of expanded *Giardia* with cytoskeletons immunolabeled with an antibody against acetylated tubulin. Positions of Z sections are color-coded according to the color scale bar. (e) Zoomed-in view of the yellow box in (d) showing immunolabeled (1) acetylated tubulin and (2) protein DAP86676. (f) Cross sectional projection of the region highlighted by yellow boxes in (e). (g) Intensity profiles (dots) and Gaussian fits (lines) of the boxed region in (f). arb.: arbitrary units. Scale bars in pre-expansion units: (d) 1  $\mu\text{m}$ ; (e, f) 200 nm. Expansion factor:  $\sim 3.5\times$ . Panels (e-g) adapted from ref. <sup>134</sup>.

In neurobiology, ExM has been applied to visualize synapses and synaptic proteins such as pre- and post-synaptic scaffolding proteins<sup>1,7,9,49,71,145–151</sup>, excitatory and inhibitory neurotransmitter receptors<sup>7,33,152,153</sup>, neurotransmitter transporters<sup>71,149,152,154</sup>, ion channels<sup>9,155</sup>, signaling molecules<sup>9</sup>, adhesion proteins<sup>153</sup>, synaptic vesicle proteins<sup>148,151,152</sup>, and others<sup>33,49,60,145,150,152–155</sup>, to delineate the morphology of cells such as neurons<sup>1,4,7,54,156,157</sup>, microglia<sup>150,158</sup>, astrocytes<sup>159</sup>, nanoscale brain structures such as dendritic spines<sup>4,7</sup>, mossy fiber boutons<sup>1</sup>, dense neuropils<sup>60</sup>, and organelles<sup>160</sup>, blood-brain barriers<sup>161</sup>, and others<sup>162–164</sup>, as well as pathological protein aggregates such as  $\beta$ -amyloids<sup>9</sup> and  $\alpha$ -synuclein inclusions<sup>165</sup>, and to analyze cell-cell interactions and connectivity such as those between neurons<sup>4,7,49,166–169</sup>, epithelial cells and neurons<sup>170,171</sup>, microglia and the vasculature<sup>158</sup>, and others<sup>172</sup>, in diverse sample types such as cultured neurons<sup>7,153,164</sup>, mouse brains<sup>1,4,7,9,49,146–152,155,156,158–160,166</sup>, spinal cords<sup>39,171</sup>, and retinas<sup>47,154,157</sup>, rat brains<sup>163</sup>, *Drosophila* brains<sup>39,60,162,167,168,170</sup> and ventral nerve cords<sup>145</sup>, zebrafish<sup>33,172</sup>, *Caenorhabditis elegans*<sup>54</sup>, brain sections of non-human primates<sup>4</sup>, in both normal and disease model organisms, and human clinical specimens<sup>161,165</sup>.

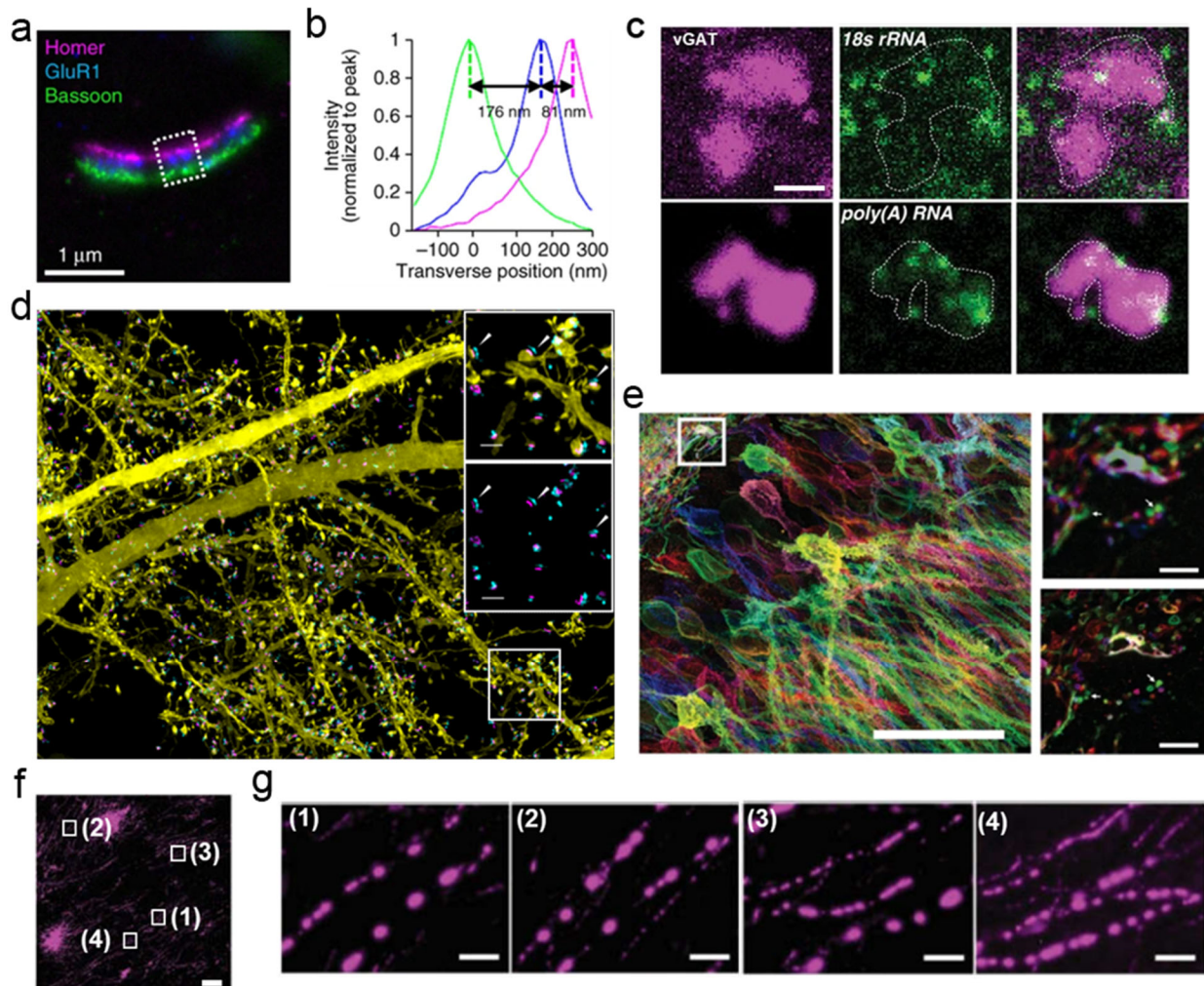


**Figure 6 Applications of ExM in neurobiology**

**(a, b) iExM imaging of synapses in cultured neurons.** (a) Epifluorescence image of a synapse in iExM-processed cultured mouse hippocampal neurons immunostained against Homer1 (magenta), glutamate receptor 1 (GluR1, blue), and Bassoon (green). The boxed region is analyzed in (b). (b) Transverse profile of the boxed region in (a) after normalizing to the peak (Homer1 in magenta, GluR1 in blue, Bassoon in green). Expansion factor:  $\sim 13\times$ . Panels (a, b) adapted from ref. <sup>7</sup> (c) **ExM imaging of messenger and ribosomal RNAs in presynaptic compartments in mouse brain tissues.** The inhibitory presynapse was labeled with antibodies against vGAT (left column, magenta); the 18s rRNA and poly(A) RNA were labeled with fluorescent in situ hybridization (FISH) probes (middle column, green). Right column shows the merge of the images in the left and middle columns. Outlines indicate vGAT-positive presynaptic compartments. Scale bar in pre-expansion units:  $1.5\ \mu\text{m}$ . Expansion factor:  $\sim 3.4\times$ . Adapted from ref. <sup>71</sup> (d) **Lattice light sheet microscopy imaging of synaptic markers and nanoscale neuronal structures in ExM-processed large 3D mouse brain tissue volumes.**  $xy$  Maximum intensity projection (MIP) of the 3D volume from the primary somatosensory cortex of Thy1-YFP mouse with immunostained Bassoon (cyan) and Homer1 (magenta). Insets

zoom in on the bottom right boxed region. Top inset shows Bassoon/Homer1 pairs (three pairs are marked with white arrows) together with YFP-marked neuronal structures. Bottom inset shows only the Bassoon/Homer1 pairs. Expansion factor:  $\sim 3.4\times$ . Adapted from ref. <sup>39</sup> **(e)**

**proExM imaging of Brainbow-labeled mouse brain tissues.** Left, *xy* MIP of a confocal microscopy volume of proExM-expanded mouse hippocampus expressing virally delivered Brainbow epitopes that were immunostained with antibodies. Pre- and post-expansion images of the boxed region in the image on the left are showing in the top right and bottom right images, respectively. Arrows highlight same brain structures before and after expansion. Scale bars in pre-expansion units: left, 50  $\mu\text{m}$ ; right, 5  $\mu\text{m}$ . Expansion factor:  $\sim 4\times$ . Adapted from ref. <sup>4</sup> **(f, g)**

**ExR imaging of periodic nanoclusters of A $\beta$ 42 peptide in brain tissues of Alzheimer's mouse models.** *xy* MIP image of an ExR-processed region in the fornix of a 5xFAD mouse with immunolabeled A $\beta$ 42 peptide. **(g)** Zoomed-in views of the boxed regions in **(f)**, showing periodic A $\beta$ 42 nanoclusters. Scale bars in pre-expansion units: **(f)**, 10  $\mu\text{m}$ ; **(g)**, 1  $\mu\text{m}$ . Expansion factor:  $\sim 20\times$ . Adapted from ref. <sup>9</sup>

# Chapter 2 Cleavable Fixative for Improved Ultrastructure Preservation in ExM

## 2.1 Introduction

Proteins are foundational for almost all biological processes. Optical fluorescence microscopy, which has been used most to investigate the molecular basis of life processes, has led to many biological insights due to the molecular contrast it provides. However, proteins are very small, averaging less than ten nanometers<sup>173</sup>, and are densely packed within cells, with an average protein-protein distance around only three nanometers<sup>174</sup>. The size and density make investigating the structure-function relationship and understanding the molecular mechanism of human diseases very challenging using a conventional diffraction limited microscope. Thus, super-resolution fluorescent microscopy that breaks the diffraction limit has gained popularity in recent decades. Many neurological diseases involve changes in the expression of proteins with key functions in neural excitability and neural communication. Mapping the subtle molecular changes of the synapses such as in neurotransmitters, receptors, and ion channels across the whole brain circuit would facilitate investigating of brain disorders. However, mapping requires a new multiplexing and multiscale imaging tool for three-dimensional (3-D) nanomapping of individual proteins throughout the whole tissue.

ExM, as introduced in Chapter 1, is a new kind of superresolution fluorescent microscopy that involves a series of chemical processes, typically: anchoring, gelation, softening, and expansion<sup>1</sup>. In brief, a swellable polymer is synthesized through a preserved specimen of tissue, anchoring key molecules to the polymer. Then, the specimen is chemically softened, and water is added to cause the polymer-specimen hybrid to swell by 100x or more in volume. However, before all these processes, there is a key step — fixation — for ultrastructure preservation in ExM (ultrastructure preservation is defined as maintaining the details of the cellular structure at molecular level in a state that closely resembles their native state). The fixatives that widely used in biological labs are paraformaldehyde (PFA) and/or glutaraldehyde (GA). Both fixatives work by forming crosslinks between proteins to lock the proteins in place<sup>175</sup>. If the fixation is not strong enough, the ultrastructure of the cells could not be well preserved. However, if the fixation is too strong, the epitope masking effect will be severe, posing a challenge to the labeling efficiency. In ExM, the preserved sample requires a softening step before expansion to

enable the isotropic expansion and the use of strong fixation will prevent expansion, thus a harsh softening condition to free the expansion process is required, for example, using broad-spectrum proteolytic digestion such as proteinase K to cut protein sequence nonspecifically or denaturing the proteins in detergent buffer with high heat treatment as in earlier versions of ExM<sup>4,7</sup>. Both methods will cause the loss of protein information. Therefore, fixation is of crucial importance for ultrastructure preservation and isotropic expansion in ExM.

Current ExM protocol variants use non-cleavable fixatives, such as PFA and/or GA which make the decrowding of protein complexes difficult. Due to the crosslinking between proteins, there is a high chance that the entire protein complex will be pulled to one side of the polymer mesh after expansion, rendering the visualization of individual proteins impossible. Therefore, using ExM to map molecular changes with nanoscale resolution, for example at synapse where many protein complexes are located, new chemistries for fixation are needed. Here, we developed a new form of ExM and improved the fixation protocol beyond that of earlier versions of ExM by inventing novel chemicals. We have screened commercially available cleavable crosslinkers with different functional groups that target the amines on proteins, such as aldehyde group, epoxide group and N-Hydroxysuccinimide (NHS) ester. We have also designed and synthesized chemicals that are small, fast-diffusing, and specifically reactive towards targeted functional groups on proteins. The results show that our new form of ExM allows for (1) biomolecules of interest to be locked in place with better spatial precision; (2) epitopes to be better preserved with milder softening condition; and (3) more homogeneous expansion, so that individual proteins being pulled apart isotropically is possible. Thus, the very three-dimensional biomolecular information that we want to read out in order to understand the organization of proteins can be preserved to the maximum extent possible.

## **2.2 Results**

### **2.2.1 Strong fixative is needed for ultrastructure preservation in ExM**

Microtubules have commonly been used to validate the resolution of the superresolution microscopy due to their defined shape. They are polymers formed by alpha and beta tubulin, so we use microtubules as the model protein complex to test our fixatives. The criteria of a good fixative to achieve ultrastructure preservation are that (1) it needs to be small, so they could diffuse into the cell/tissue fast enough; (2) the reaction rate between fixative and proteins needs

to be fast enough to stabilize the proteins and kill the autolysis process; and (3) it is able to preserve as many proteins as possible. Any protein information lost during the fixation step will be lost forever, and therefore it is crucial to preserve proteins to the maximum during fixation. The commonly used fixatives for microtubule fixation are methanol, PFA and/or GA in fluorescence microscopy. Therefore, we first tested microtubule fixation by those methods in ExM. We found that both methanol and PFA are too weak for ultrastructure preservation. Those two fixatives cannot preserve the morphology of microtubules (**Figure 7 a-f**), possibly because tubulins are badly fixed and/or after the downstream processes, the unfixed tubulins were washed out during the washing steps or the antibody incubation step.

Next, we tested GA which is routinely used in electron microscopy sample preparation and has demonstrated its superior ability in ultrastructure preservation<sup>176</sup>. We found that the fixation is strong, and the shape of the microtubules was well preserved before expansion; however, many cracks appear both in gel and in the microtubule structure after expansion (**Figure 7 c, g**), possibly because the crosslinks formed between proteins prevent the expansion of the polymer. We also tested the PFA/GA fixation which is used in our previous versions of ExM<sup>177,178</sup>. We found the ultrastructure is well preserved before expansion; however, after expansion we found cracks and discontinuity in the structure (**Figure 7 d, h**), possibly because the presence of the GA prevents the expansion. Note the antibodies are delivered post-expansion, therefore high heat treatment has been used for the softening process instead of protease K treatment, as epitopes will no longer be recognizable for immunostaining after the protease K treatment, and no fluorescence signal will be observed.

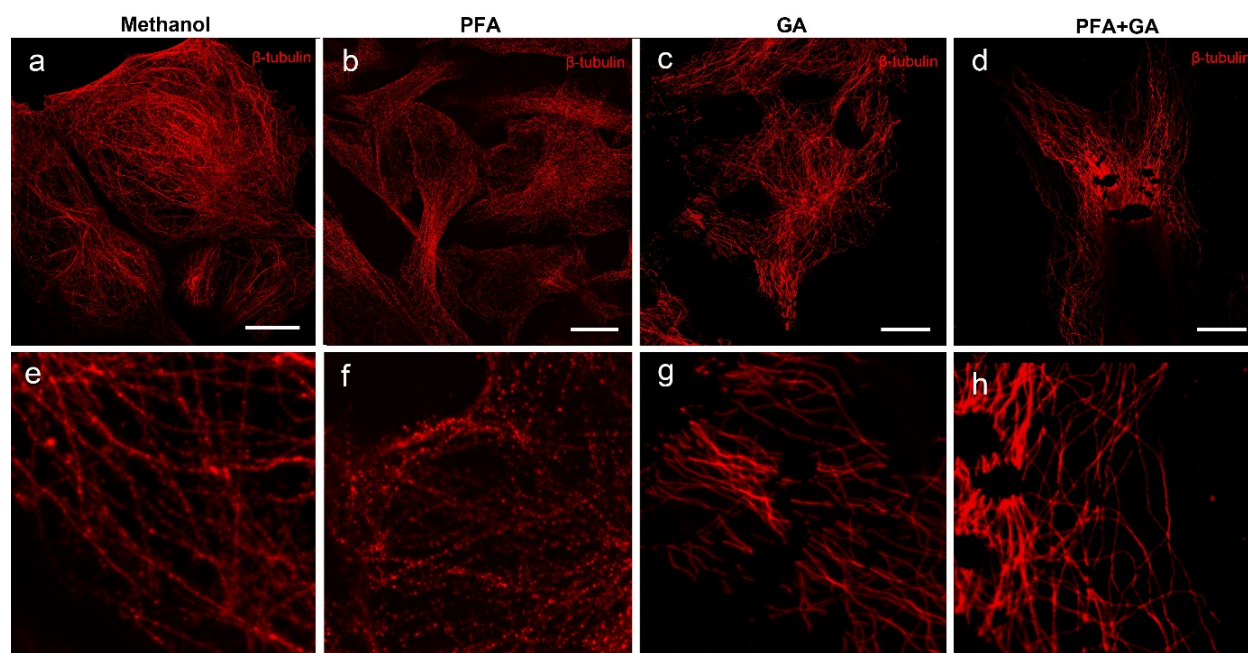


**Figure 7 Strong fixative preserves ultrastructure but will prevent isotropic expansion**

HeLa cells were fixed by (a) methanol for 7 min at  $-20^{\circ}\text{C}$  (b) 4% PFA for 10 min at room temperature (RT) (c) 0.5% GA for 10 min at RT and, (d) 3% PFA/0.1% GA for 10 min at RT, then processed by ExM and immunostained against beta-tubulin before expansion. (e-h). Zoomed in view of the microtubules in a-d, respectively. Scale bar in post-expansion units: 50  $\mu\text{m}$ .

We then asked whether the specimen preserved by PFA/GA could be expanded isotropically under mild softening conditions, so that the ultrastructure and the protein sequence could be preserved to the maximum and the isotropic expansion is ensured. We tested various mild softening conditions by substituting a non-specific proteolytic enzyme with enzymes that only cut proteins at specific sites (a complete list of enzymes that we have tested and their corresponding results are shown in **Supplementary Table 1**). However, we found that all these mild softening conditions are not able to ensure the isotropic expansion and the protein preservation at the same time. For example, discontinuous microtubules are observed with ArgC, LysC, GluC and LysN treatment, suggesting protein loss during digestion, even though they are milder compared to Proteinase K (**Figure 8**). In some cases, there are also cracks shown within the structure, for example, the sample treated with GluC (**Figure 8c**), suggesting the crosslinkage caused by fixatives still exist therefore cannot ensure the isotropic expansion. Thus, a new



fixative that allows for ultrastructure, protein sequence preservation and isotropic expansion is needed.

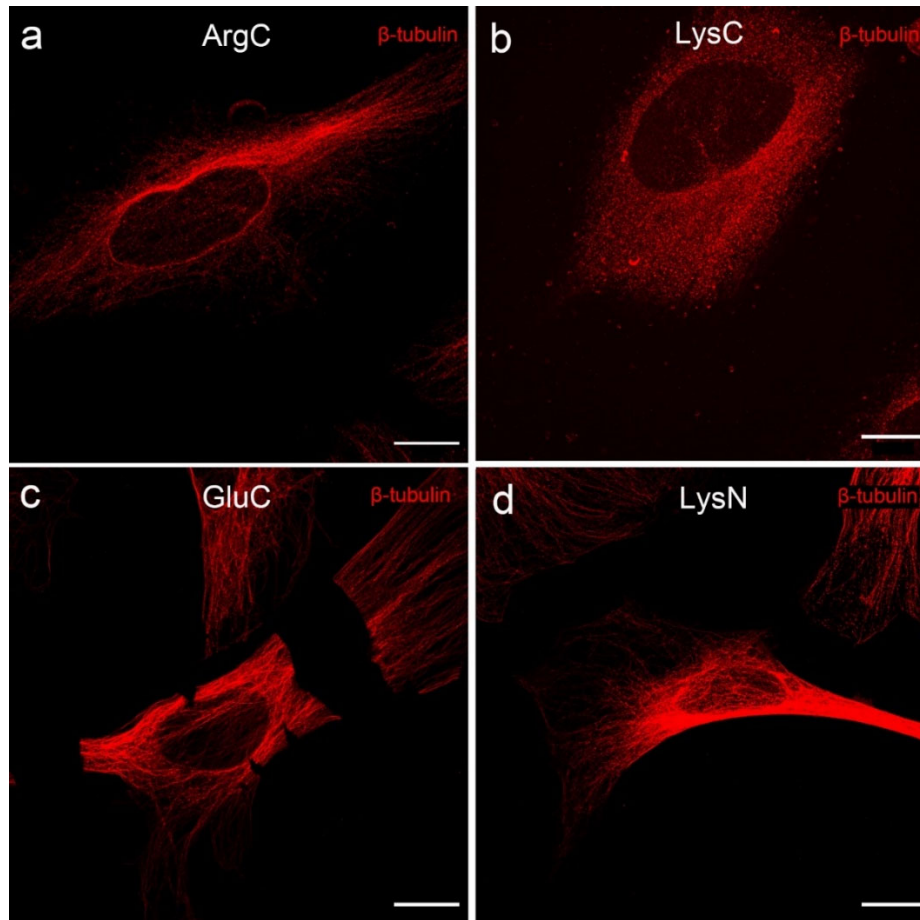


**Figure 8 Mild softening methods using specific proteolytic enzymes cannot ensure the structure preservation and isotropic expansion when the strong fixative is applied**

**(a-d)** HeLa cells were fixed using standard PFA/GA, which preserves the ultrastructure of microtubules. The cells were then subjected to the standard ExM protocol, with modifications only in the softening method. Specifically, cells were softened using specific proteolytic enzymes **(a)** ArgC, **(b)** LysC, **(c)** GluC, and **(d)** LysN. Post-softening, cells were indirectly immunostained with Alexa Fluor 546 against beta-tubulin, followed by expansion. Scale bar in post-expansion units: 50  $\mu\text{m}$ .

### 2.2.2 Designing and screening of new fixatives

We have shown that a strong fixative is needed for ultrastructure preservation, but it will prevent downstream expansion due to the crosslinks formed between proteins. Thus, we sought to design a series of new fixatives with the following principles: first, the fixatives are small so they can rapidly diffuse inside the sample; second, the fixatives have reactive groups that target the functional groups on proteins on both ends; third, the fixatives bear a cleavable bond, so we could cleave the bond after the polymerization, in which proteins are anchored to the gel network, and release the linkage before the expansion. The reactive groups we chose are aldehyde group and epoxide group that have commonly been used in protein crosslinking. The cleavable bonds we chose are the ones with known cleavage mechanism: the diol bond that can be cleaved by oxidation, the disulfide bond that can be cleaved by reduction and the sulfone bond which can be cleaved by sodium hydroxide. We have also screened commercially available crosslinkers with N-hydroxysuccinimide ester group that targets the most prevailing amine groups on proteins. The modular design of fixatives is illustrated in **Figure 9a**. We have also found one special chemical called 1,2,3,4-Diepoxybutane (DEB) that does not bear a cleavable bond, but the bond will be formed after crosslinking with two proteins between epoxide and amines on proteins via ring-opening reaction<sup>179</sup>. The illustration of this cleavable bond formation via crosslinking is shown in **Figure 9b**.

We next did initial screening of these fixatives by testing their crosslinking ability in vitro with purified  $\alpha$ -Lactalbumin protein and analyzing it with SDS-PAGE (see full list of chemicals we have tested in **Supplementary Table 2**). We found that only one of our designed fixatives, A1 (for chemical structure information, check **Supplementary Table 2**), has higher crosslinking ability than GA (at room temperature) and one commercially available BSOCOES performed well. We varied fixation time, temperature, pH and concentration for each crosslinker, but we found that those crosslinkers alone cannot preserve the ultrastructure very well. However, when supplemented with one percent PFA, the fixation of A1 and BSOCOES turns out to be very promising, as the structure of microtubules has been well preserved compared to the standard PFA/GA fixation (**Figure 9c, d**). We reason that this is because PFA is small so they can rapidly diffuse inside the cell to stabilize the proteins by stopping most of the autolysis process via add-on reaction, and then the new fixative comes in to crosslink the proteins, lock the biomolecules in place and preserving the ultrastructure. The widely used PFA/GA mixture in superresolution microscopy<sup>180</sup> for ultrastructure preservation of microtubules probably works in the same

fashion. Since PFA crosslinking is reversible in high salt solution<sup>181</sup>, we hypothesize that the fixatives would still be compatible with our new ExM protocol.

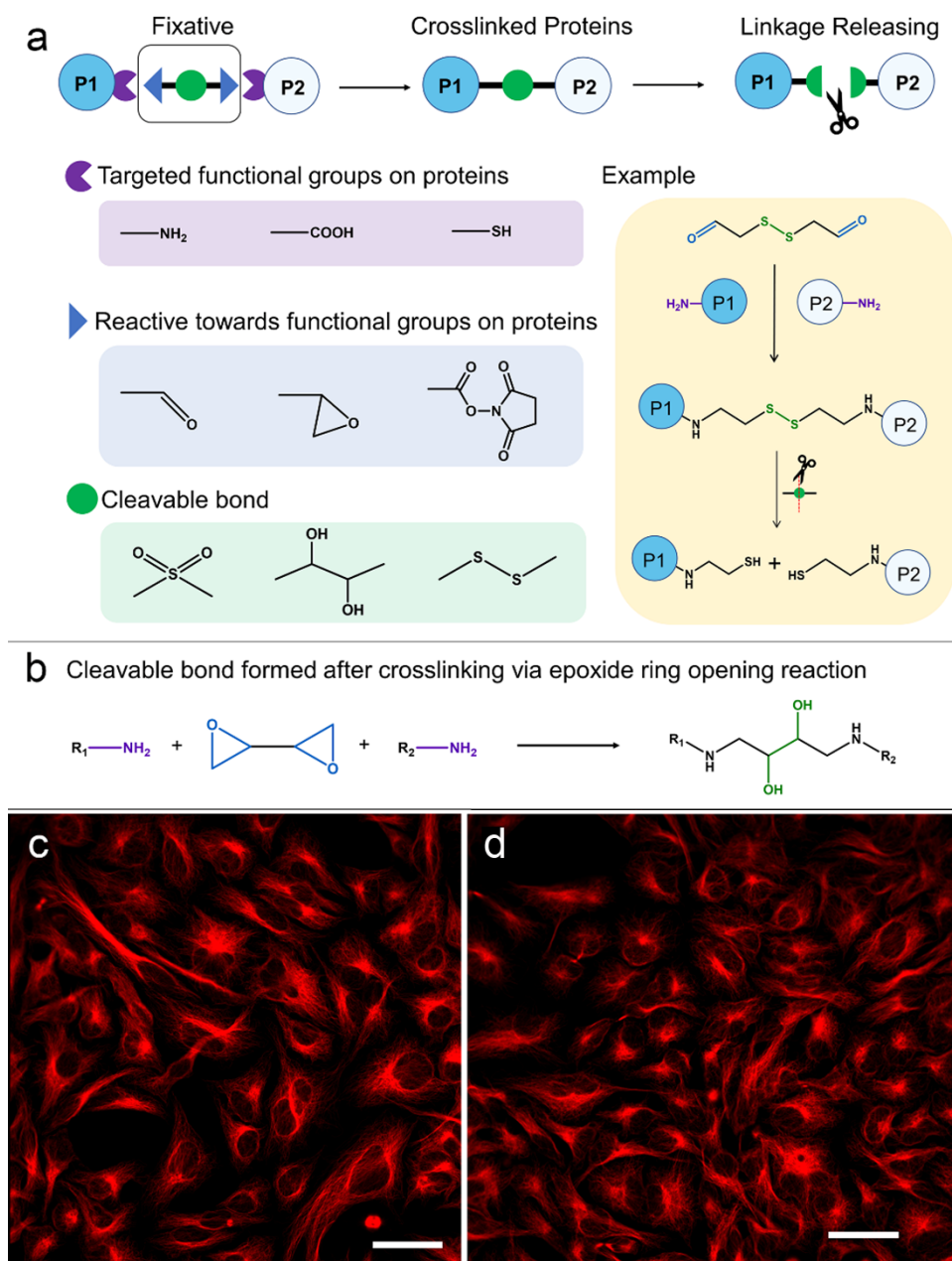


**Figure 9 Design and screening of new fixatives**

(a) Modular design of cleavable crosslinkers as new fixative in ExM. The designed crosslinker has reactive groups on both ends consisting of an aldehyde, epoxide, or NHS-ester group, which are known to be reactive toward proteins, with the most abundant groups being amine, sulfur or carboxyl groups. The crosslinker bears a cleavable sulfone, diol, or disulfide bond so that the

linkage between two proteins can be released. The example shows a candidate fixative, with aldehyde groups on both ends, that crosslinks proteins by targeting amines, thereby forming a disulfide bond that is cleavable with reduction to enable release for expansion in the downstream ExM process. **(b)** Another cleavable fixative type is DEB, which does not bear a cleavable bond prior to protein crosslinking but will form a cleavable diol post crosslinking with proteins. **(c-d) Testing of ultrastructure preservation using new fixative candidates on cultured HeLa cells without ExM processing.** HeLa cells were fixed by **(c)** A1/PFA, **(d)** BSOCOES/PFA and immunostained with Alexa Fluor 546 against beta-tubulin. Scale bar in pre-expansion units: 50  $\mu\text{m}$ .

### **2.2.3 Ultrastructure preservation of microtubules with new fixatives in new form of ExM**

**Figure 10a-c** illustrate the workflow of the standard ExM and the new form of ExM using cleavable fixative. A good fixative here involves two parts: a good protein fixation ability and a high cleavage efficiency to free the expansion process. In previous sections, we have two crosslinkers that can be the candidates of our new cleavable fixatives due to their protein preservation ability. Then we asked how those fixatives are compatible with this new form of ExM and how well they can preserve the ultrastructure of microtubules after cleavage and expansion. Therefore, we performed the same fixation, anchoring and polymerization under the same conditions as in the previous section. Then we did cleavage and applied antibodies after the cleavage, followed by expansion. The results of ultrastructure preservation of microtubules using aforementioned two cleavable fixatives in ExM post-cleavage and expansion are shown in **Figure 10 d-e**. In **Figure 10d**, cells were fixed using A1/PFA and treated with sodium hydroxide prior to expansion. While no cracks were detected within the structure, the preservation of ultrastructure, based on the continuity of the microtubules examined by eye, was better than methanol or PFA fixation but inferior to that observed with PFA/GA. In **Figure 10e**, cells were fixed with BSOCOES/PFA and cleaved with sodium hydroxide before expansion. Still, there are no cracks found within the structure or the hydrogel, however, the preservation of ultrastructure, based on the continuity of the microtubules examined by eye, was better than methanol or PFA fixation but inferior to that observed with PFA/GA. We think this is because the reactivity of the crosslinker is not fast enough and/or the molecular weight of the crosslinker is rather large compared to formaldehyde or glutaraldehyde, therefore the penetration speed is not fast enough to lock proteins in place and preserve their integrity and relative organization.

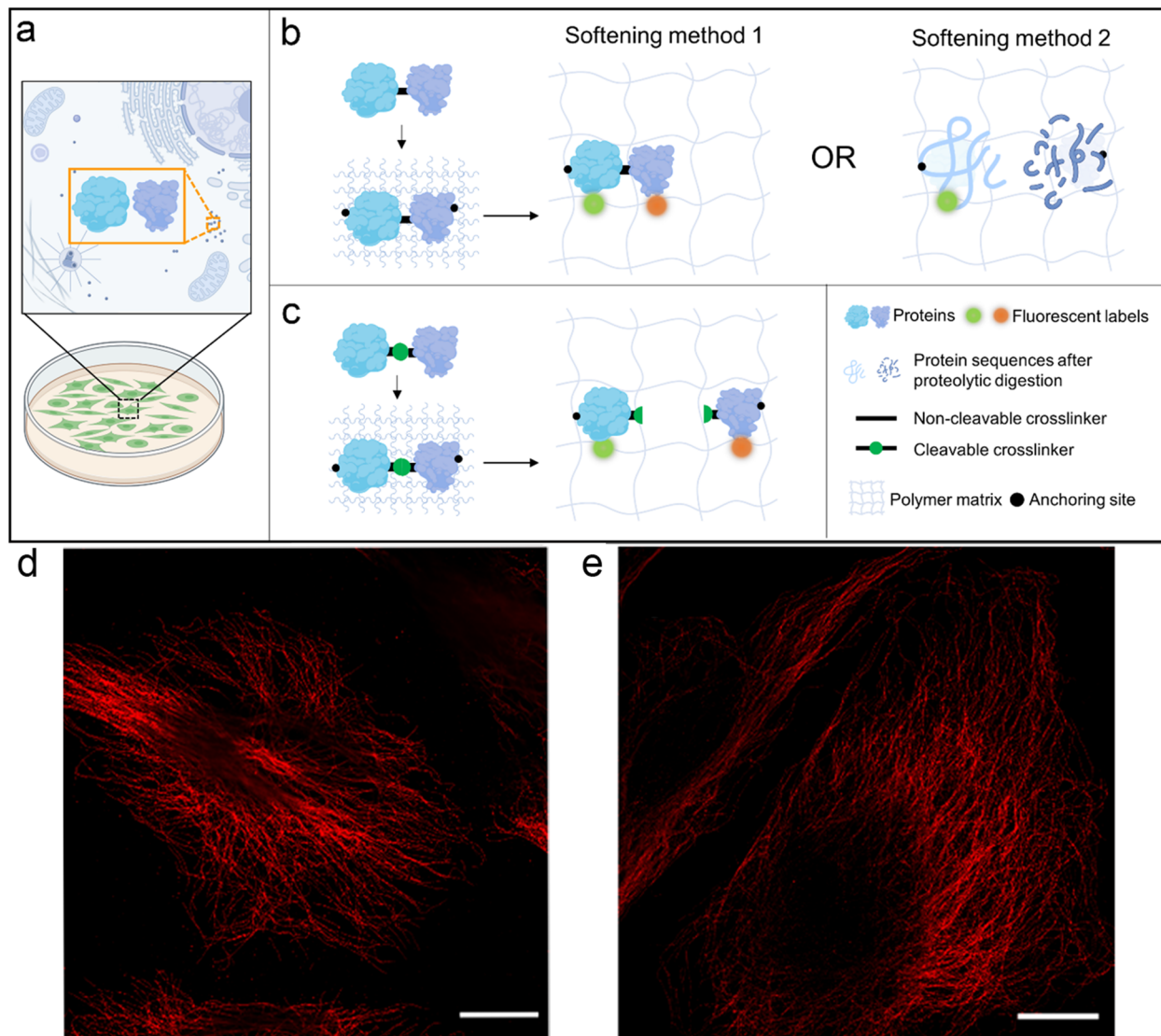


**Figure 10 Ultrastructure preservation of the designed fixative using the new form of ExM.**

(a) Shows live cells to be processed with ExM and the zoomed in view of two random cytoplasmic proteins that are close to each other. (b) Cells that have been fixed with non-cleavable fixative, processed by standard ExM and softened via 1) high heat in detergent solution or 2) non-specific protease K digestion. (c) Cells that have been fixed with cleavable fixative, processed by the new form of ExM and softened in cleavage solution at RT. (a-c) created using Biorender (<https://biorender.com/>). (d-g) Representative images of HeLa cells processed by new form of ExM using different cleavable fixatives and cleaved before immunostaining and expansion. All cells were indirectly immunostained with Alexa Fluor 546 against beta-tubulin. HeLa cells were (d) fixed by A1/PFA and cleaved with sodium hydroxide (e) fixed by BSOCOES/PFA and cleaved with sodium hydroxide before immunostaining and gel expansion. Scale bar in post-expansion units: 50  $\mu\text{m}$ .

Consequently, we began to ask if there was a chemical that could quickly stabilize proteins and anchor them to the gel simultaneously. This approach would prevent crosslinking between proteins by fixing biomolecules directly to the gel network, instead of forming the protein-protein network with crosslinkers first, and then being anchored to the gel network. Acrolein is an  $\alpha,\beta$ -unsaturated aldehyde that contains an aldehyde group for reacting with biomolecules and a double bond for polymerization. It can quickly stabilize the specimen by rapidly penetrating the tissue and reacting with cellular components, effectively halting cellular activities and biochemical reactions that may otherwise degrade the sample's ultrastructure. Due to its small size and ability to attach handles to proteins, facilitating their incorporation into the gel network, we used acrolein as our reagent to "fix" the biomolecules to the gel. The concept of this idea is illustrated in **Figure 11a**. First, the specimen is stabilized by acrolein, and after the aldehyde group on acrolein reacts with the amines on proteins, the proteins are armed with a vinyl group that allows the biomolecules to be incorporated into the gel network. The gelation step is the same as the standard proExM conducted at physiological temperature. The formed gel then undergoes detergent treatment for denaturation, followed by immunostaining and expansion in water (details are provided in the methods section). We found that at room temperature, acrolein alone is not sufficient and needs to be supplemented with 1% PFA to achieve good ultrastructure preservation, as shown in **Figure 11b-c**. The details of the optimized version, which uses acrolein as a direct fixation reagent for the gel network and conducts all key steps—fixation, anchoring, gelation—at cold temperatures as part of a novel fixation strategy, will be provided in the next chapter.

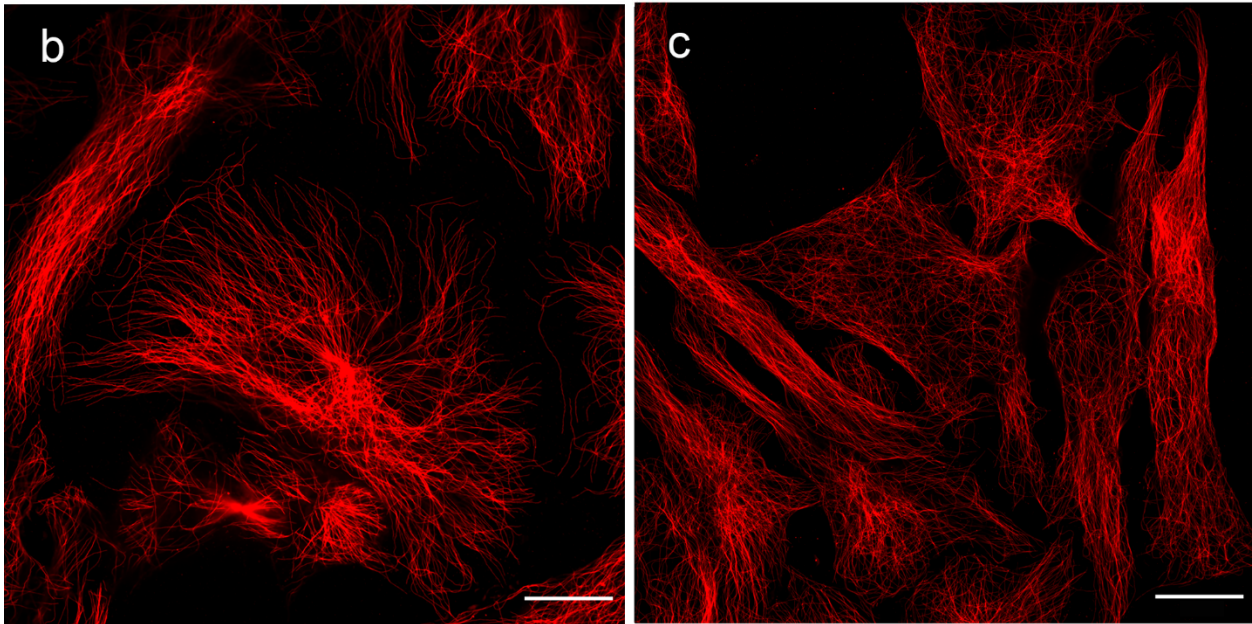
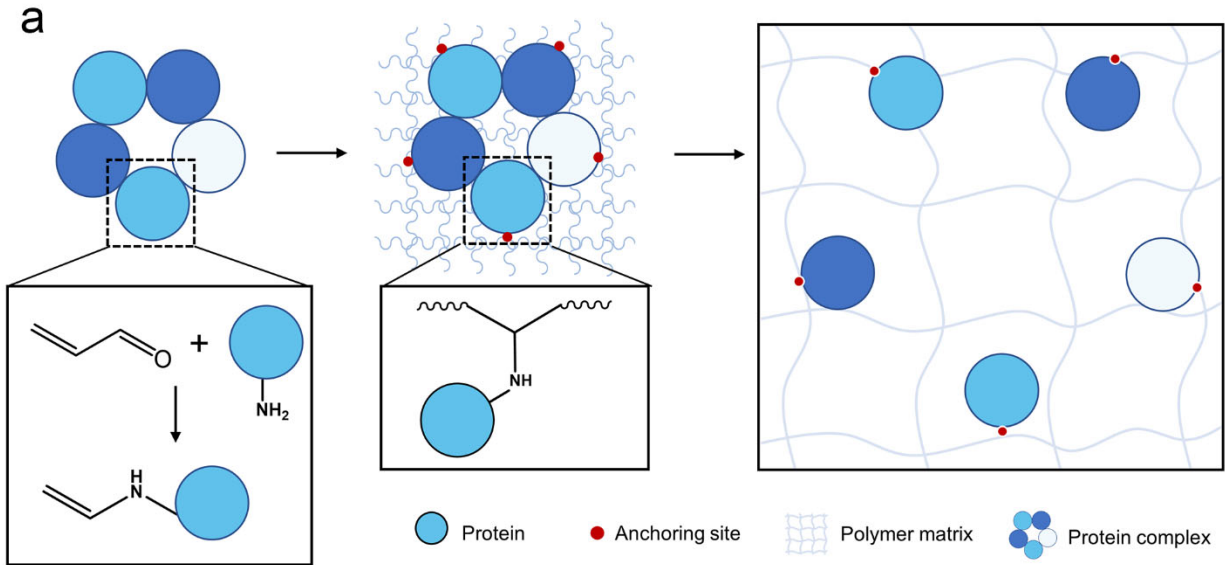


**Figure 11 The direct fixation of the proteins to the gel network by using acrolein**

(a) The concept of the direct fixation of biomolecules to the gel network using acrolein – the protein complex is stabilized by acrolein which is fast reactivity and rapid penetration. The reaction between the aldehyde group of acrolein and the amine on proteins and after proteins are armed with a vinyl group that allows them to be incorporated into the polymer network. After the polymerization, softening and expansion, the proteins can be expanded isotopically. However, when experiments were conducted at room temperature, acrolein needed to be supplemented with PFA to achieve better ultrastructure preservation. (b-c) The results of HeLa cells processed by standard ExM except proteins were fixed to the gel with acrolein/PFA. The microtubules were post-immunostained with beta-tubulin. Scale bar in post-expansion units: 50  $\mu\text{m}$ .

## 2.3 Discussion

As ExM keeps evolving<sup>177,182</sup>, and the resolution of ExM gets higher, the ultrastructure preservation in ExM becomes even more important. Therefore, the fixation becomes a critical step in the next generation ExM. In this section, we developed a novel form of ExM using a cleavable crosslinker as the fixative. This new cleavable fixative can achieve good ultrastructure preservation and minimize protein crosslinking by breaking the crosslinks before expansion, thus allowing more homogeneous expansion. Moreover, antibodies are allowed to be delivered post-expansion, which brings two important advantages<sup>183,184</sup>: 1) avoiding intensity decreasing caused by fluorophore attacking during polymerization; and 2) reducing the linkage error<sup>185</sup>. The other option to reduce the linkage error is to use nanobodies. However, this approach still has many limitations. For example, the availability of nanobodies is very limited compared to IgG antibodies. Additionally, the development and production processes for nanobodies can be more complex and costly. Despite their smaller size and potentially higher specificity, which can be advantageous in reducing linkage error, the current limitations in accessibility and production make them less practical for widespread use in many experimental settings.

Although the use of cleavable fixatives in the new form of ExM can balance the two contrary and competing demands—strong chemical cross-linking to preserve the nanoscale organization of biomolecules and the need for clean, isotropic separation of biomolecules from each other in the expansion step—there is still room for improvement in the preservation of ultrastructure. For example, we found that acrolein can be used as the anchoring reagent to fix biomolecules to the gel network and minimize cross-linking between biomolecules. However, this process must be conducted at cold temperatures to prevent structural perturbation due to the absence of fixatives. The gelation step also needs to be performed at cold temperatures and rapidly for the same reason. The details of this method, which allows for conducting all key steps (fixation, anchoring, and gelation) before biomolecules are secured to the gel network, will be described in the next chapter.



## 2.4 Methods

### Cell culture

HeLa cells (ATCC) were cultured in Dulbecco's Modified Eagle Medium (DMEM; Corning, catalog no. 10013CV) with 10% heat-inactivated fetal bovine serum (FBS; Thermo Fisher, catalog no. A3840001) and 1% penicillin-streptomycin (Thermo Fisher, catalog no. 15140122) at 37 °C in a humidified 5% CO<sub>2</sub> incubator to reach 50~70% confluency.

### Reagents and standard ExM Monomer Solution Preparation

Sodium acrylate (SA; Pfaltz & Bauer, catalog no. S03880) was used as the primary monomer essential for gel expansion. Acrylamide (AAm; Sigma Aldrich, catalog no. A9099-25G) served as the co-monomer. N,N'-Methylenebisacrylamide (Bis; Sigma-Aldrich, catalog no. 146072) was employed as the crosslinker, prepared as a 2% (w/v) stock solution in deionized water and stored at 4°C. The initiation system comprised ammonium persulfate (APS) and N,N,N',N'-Tetramethylethylenediamine (TEMED), both prepared as 10% (w/v) stock solutions in deionized water and stored at -20°C. The monomer solution was prepared following the proExM protocol which comprised of 8.6% (w/v) SA, 2.5% (w/v) AAm, 0.15% (w/v) Bis, 2 M NaCl, 0.1% (w/v) TEMED, and 0.1% (w/v) APS, in phosphate buffered saline (PBS).

### Effect of commonly used fixative on microtubule preservation

We tested four different fixation conditions to investigate their effect on microtubule preservation by post-expansion staining: (1) methanol for 7 minutes at -20°C, (2) 4% PFA in PBS for 10 minutes at room temperature (RT), (3) 0.5% GA in PBS for 10 minutes at RT, and (4) 3% PFA/0.1% GA in PBS for 10 minutes at RT. HeLa cells cultured in a 24-well plate with 12-mm-diameter coverslips were first gently rinsed twice with prewarmed (37°C) Dulbecco's Phosphate-Buffered Saline (DPBS; Thermo Fisher, catalog no. 14190136) to remove any residual media. The corresponding fixative solution was then added, and cells were incubated for the times under conditions mentioned previously. Cells were subsequently washed three times with PBS, 5 minutes each at RT. After removing the PBS, cells were incubated in 0.1 mg/mL 6-((acryloyl)amino)hexanoic acid, succinimidyl ester (AcX, Thermo Fisher, catalog no. A20770) in PBS for at least 2 hours at RT without shaking. AcX was prepared as a 10 mg/mL stock solution in DMSO and stored at -20°C. After anchoring with AcX, the cells were washed three times with 1x PBS, 5 minutes each. The coverslips with cells were then transferred to a gelation

chamber (the detailed construction of the gelation chamber can be found in ref.<sup>186</sup>). The standard ExM monomer solution (with APS and TEMED added last) was then added to the cells and allowed to gel at 37°C for 1.5 hours in a humidified box.

### **Denaturation, post-expansion immunostaining, and expansion**

After the gelation process, the gel was subjected to a denaturation step for subsequent staining. The reagents being used for denaturation are Tris(hydroxymethyl)aminomethane (Tris; Thermo Fisher, catalog no. AM9855G), Sodium chloride (NaCl, Thermo Fisher, catalog no. AM9759), Sodium hydroxide (NaOH; Sigma, catalog no. S8263), Sodium n-dodecyl sulfate (SDS; ThermoFisher, catalog no. AM9820). 20mL denaturation buffer was prepared by mixing 12.38 mL of deionized water, 1 mL of 1M Tris (pH 8.0), 0.8 mL of 5M NaCl, 60 µL of 5M NaOH, and 5.76 mL of 20% SDS, with the pH adjusted to 9.0. The gel was incubated in a denaturation buffer for 1.5 hours at 95°C. Following denaturation, the gel was washed three times with 1x PBS for 30 minutes each to remove any residual denaturation buffer.

For immunofluorescence staining, all processes were conducted at room temperature (RT) unless otherwise specified. The protocol began with blocking to reduce nonspecific binding by incubating the gel in 400 µL of MAXblock Blocking Medium (Active Motif, catalog no. 15252) for 30 minutes to 1 hour. This was followed by a single wash with MAXwash™ Washing Medium (Active Motif, catalog no. 15254) for 10 minutes to prepare the gel for antibody incubation. For primary antibody staining, rabbit anti-tubulin (abcam, catalog no. ab6046) was diluted 1:100 in MAXbind™ Staining Medium (Active Motif, catalog no. 15253). Approximately 250 µL of the primary antibody solution was added to each well of a 24-well plate, and the gel was incubated for 5 hours at RT or overnight at 4°C. After primary antibody binding, the gel was washed three times with 1x PBS, each wash lasting 30 minutes, to remove unbound primary antibodies. For secondary antibody staining, goat anti-rabbit AF546 (Thermo Fisher, catalog no. A-11035) was diluted 1:100 in MAXbind™ Staining Medium. Similar to the primary antibody step, 250 µL of the secondary antibody solution was added to each well, followed by incubation for 5 hours at RT or overnight at 4°C. The gel underwent a final series of three 30-minute washes with 1x PBS to ensure the removal of excess secondary antibody. Finally, the gel was first expanded in deionized water for two 30-minute sessions, followed by an overnight incubation.

### **Testing mild softening method with non-specific enzymes**

HeLa cells cultured in a 24-well plate with 12-mm-diameter coverslips were first gently rinsed twice with prewarmed (37°C) DPBS to remove any residual media. All the following steps were performed at RT unless otherwise specified. The fixative solution composed of 3% PFA and 0.1% GA was then added, and cells were incubated for 10 min. Cells were subsequently quenched with 0.1% (w/v) sodium borohydride (Sigma Aldrich, catalog no. 213462-25G) in PBS for 7 min followed by incubation in 100mM glycine (Sigma Aldrich, catalog no. G7126-100G) in PBS for 10 min. Then cells were washed three times with PBS, 5 minutes each. After removing the PBS, cells were incubated in 0.1 mg/mL AcX in PBS for at least 2 hours without shaking. After anchoring with AcX, the cells were washed three times with 1x PBS, 5 minutes each. The coverslips with cells were then transferred to a gelation chamber. The standard ExM monomer solution (with APS and TEMED added last) was then added to the cells and allowed to gel at 37°C for 1.5 hours in a humidified box.

Next, the gel was incubated in enzyme digestion buffer (without the enzyme) for 30 minutes at RT (refer to **Supplementary Table 1** for each enzyme's corresponding condition). The digestion buffer was then replaced with the same buffer containing the enzyme, and the gel was incubated for the corresponding time and temperature (also see **Supplementary Table 1**). After the digestion and gel was washed three times with PBS, the gel was then incubated in 400  $\mu$ L of MAXblock Blocking Medium for 30 minutes to 1 hour. This was followed by a single wash with MAXwash™ Washing Medium for 10 minutes to prepare the gel for antibody incubation. For primary antibody staining, rabbit anti-tubulin (abcam, catalog no. ab6046) was diluted 1:100 in MAXbind™ Staining Medium. Approximately 250  $\mu$ L of the primary antibody solution was added to each well of a 24-well plate, and the gel was incubated for 5 hours at RT or overnight at 4°C. After primary antibody binding, the gel was washed three times with 1x PBS, each wash lasting 30 minutes, to remove unbound primary antibodies. For secondary antibody staining, goat anti-rabbit AF546 (Thermo Fisher, catalog no. A-11035) was diluted 1:100 in MAXbind™ Staining Medium. Similar to the primary antibody step, 250  $\mu$ L of the secondary antibody solution was added to each well, followed by incubation for 5 hours at RT or overnight at 4°C. The gel underwent a final series of three 30-minute washes with 1x PBS to ensure the removal of excess secondary antibody. Finally, the gel was expanded in deionized water for two 30-minute sessions, followed by an overnight incubation.

## **Testing of ultrastructure preservation of microtubules using cleavable fixative candidates on HeLa cells**

Two fixative candidates were tested: one commercially available and one custom-made. The commercial fixative was bis[2-(succinimidyl)oxycarbonyloxy]ethyl]sulfone (BSOCOES, Thermo Fisher, catalog no. 21600) in powder form, and the custom-made fixative was sulfonyl-bis-acetaldehyde (A1) in liquid form. BSOCOES was prepared as a 100 mM stock solution in anhydrous dimethyl sulfoxide (DMSO, Thermo Fisher, catalog no. D12345) and stored at -20°C.

For samples without ExM processing: HeLa cells cultured in a 24-well plate with 12-mm-diameter coverslips were first gently rinsed twice with prewarmed (37°C) DPBS to remove any residual media. A 40 mM fixative supplemented with 1% PFA in PBS was then added, and cells were incubated for 8 hours at RT. Cells were subsequently washed three times with PBS, 5 minutes each at RT. After removing the PBS, the samples underwent immunofluorescence staining. All processes were conducted at RT unless otherwise specified. First, the samples were incubated in 250 µL of MAXblock™ Blocking Medium for 15 minutes. This was followed by a single wash with MAXwash™ Washing Medium for 10 minutes to prepare the samples for antibody incubation. For primary antibody staining, rabbit anti-tubulin (abcam, catalog no. ab6046) was diluted 1:100 in MAXbind™ Staining Medium. Approximately 250 µL of the primary antibody solution was added to each well of a 24-well plate, and the samples were incubated for 2 hours at RT or overnight at 4°C. After primary antibody binding, the samples were washed three times with 1x PBS, each wash lasting 10 minutes, to remove unbound primary antibodies. For secondary antibody staining, goat anti-rabbit AF546 (Thermo Fisher, catalog no. A-11035) was diluted 1:100 in MAXbind™ Staining Medium. Similar to the primary antibody step, 250 µL of the secondary antibody solution was added to each well, followed by incubation for 2 hours at RT or overnight at 4°C. The samples then underwent a final series of three 10-minute washes with 1x PBS to ensure the removal of excess secondary antibody before being prepared for imaging.

For samples with ExM processing (including cleavage of the cleavable fixative): HeLa cells cultured in a 24-well plate with 12-mm-diameter coverslips were first gently rinsed twice with prewarmed (37°C) DPBS to remove any residual media. A 40 mM fixative supplemented with 1% PFA in PBS was then added, and cells were incubated for 8 hours at RT. Cells were subsequently washed three times with PBS, 5 minutes each at RT. After removing the PBS, cells were incubated in 0.1 mg/mL AcX in PBS for at least 2 hours at RT without shaking. After

anchoring with AcX, the cells were washed three times with 1x PBS, 5 minutes each. The coverslips with cells were then transferred to a gelation chamber. The standard ExM monomer solution (with APS and TEMED added last) was then added to the cells and allowed to gel at 37°C for 1.5 hours in a humidified box. After the gelation process, the gel was subjected to a cleavage and softening step. The gel was incubated in a buffer consisting of 8M urea (Thermo Fisher, catalog no. 29700) and 50 mM dithiothreitol (DTT, Thermo Fisher, catalog no. D1532) in water and adjusted the pH to 9.3. The gel was shaken at RT for 20 minutes, followed by incubation at 95°C for 30 minutes. Afterward, the gel was washed three times with 1x PBS for 30 minutes each. The gel was then incubated in 400 µL of MAXblock Blocking Medium for 30 minutes to 1 hour. This was followed by a single wash with MAXwash™ Washing Medium for 10 minutes to prepare the gel for antibody incubation. For primary antibody staining, rabbit anti-tubulin (abcam, catalog no. ab6046) was diluted 1:100 in MAXbind™ Staining Medium. Approximately 250 µL of the primary antibody solution was added to each well of a 24-well plate, and the gel was incubated for 5 hours at RT or overnight at 4°C. After primary antibody binding, the gel was washed three times with 1x PBS, each wash lasting 30 minutes, to remove unbound primary antibodies. For secondary antibody staining, goat anti-rabbit AF546 (Thermo Fisher, catalog no. A-11035) was diluted 1:100 in MAXbind™ Staining Medium. Similar to the primary antibody step, 250 µL of the secondary antibody solution was added to each well, followed by incubation for 5 hours at RT or overnight at 4°C. The gel underwent a final series of three 30-minute washes with 1x PBS to ensure the removal of excess secondary antibody. Finally, the gel was expanded in deionized water for two 30-minute sessions, followed by an overnight incubation.

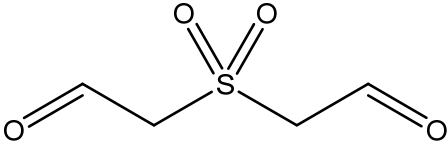
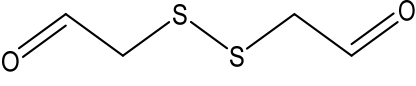
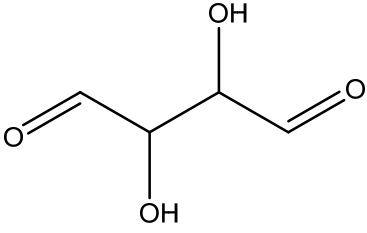
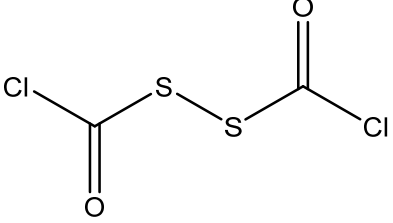
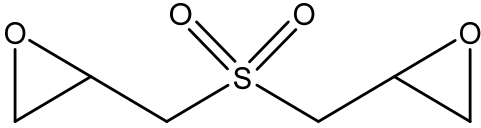
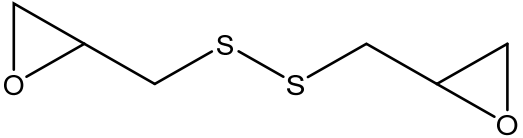
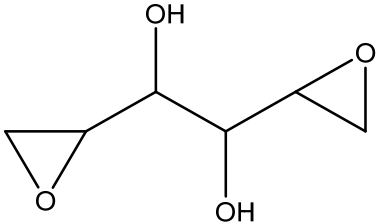
## 2.5 Supplementary Information

**Supplementary Table 1** A list of enzymes has been tested as a mild softening method when the specimen is preserved by standard GA/PFA fixation.

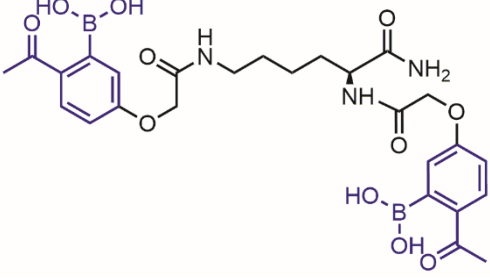
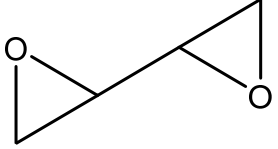
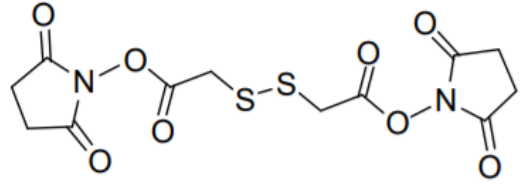
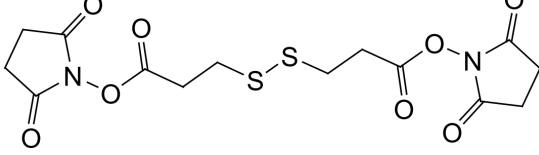
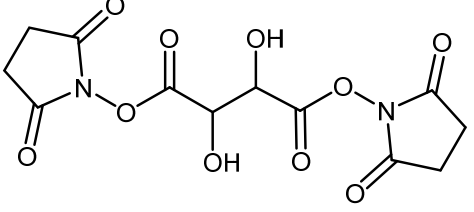
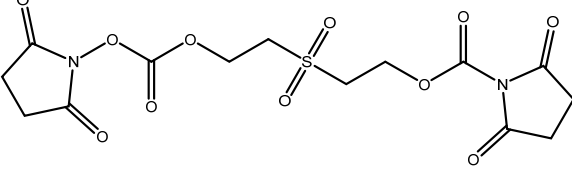
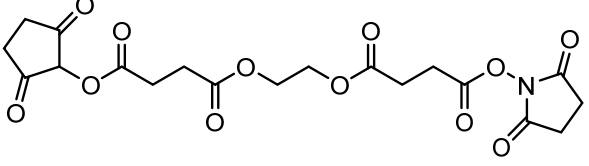
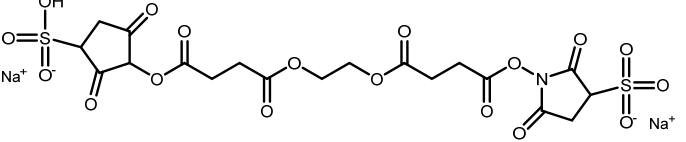
Enzymes	Vendor	Cat#	Condition	Results
Trypsin	New England Biolabs	<a href="#">P8101S</a>	50 ug/mL 50 mM Tris, pH 8 5 mM CaCl <sub>2</sub> 37°C, overnight	Microtubules appear discontinuous
LysC	New England Biolabs	<a href="#">P8109S</a>	20 ug/mL 50 mM Tris, pH 8.5 1 mM EDTA 37°C, overnight	Microtubules appear discontinuous
GluC	New England Biolabs	<a href="#">P8100S</a>	50 ug/mL 100 mM ammonium bicarbonate buffer, pH 8 0.5 mM Glu-Glu 25°C, overnight	Observed cracks within the gel & microtubules appear discontinuous
AspN	New England Biolabs	<a href="#">P8104S</a>	50 ug/mL 50 mM ammonium bicarbonate buffer, pH 8 2.5mM ZnSO <sub>4</sub> 37°C, overnight	Microtubules appear discontinuous
rLys-C	Promega	<a href="#">V1671</a>	15 ug/mL 50 mM Tris, pH 8.5 1 mM EDTA 37°C, overnight	Microtubules appear discontinuous
Arg-C	Promega	<a href="#">V1881</a>	10 ug/mL 50 mM Tris, pH 7.8 2 mM EDTA, 10 mM DTT 37°C, overnight	Microtubules appear discontinuous
LysN	Promega	VA1180	50 mM Tris, pH 8 2 mM ZnSO <sub>4</sub> 37°C, overnight	Observed cracks within the gel & microtubules appear discontinuous
LysC/Trypsin	Promega	<a href="#">V5071</a>	20 ug/mL 50 mM Tris, pH 8	Microtubules appear discontinuous

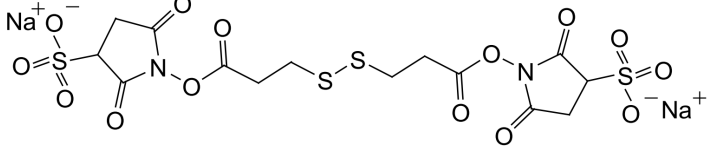
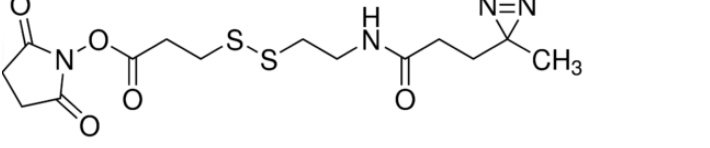
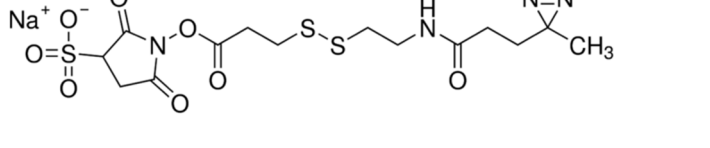
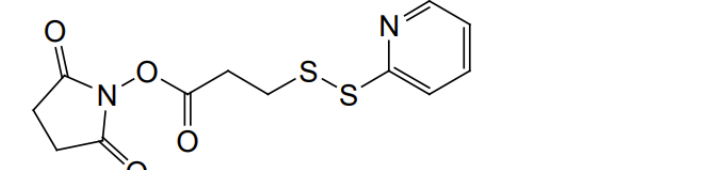
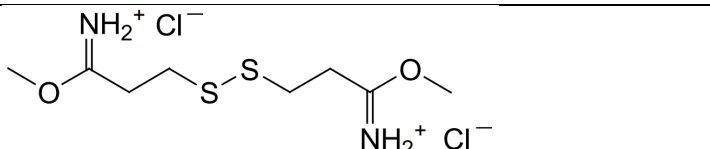
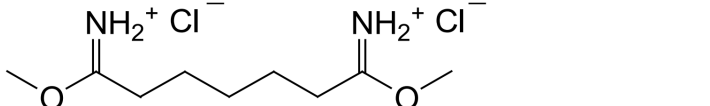
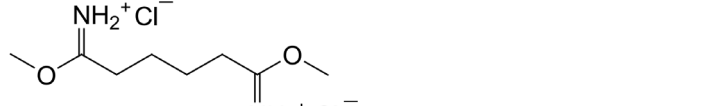
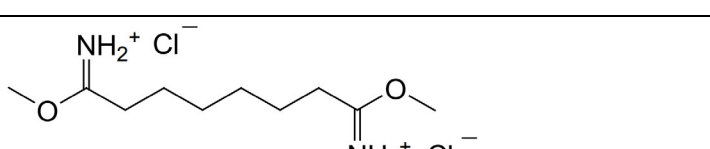
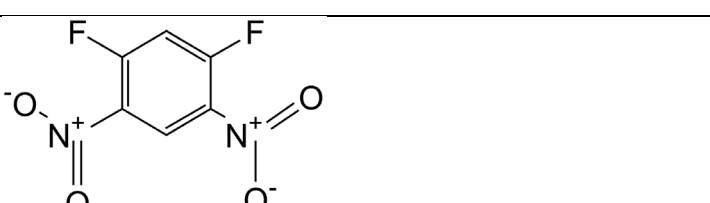
			37°C, overnight	
Chymotrypsin	Promega	<a href="#">V1061</a>	25 ug/mL 100 mM Tris, pH 8 25°C, overnight	Microtubules appear discontinuous

**Supplementary Table 1 A list of chemicals have been tested as cleavable fixatives.**

Name	Chemical Structure
A1 Sulfonyl-bis-acetaldehyde	
A2 2,2'-disulfanediyldiacetaldehyde	
CL1 Tartaric aldehyde	
CL2 Bis(chlorocarbonyl)(carbamoyl)disulfane	
B1 2,2'-(sulfonylbis(methylene))bis(oxirane)	
B2 1,2-bis(oxiran-2-ylmethyl)disulfane	
B3 1,2-di(oxiran-2-yl)ethane-1,2-diol	



Boronate traceless crosslinker	
1,2,3,4-diepoxybutane (DEB)	
Bis(2,5-dioxopyrrolidin-1-yl) disulfanediyl diacetate (Bis-DSP) 2,2'-	
Dithiobis(succinimidyl propionate) (DSP)	
Disuccinimidyl tartrate (DST)	
Bis[2-(succinimidooxycarbonyloxy)ethyl]sulfone (BSOCOES)	
Ethylene glycol bis(succinimidyl succinate) (EGS)	
Ethylene glycol bis(sulfosuccinimidyl succinate) (Sulfo-EGS)	

3,3'-dithiobis(sulfosuccinimidyl propionate) (Sulfo-DSP)	
<b>SDAD</b> (NHS-SS-Diazirine) (succinimidyl 2-((4,4'-azipentanamido)ethyl)-1,3'-dithiopropionate)	
<b>Sulfo-SDAD</b> (Sulfo-NHS-SS-Diazirine) (sulfosuccinimidyl 2-[(4,4'-azipentanamido)ethyl]-1,3'-dithiopropionate]	
Succinimidyl 3-(2-pyridyldithio)propionate ( <b>SPDP</b> )	
Dimethyl dithiobispropionimide•2HCl ( <b>DTBP</b> )	
Dimethyl pimelimidate•2 HCl ( <b>DMP</b> )	
Dimethyl adipimidate (DMA)	
Dimethyl suberimidate•2 HCl ( <b>DMS</b> )	
1,5-difluoro-2,4-dinitrobenzene ( <b>DFDNB</b> )	

# Chapter 3 Subzero Temperatures Expansion Microscopy for Ultrastructural Preservation

## 3.1 Introduction

All ExM protocols have the same basic four steps. First, biomolecules are covalently equipped with handle-like, or anchor-like, molecules bearing a polymerizable group. Second, a hydrogel is then formed (mesh size  $\sim 1\text{-}2\text{ nm}$ <sup>187</sup>) that weaves its way throughout the specimen, inside and outside cells, and intercalating between biomolecules, binding to the anchors (and thus anchoring the biomolecules to the polymer mesh). Third, the specimen is softened (typically through enzymatic, heat, and/or detergent treatment). Finally, the sample is exposed to water which causes swelling (typically by 4x-10x, although the process can be iterated<sup>177,188</sup>). Before any of these steps begin, there is an inevitable preprocessing step: a sample is chemically fixed, an important step because it preserves the integrity and/or relative organization of biomolecules. In other branches of nanoimaging, such as electron microscopy, to improve integrity and relative organization, chemical fixation sometimes is conducted at cold temperatures in a process called freeze substitution, in which a frozen sample at liquid nitrogen temperature<sup>189</sup> is exposed to a liquid organic solvent containing a covalent crosslinking fixative (e.g., glutaraldehyde)<sup>190,191</sup>. The idea is that the fixative binds biomolecules while in a cold, but liquid state, so that covalent fixation occurs while the sample is in a high-integrity state, preserving relative organization.

Recently, a pioneering attempt was made to create such a process compatible with ExM, in a protocol called CryoExM<sup>192</sup>. In CryoExM, the sample was first rapidly frozen (to  $-180\text{°C}$ ) and then immersed in cold acetone, followed by raising the temperature of the acetone, gradually substituting ethanol and finally PBS for the acetone as the temperature rose above  $0\text{°C}$ , ending with the cells in cold liquid PBS. At that time, the chemical fixative formaldehyde was introduced at  $37\text{°C}$  in PBS, which began to covalently crosslink biomolecules with each other; acrylamide was also included, to enable some fraction of the formaldehydes attached to target molecules to bind a polymer-incorporable anchor to the target biomolecule (MAP-style fixation<sup>193</sup>). Given that the sample, in this protocol, was raised above freezing, and even to physiological temperatures, before chemical fixation began, we wondered if the introduction of the chemical fixative, and the anchoring molecule, could be done while the sample was still at cold temperatures, in the ExM context. After all, in electron microscopy-style methods, the

glutaraldehyde would be introduced while the sample was still quite cold. Copying this strategy literally, however, could compromise the later expansion process, as glutaraldehyde fixation causes such strong crosslinking of biomolecules to each other, that it has seldom been used in expansion protocols, and only at concentrations much lower (0.1% vs. 2%) than in electron microscopy, to avoid hampering expansion<sup>194</sup>. One could stain with antibodies pre-expansion, of course, and then use extremely strong proteolysis to disrupt the glutaraldehyde-crosslinked proteins (in principle), but such staining would miss any proteins that are in very crowded environments - several studies have shown that expanding proteins away from each other, before staining, can vastly improve labeling of proteins, in many cases converting virtually invisible proteins into visible ones<sup>174,178,184,188,193,195,196</sup>.

Therefore, there are seemingly contrary and competing demands in ExM: the need for strong chemical cross-linking to preserve the integrity and relative organization of biomolecules and the later need for clean, isotropic separation of biomolecules during the expansion step. In this chapter, we introduce a new protocol where we employ a chemical agent, acrolein, in methanol for simultaneous specimen fixation and biomolecule anchoring to the hydrogel matrix at subzero temperatures, aiming to minimize biomolecule crosslinking, which can impede subsequent expansion. The hydrogel-specimen hybrid was formed at subzero temperatures to minimize cellular organization perturbation. Because the molecules are fixed to the hydrogel network, and not directly to each other – key to balancing nanoscale information preservation, and clean molecule separability - we call this technology subzero temperature expansion microscopy, or subExM. The key innovations of this protocol include equipping molecules with polymerizable handles at -20°C using acrolein, permeating the specimen with the gelation solution (in water, with freezing point depression) also at -20°C, and then triggering polymerization at -20°C using UV light. The results of our protocol showed an increased fluorescent signal intensity in microtubules stained post-expansion, compared to CryoExM<sup>192</sup>. SubExM-processed microtubules showed more continuous fluorescent signals. SubExM also demonstrates better preservation of mitochondria and the Golgi apparatus, with improved signal intensity. In summary, our method introduces a new approach to fixation that preserves ultrastructure by directly fixing biomolecules to the gel network instead of forming crosslinks between biomolecules. This approach allows the entire ExM process, from anchoring to polymer formation, to be conducted at cold temperatures, minimizing perturbations to the structure.

## 3.2 Results

### 3.2.1 Development of subzero expansion microscopy

ExM involves a series of chemical processes, including anchoring, polymerization, softening (e.g., denaturation), and expansion. However, as mentioned before, a key challenge is balancing the need for strong cross-linking to maintain biomolecular integrity with the requirement for clean, isotropic separation during expansion. To address this seeming contradiction, one approach involves using a strong chemical crosslinker, such as glutaraldehyde, to crosslink proteins. Subsequently, specific proteases can be applied under mild conditions to digest the proteins, as described in Chapter 2. Another method is to employ a cleavable fixative that is sufficiently strong to maintain the integrity and relative organization of biomolecules during fixation, and then separate biomolecules by breaking the crosslinkages before expansion, which is also detailed in Chapter 2. However, the preservation of ultrastructure is suboptimal with these two methods. Thus, we explored the possibility of crosslinking biomolecules to each other, via the polymer itself as an intermediate, and to do this rapidly, while still in a high-integrity condition, such as at low temperatures. Then, the biomolecules would be locked in a configuration close to the native state, due to the rapid, high-integrity anchoring to the polymer, all while cold, while simultaneously being readied for separation in the swelling step, because the biomolecules are not directly covalently bound to each other – they are only anchored to the very substrate that will swell them apart from their neighbors. We thus set out to develop a strategy for applying “handles” to proteins, and to form a densely permeating hydrogel network that anchors the proteins via the handles, all at -20°C.

To carry out biomolecule anchoring at subzero temperatures, we sought to find an anchoring reagent that carries both a chemical group that covalently reacts with biomolecules at cold temperatures, and a handle for polymerization into the ExM gel matrix. In addition to these chemical reactivity requirements, ideally the reagent needs to be small enough for fast diffusion throughout cells at cold temperatures. Acrolein is the smallest reagent carrying an aldehyde group and a polymerizable carbon-carbon double bond. The aldehyde group can covalently react with biomolecules at cold temperatures as proven by the wide usage of aldehydes in electron microscopy-style cold temperature freeze substitution protocols. The carbon-carbon double bond placed right next to the aldehyde group is also a handle that is commonly used in radical-based polymerization reactions. We chose to dissolve acrolein in methanol, an organic solvent with low

freezing point (-97.6 °C) and commonly used to fix biological samples at -20 °C, to ensure that the biological sample would be rapidly fixed and anchored in an organic solvent state (where presumably the biomolecules such as proteins are fixed, not by crosslinking, but by precipitation), all at subzero temperatures.

In addition to the cold temperature anchoring strategy with acrolein-methanol solution, we sought to also develop a gel recipe and protocol that forms ExM gel at -20 °C. Such as cold temperature polymerization strategy requires the gel mixture to remain liquid at -20 °C such that the gel monomers can diffuse evenly throughout the biological specimen. In addition, it also requires that the polymerization reaction be initiated in a temperature-independent way. To fulfil the first requirement, we designed a gel recipe with 48% (w/v) *N,N*-dimethylacrylamide (DMAA, a neutral ExM monomer that is a liquid with freezing point of -40 °C), 10% (w/v) of sodium acrylate (an ionic ExM monomer to help with expansion), 0.1% (w/v) *N,N'*-methylene-bis-acrylamide (a ExM gel crosslinker), in water. The high percentage of DMAA led to freeze point suppression such that this gel recipe remains liquid at -20 °C. We used 0.5% (w/v) of a photo-initiator I-2959 to trigger polymer formation with UV light. Photo-polymerization is heat-independent thus might enable rapid ExM gel formation at -20 °C.

Combining the acrolein-methanol fixation/anchoring and the photopolymerization approaches outlined above, we developed a subExM workflow for cultured cells (Fig. 12). The entire anchoring and gelation processes (Fig. 1a) are conducted at -20 °C, starting with treating live cultured cells for 8 minutes with 0.5% acrolein dissolved in methanol to fix the sample and install gel anchors on biomolecules (Fig. 12a, top). Immediately after acrolein-methanol treatment, the cells are incubated for 5 minutes with the aforementioned photo-polymerization monomer solution followed by UV light exposure for 3 minutes to form the ExM gel. Overall, the anchoring and gelation steps took less than 20 minutes to complete. Then, the hydrogel-cell hybrid enters a denaturation, expansion, and staining sequence similar to that in existing post-expansion staining ExM protocols such as MAP, ExR, U-ExM, CryoExM<sup>184,188,192,193</sup>.

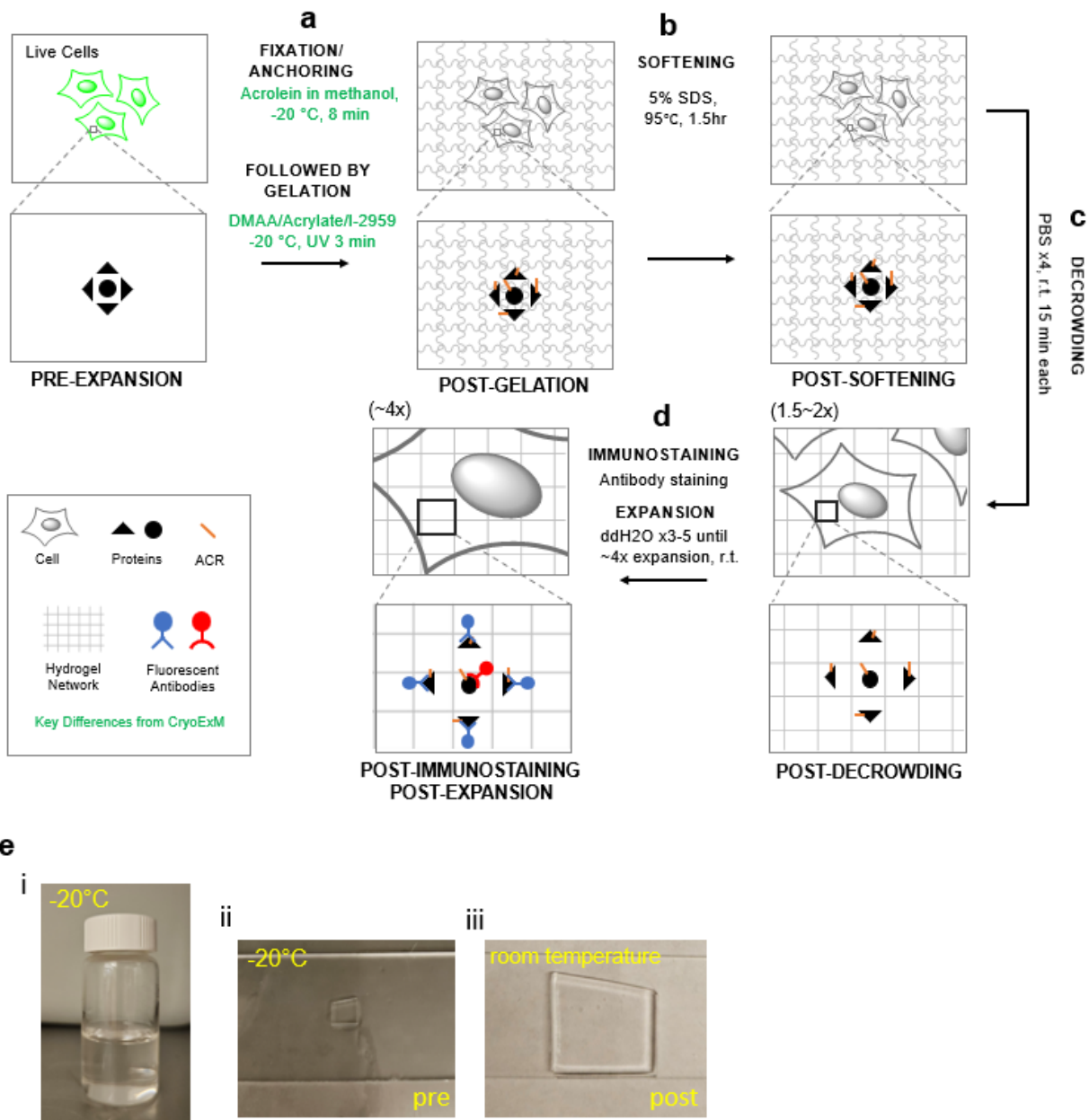


**Figure 12 Subzero Temperature Expansion Microscopy (subExM) workflow for Cultured Cells**

(a–d) Workflow for expanding cultured cells with subExM. Key differences from published CryoExM are shown in green text. ACR, acrolein; DMAA, N,N-dimethylacrylamide; SDS, sodium dodecyl sulfate; I-2959, 2-Hydroxy-4'-(2-hydroxyethoxy)-2-methylpropiophenone; PBS, phosphate buffered saline. For steps after decrowding (c), linear expansion factor of the hydrogel-specimen composite is shown in parentheses above the schematic of the step. (a) cultured U2OS cells are stabilized with cold acrolein in methanol at  $-20^{\circ}\text{C}$ , fixing and anchoring biomolecules; cells are then infiltrate with monomer solution at  $-20^{\circ}\text{C}$ ; after infiltration, cells are

then placed in a gelation chamber and exposed to UV light at  $-20^{\circ}\text{C}$  to form the hydrogel. **(b)** With biomolecules now securely embedded in the gel network, samples are incubated in a softening buffer to denature proteins at above-zero temperatures; softened samples are then washed in PBS buffer and will be partially expanded. **(d)** Next, samples are immunostained and expanded fully by immersion in water. **(g)** Photographs illustrating (i) the monomer solution, which remains in a liquid state at  $-20^{\circ}\text{C}$ ; (ii) the post-cryogelation hydrogel formed at  $-20^{\circ}\text{C}$  (the specimen-polymer hybrid remains as a hydrogel after two days at  $-20^{\circ}\text{C}$ ); (iii) the expanded hydrogel after immersion in water at RT.

### **3.2.2 subExM enables better ultrastructure preservation of microtubules**

To validate the preservation of microtubule ultrastructure by subExM compared to CryoExM protocols, we conducted a continuity analysis — quantitative measurements of microtubule intensity, gap ratio in total length, and average gap size. This analysis involved tracing selected microtubules within the sample, measuring tubulin intensity along these tracings, and establishing a background intensity level. A "gap" in the microtubule was identified if its intensity fell below a threshold defined as the mean plus the standard deviation of the background signal. The results, presented in Figure 13, offer a detailed quantitative comparison between the two techniques. Figure 13a displays an expanded  $\beta$ -tubulin-immunostained U2OS cell sample prepared by plunge freezing and freeze substitution with acetone, with the subsequent ExM process carried out at  $37^{\circ}\text{C}$  as described in the CryoExM protocol. The inset in Figure 13a highlights a magnified view of the area indicated by the yellow box. In contrast, Figure 13b shows an expanded  $\beta$ -tubulin-immunostained U2OS cell sample prepared using the subExM protocol, with polymerization performed at  $-20^{\circ}\text{C}$ . The inset of Figure 13b magnifies the area marked by the yellow box. We quantified 48 microtubule segments from samples prepared via the CryoExM method and 57 microtubule segments from samples prepared via the subExM method. Microtubules subjected to subExM exhibited a 3.6-fold higher mean intensity ( $318.4 \pm 108.2$ ) and an absence of gaps, in contrast to those processed by CryoExM, which showed a lower mean intensity ( $89.5 \pm 42.6$ ) and measurable gaps. These findings emphasize the enhanced microtubule continuity achieved with subExM.



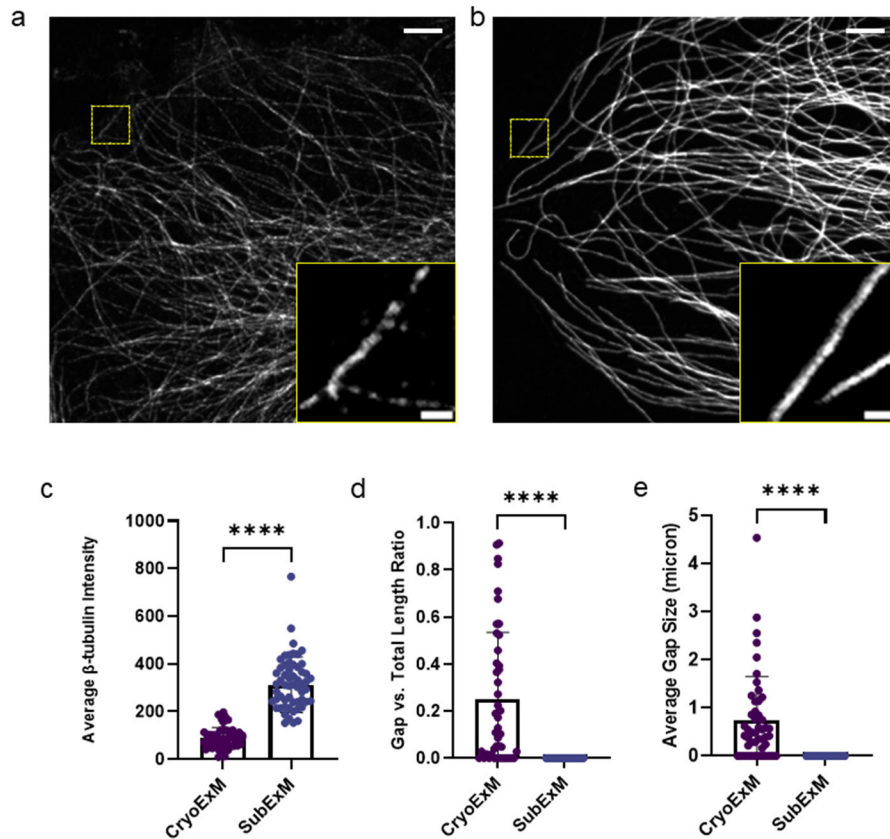


**Figure 13 subExM enables better ultrastructure preservation of microtubules**

(a) A confocal image (maximum intensity projection from a representative experiment) of expanded  $\beta$ -tubulin-immunostained U2OS cells, cryofixed via plunge freezing, followed by freeze substitution with acetone. The subsequent ExM process was performed as described in CryoExM, with polymerization carried out at 37°C. The inset shows a magnified view of the region highlighted in yellow in a. (b) A confocal image (maximum intensity projection from a representative experiment) of expanded  $\beta$ -tubulin-immunostained U2OS cells, fixed and polymerized at -20°C. The inset shows a magnified view of the region highlighted in yellow in b. (c-e) **Quantification of intensity** (c), gap ratio in total length (d), and average gap size ( $\mu\text{m}$ , post-expansion) (e) in expanded U2OS cells post-CryoExM or subExM processing. CryoExM:  $89.5 \pm 42.6$  (mean  $\pm$  standard deviation,  $n=48$  microtubule segments, 4 wells of cell culture from two culture batch); subExM:  $318.4 \pm 108.2$  (mean  $\pm$  standard deviation,  $n=57$  microtubule segments, 5 wells of cell culture from two culture batch); CryoExM:  $0.25 \pm 0.28$  (mean  $\pm$  standard deviation,  $n=48$  microtubule segments from two culture batch); subExM:  $0 \pm 0$  (mean  $\pm$  standard deviation,  $n=57$  microtubule segments from two culture batch); CryoExM:  $0.75 \pm 0.89$  (mean  $\pm$  standard deviation,  $n=48$  microtubule segments from two culture batch); subExM:  $0 \pm 0$  (mean  $\pm$  standard deviation,  $n=57$  microtubule segments from two culture batch). Data from two independent experiments, \*\*\*\* $p < 0.0001$ . Scale bars in post-expansion units: 10  $\mu\text{m}$  (a, b), 2  $\mu\text{m}$  (inset of a, b). Two-tailed unpaired t-tests with Welch's correction used for statistics.

### **3.2.3 Enhanced protein retention of different cellular structures using subExM**

To further examine the performance of subExM when applied to other cellular organelles, such as mitochondria and Golgi apparatus, we conducted a comparative analysis focusing on protein preservation between subExM and the CryoExM protocols. Figures 14a and 14b illustrate the results for TOM20-immunostained HeLa cells, with the former prepared using the CryoExM protocol and the latter with subExM. The cells processed via subExM exhibited a higher TOM20 intensity, with a mean and standard deviation of  $1210.7 \pm 405.1$ , compared to  $278.5 \pm 174.5$  for CryoExM, the quantitative results is shown in Fig3c. Similarly, Figures 14d and 14e present GM130-immunostained HeLa cells prepared following the CryoExM and subExM protocols, respectively. The subExM-treated cells showed a significantly enhanced intensity, with a mean and standard deviation of  $2164.4 \pm 792.7$ , compared to  $119.2 \pm 118.8$  for CryoExM. The quantitative results is depicted in Figure 14f and the results show subExM method outperformed CryoExM in preserving the Golgi apparatus structure as well as the protein retention.

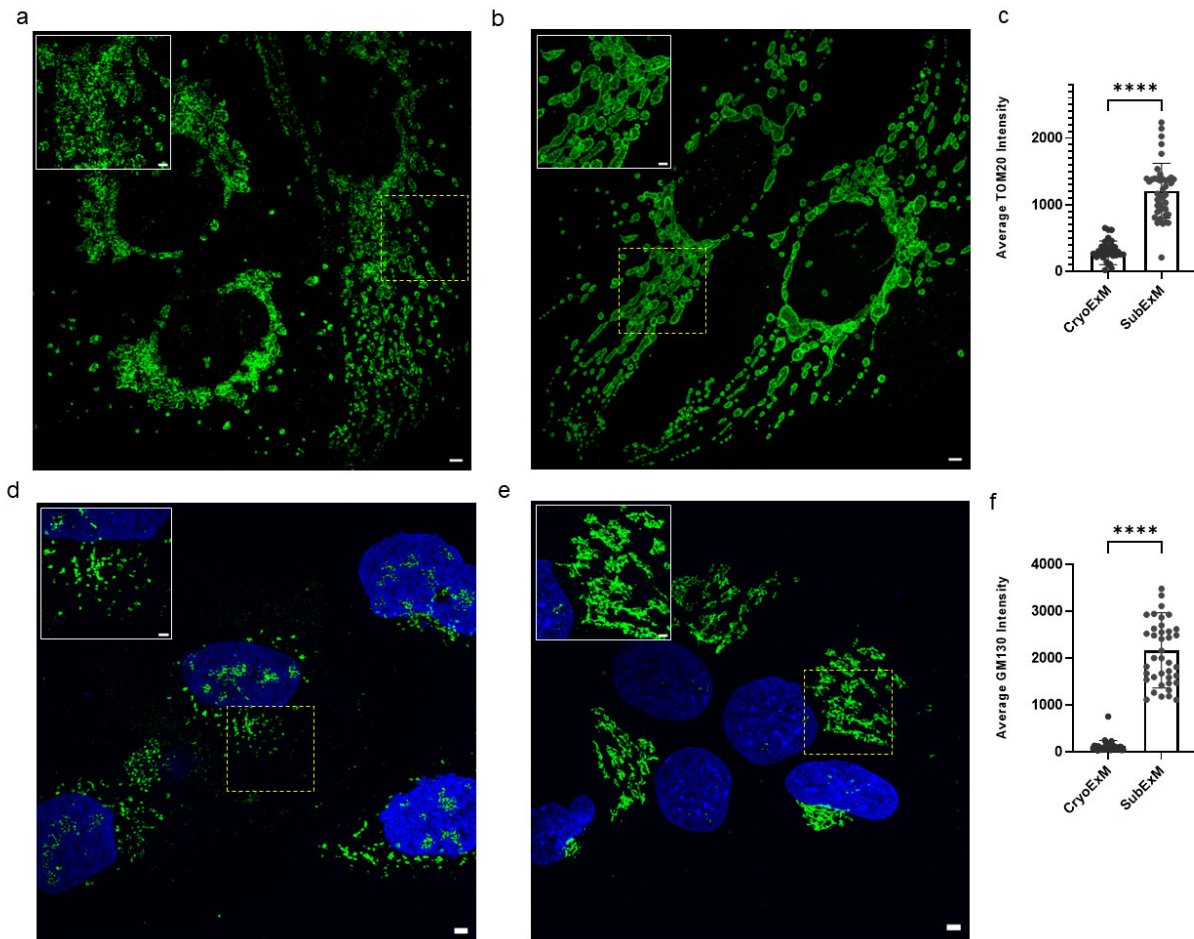


**Figure 14 Enhanced protein retention of different cellular structures using subExM**

(a) Maximum intensity projection of a confocal image from a typical experiment, showing TOM20-immunostained HeLa cells. Cells were cryofixed via plunge freezing and underwent freeze substitution with acetone. The subsequent expansion microscopy (ExM) process followed the CryoExM protocol, with polymerization conducted at 37°C. The inset shows a detailed view of the area highlighted in yellow. (b) A similar confocal image of TOM20-immunostained HeLa cells, which were processed using subExM with polymerization at -20°C. The inset shows a detailed view of the area highlighted in yellow. (c) Quantitative analysis of TOM20 intensity in expanded HeLa cells. The mean and standard deviation are  $278.5 \pm 174.5$  for CryoExM and  $1210.7 \pm 405.1$  for subExM. (d) Confocal image (maximum intensity projection from a typical experiment) of GM130-immunostained HeLa cells, also cryofixed and freeze-substituted with acetone, followed by the CryoExM protocol. Polymerization was performed at 37°C. The inset shows a magnified view of the yellow-highlighted region. (e) Confocal image (maximum intensity projection from a typical experiment) of GM130-immunostained HeLa cells, subExM processed with polymerization at -20°C. The inset shows a detailed view of the area highlighted

in yellow. (f) Quantification analysis of GM130 intensity in expanded HeLa cells. The mean and standard deviation are  $119.2 \pm 118.8$  for CryoExM and  $2164.4 \pm 792.7$  for subExM.

Analysis of TOM20 Intensity: evaluated across  $n=36$  mitochondria for CryoExM and  $n=42$  mitochondria for subExM, derived both from three culture batches, \*\*\*\* $p < 0.0001$ . For GM130 Intensity: examined  $n=36$  fields of view within the Golgi apparatus for CryoExM from three culture batches and  $n=40$  fields of view for subExM from two culture batches, \*\*\*\* $p < 0.0001$ . Scale bars in post-expansion units:  $10 \mu\text{m}$  (main images),  $5 \mu\text{m}$  (insets). Statistical analyses used unpaired two-tailed t-tests with Welch's correction.

### 3.3 Discussion

SubExM provides a solution to the seemingly contradictory and competing demands in ExM: the need for strong chemical cross-linking to preserve the integrity and relative organization of biomolecules, and the subsequent need for clean, isotropic separation of biomolecules during the expansion step. By using acrolein for simultaneous fixation and anchoring, the method "fixes" the biomolecules to the gel network instead of forming crosslinks between biomolecules, thus avoiding excessive crosslinking. Additionally, forming the gel at subzero temperatures further minimizes alterations to the cellular ultrastructure. Our continuity analysis has shown that subExM performs better than cryofixation-based methods, where anchoring and polymerization still occur at above-zero temperatures, in preserving microtubule ultrastructure. This is evidenced by enhanced protein retention and significant improvements in structural continuity. These outcomes highlight the effectiveness of subExM and extend its potential applicability to various structures, as shown by our observations of mitochondria and the Golgi apparatus with improved protein retention. The enhanced preservation of ultrastructure provided by subExM can offer new insights into cellular architecture and functions. Additionally, the simplicity and speed of this method, combined with the use of readily available reagents and no need for specialized equipment, make it accessible and practical for a wide range of research laboratories.

Nonetheless, future research is needed to further refine the subExM protocols. A current drawback is the challenge in performing distortion analysis, which is typically achieved by comparing super-resolution images of pre-expansion staining with diffraction-limited confocal images of post-expansion staining of the same sample. This analysis is important for assessing the expansion uniformity. The subExM protocol, necessitating the concurrent execution of fixation, anchoring, and polymerization at subzero temperatures without intermediate steps, precludes traditional immunostaining prior to polymerization, thus complicating distortion analysis. A potential solution involves the incorporation of an intrinsic ruler, as demonstrated by the GelMap method<sup>197</sup>, for accurate distortion assessment. Moreover, while the current protocol is optimized for cultured cells, additional optimization is necessary for adapting this technique to a wider array of biological specimens.

## 3.4 Methods

### Cell culture

Human bone osteosarcoma epithelial cells (U2OS; ATCC) and HeLa cells (ATCC) were cultured in Dulbecco's Modified Eagle Medium (DMEM; Corning, catalog no. 10013CV) with 10% heat-inactivated fetal bovine serum (FBS; Thermo Fisher, catalog no. A3840001) and 1% penicillin-streptomycin (Thermo Fisher, catalog no. 15140122) at 37 °C in a humidified 5% CO<sub>2</sub> incubator to reach 50~70% confluency.

### Reagents and subExM monomer solution preparation

Sodium acrylate (SA; Pfaltz & Bauer, catalog no. S03880) served as the hydrophilic monomer which is critical for the gel's expansion. N,N-Dimethylacrylamide (DMAA, Acros Organics, catalog no. 432021000) was employed as a co-monomer. N,N'-Methylenebisacrylamide (Bis-acrylamide, Sigma-Aldrich, catalog no. 146072) was used as a crosslinker, prepared as a 2% (w/v) stock solution in deionized water and stored at 4°C. The photoinitiator Irgacure 2959 (I-2959, Sigma-Aldrich, catalog no. 410896) was chosen for its efficient free radical generation under UV light, initiating polymerization without requiring thermal activation.

10 mL of subExM gelation solution was prepared by following steps: first, 1 g of sodium acrylate and 500 mg of the photoinitiator I-2959 were weighed and added to 3.5 mL of deionized water in a 20 mL glass vial. Subsequently, 5 mL of DMAA was added to the mixture. A 500 µL of Bis-acrylamide stock solution was then added to introduce crosslinks within the polymer network. To prepare the Bis stock solution, 200 mg of Bis-acrylamide was dissolved in deionized water to a final volume of 10 mL. Then, the mixture was subjected to vigorous vortexing for 1 minute to ensure homogeneity. Subsequent to the initial vortex mixing, the mixture underwent sonication in an ice-water bath for 15 minutes to ensure uniform dispersion of components and to expel entrapped air, enhancing the polymer network's quality. This was followed by an additional vortex mixing step for 1 minute to further homogenize the mixture. In cases where the mixture did not achieve homogeneity, it was subjected to continuous stirring for 5 minutes, facilitating the thorough mixing of the components. This can give us approximately 4~4.5-fold linear expansion depending on the purity of the sodium acrylate.

### **Plunge-freezing and freeze substitution**

The experimental procedure was performed as described in the literature<sup>192</sup>. To enhance the consistency of our results, we opted for a commercially manufactured cryoplunger, the Gatan CP3, instead of the homemade plunger. The vitrified cells were prepared by positioning 12-mm coverslips, bearing the biological specimen, using precision tweezers to hold them at their midpoint. Excess culture medium was carefully blotted away with filter paper before the coverslips were swiftly submerged into liquid ethane using the Gatan CP3 cryoplunger. Subsequent to plunge-freezing, the coverslips were immediately transferred into a pre-chilled 5-ml Eppendorf tube filled with solidified acetone (ThermoFisher Scientific, catalog no. AC326801000) at liquid nitrogen temperature. To ensure optimal cryofixation, the tubes were positioned at a 45-degree angle on dry ice and gently agitated overnight, allowing a gradual temperature increase to  $-80^{\circ}\text{C}$ . This was followed by a controlled warming phase, absent dry ice, lasting 1.5 hours until the temperature stabilized near  $0^{\circ}\text{C}$ . Rehydration of the samples was conducted through a series of ethanol:water baths for 5 minutes each, following a descending concentration gradient: 100% ethanol (twice), 95% ethanol (twice), 70% ethanol, 50% ethanol, then in PBS. The cells were then preserved in PBS for further expansion microscopy process.

### **Hydrophobic glass slide preparation**

To render glass slides hydrophobic for subsequent use in gelation chamber assembly, an initial step involved immersing the slides in a 0.2% (v/v) trichloro(octadecyl)silane solution (Fisher Scientific, catalog number AC147400250) in hexane, for 90 seconds. Following immersion, the slides underwent a sequential cleansing process involving a rinse with 70% isopropanol and subsequently with deionized water (ddH<sub>2</sub>O), to eliminate any residual silane compound or hexane. The drying process was carried out at  $37^{\circ}\text{C}$ , after which the slides were cleaned with a dry kimwipe to remove any chemical residues.

For the construction of the gelation chamber for cell culture, parafilm strips, each measuring about 4.5 cm in length and 0.2 cm in width, were carefully wrapped around the slide, creating a chamber with a 0.4-cm spacing for subsequent polymerization experiments.

### **Expansion of cell culture with subExM**

First, cells adhered to the substrate were gently rinsed twice with DPBS prewarmed to 37°C, to remove any residual media or non-adherent cells. This was immediately followed by the addition of acrolein (Restek, Catalog No. 30645), previously chilled to -20°C (Note it is critical to use fresh acrolein to ensure optimal reactivity and effectiveness in the fixation/anchoring process. Using degraded or old acrolein can compromise structure integrity of the sample). The cells were incubated with this fixative for 8 minutes at -20°C to ensure rapid and effective fixation/anchoring while preserving cellular architecture and molecular integrity. Subsequent subExM monomer solution, previously chilled to -20°C, was added directly to the cells without any intermediate washing step. This approach minimizes the loss of fixed cellular components and maintains the structural integrity for the subsequent polymerization process. The cells were then incubated for 5 minutes, allowing sufficient time for the monomer solution to permeate the cellular structure. Next, subExM monomer solution was added to the previously prepared gelation chamber, which was chilled at -20°C. Then, use a syringe needle to carefully lift the coverslip from the plate without disturbing the monomer solution and close the chamber with the cells facing down. Polymerization was initiated using UV light exposure for 3 minutes under an 8W UV lamp.

### **Expansion of cell culture with CryoExM**

Reagents being used are glutaraldehyde (EMS, catalog no. 16019), paraformaldehyde (PFA; EMS, catalog no. 15710), acetone (Thermofisher Scientific, catalog no. AC326801000), Acrylamide (Sigma Aldrich, catalog no. A9099-25G), Bis-acrylamide (Sigma-Aldrich, catalog no. 146072), SA (Pfaltz & Bauer, catalog no. S03880), ammonium persulfate (APS, Thermo Fisher, catalog no. 17874), N,N,N',N'-Tetramethylethylenediamine (TEMED; Thermo Fisher, catalog no. 17919), nuclease-free water (Thermo Fisher Scientific, catalog no. 10977015)

The cryofixed cells were incubated in a solution of acrylamide and 1.4% formaldehyde in PBS for a duration of 4 hours at a temperature of 37°C. This step was followed by incubation in a CryoExM monomer solution for 5 minutes on ice, just after the addition of 0.5% TEMED and APS to the solution. The monomer solution, composed of 19% SA, 10% AA, and 0.1% Bis-acrylamide in PBS, was prepared in advance and stored at -20°C for no less than 24 hours before the initiation of gelation. The SA stock solution was prepared by dissolving 25g of SA powder in 40.8g of nuclease-free water, achieving a 38% wt/wt concentration, and stirred at 4°C



overnight until fully dissolved. For gelation, approximately 25  $\mu$ L of the monomer solution with TEMED and APS was placed on the slide of a gelation chamber, which was prepared with parafilm strips around a slide. A syringe needle with a bent tip was used to carefully transfer the cryofixed cells on a 12mm coverslip from a 24-well plate to the gelation chamber, ensuring the cells were facing down to close the chamber. Next, the chamber was placed inside a food storage box with wet tissue paper to create a humidified environment. This setup was incubated at 37°C to allow polymerization for an hour. Post-gelation, the gel was trimmed into an asymmetric shape to facilitate later identification of the cell-containing side.

### **Denaturation, immunostaining and expansion for both subExM and CryoExM processed sample**

After the polymerization process, the gel was subjected to a denaturation step. Reagents being used are Tris(hydroxymethyl)aminomethane (Tris; Thermo Fisher, catalog no. AM9855G), Sodium chloride (NaCl, Thermo Fisher, catalog no. AM9759), Sodium hydroxide(NaOH; Sigma, catalog no. S8263), Sodium n-dodecyl sulfate (SDS; Thermifisher, catalog no. AM9820). The gel was incubated in a denaturation buffer for 1.5 hours at 95°C. 20mL denaturation buffer was prepared by mixing 12.38 mL of deionized water, 1 mL of 1M Tris (pH 8.0), 0.8 mL of 5M NaCl, 60  $\mu$ L of 5M NaOH, and 5.76 mL of 20% SDS, with the pH adjusted to 9.0. Following denaturation, the gel was washed three times with 1x PBS for 30 minutes each to remove any residual denaturation buffer.

For immunofluorescence staining, the protocol began with blocking to reduce nonspecific binding, employing 400  $\mu$ L of MAXblock Blocking Medium for 1 hour at RT. This was followed by a single wash with MAXwash™ Washing Medium for 10 minutes at RT to prepare the gel for antibody incubation. Primary antibody staining involved diluting rabbit anti-TOM20 (abcam, ab78547) or rabbit anti-GM130 (proteintech, 11308-1-AP) or rabbit anti beta-tubulin (abcam, ab6046) in MAXbind™ Staining Medium to a 1:100 dilution. Approximately 250  $\mu$ L of the primary antibody solution was added to each well of a 24-well plate, and the gel was incubated for 5 hours at RT or overnight at 4°C. After primary antibody binding, the gel was washed three times with 1x PBS for 30 minutes each to remove unbound primary antibodies. Secondary antibody staining was then performed. For mitochondria and Golgi samples, goat anti-rabbit AF488 (Thermo Fisher, catalog no. A-11008) was used, and for microtubule samples,

goat anti-rabbit AF546 (Thermo Fisher, catalog no. A-11035) was used. Similar to the primary antibody step, 250  $\mu$ L of the secondary antibody solution was added to each well, followed by incubation for 5 hours at RT or overnight at 4°C. The gel underwent a final series of three 30-minute washes with 1x PBS to ensure the removal of excess secondary antibody. Finally, the gel was first expanded in deionized water for two 30-minute sessions, followed by an overnight incubation.

### **Quantification of microtubules**

To quantify and analyze the structure preservation of microtubules. We utilized the straight line tool in Fiji<sup>198</sup>, an open-source platform for biological-image analysis, to manually trace the microtubules in our images. Critical to our methodology was the avoidance of tracing segments of microtubules that overlapped with other microtubules, ensuring that our data was not skewed by overlapping intensities. We defined a data point in a microtubule segment as a “gap” (marked ‘1’) or a “non-gap” (marked ‘0’). This determination was based on the intensity value of the data point; if its intensity was lower than a specific threshold we set, it was classified as a “gap”. This threshold was calculated as the sum of the mean value and the standard deviation of the background intensity. We further defined the gap frequency as the proportion of “gap” data points in a microtubule segment. This was calculated by dividing the number of data points defined as “gaps” by the total number of data points within the segment. Finally, we quantified the size of the gaps, which we defined as the length of the gaps in the post-expansion scale. For instance, if there were four consecutive pixels classified as “gaps”, the gap size would be calculated as four times the pixel width. The average intensity of each segment is obtained by subtracting the average background intensity from the intensity value of each segment to account for any potential background noise or interference.

## **3.5 Supplementary Information**

### **Excel Macro for Batch Processing of Gap Ratio / Size**

Sub GapsRatio()

,

' GapsRatio Macro

' Gaps vs Total Length Ratio: Calculate the ratio of the total length of gaps to the total length of the microtubules.

```

Dim ws As Worksheet
Dim wbNew As Workbook
Dim wsNew As Worksheet
Dim i As Long, j As Long, k As Long
Dim lastRowB As Long, lastRowD As Long
Dim thresholds(1 To 3) As Double
Dim gapCount(1 To 3) As Long
Dim totalDataPoints As Long

Set wbNew = Application.Workbooks.Add
Set wsNew = wbNew.Sheets(1)
k = 1

For Each ws In ThisWorkbook.Sheets

    lastRowB = ws.Cells(ws.Rows.Count, "B").End(xlUp).Row
    lastRowD = ws.Cells(ws.Rows.Count, "D").End(xlUp).Row

    'Calculate standard deviation and mean for column B
    ws.Range("K2").Value = Application.WorksheetFunction.StDev(ws.Range("B1:B" &
lastRowB))
    ws.Range("K1").Value = Application.WorksheetFunction.Average(ws.Range("B1:B" &
lastRowB))

    'Calculate mean for column D and subtract K1
    ws.Range("K4").Value = Application.WorksheetFunction.Average(ws.Range("D1:D" &
lastRowD))
    ws.Range("K5").Value = ws.Range("K4").Value - ws.Range("K1").Value

    'Set thresholds
    For i = 1 To 3
        thresholds(i) = ws.Range("K1").Value + i * ws.Range("K2").Value
    Next i

    'Reset gapCount for each sheet
    For i = 1 To 3
        gapCount(i) = 0
    
```

```

Next i

'Compare each data point in column D to the threshold
For i = 1 To lastRowD
  For j = 1 To 3
    If ws.Cells(i, "D").Value < thresholds(j) Then
      ws.Cells(i, j + 4).Value = 1
      gapCount(j) = gapCount(j) + 1
    Else
      ws.Cells(i, j + 4).Value = 0
    End If
  Next j
Next i

'Count the number of "gaps" and total data points
For i = 1 To 3
  ws.Cells(1, i + 7).Value = gapCount(i)
  ws.Cells(2, i + 7).Value = lastRowD
  ws.Cells(3, i + 7).Value = gapCount(i) / lastRowD
  ws.Cells(3, i + 7).NumberFormat = "0.00%"
Next i

'Export K5, H3, I3, J3 to a new workbook
wsNew.Cells(k, "A").Value = ws.Name
wsNew.Cells(k, "B").Value = ws.Range("K5").Value
wsNew.Cells(k, "C").Value = ws.Range("H3").Value
wsNew.Cells(k, "D").Value = ws.Range("I3").Value
wsNew.Cells(k, "E").Value = ws.Range("J3").Value
k = k + 1

Next ws

'Save the new workbook
wbNew.SaveAs "C:\% your path %\Mean&GapsRatio_New.xlsx"
wbNew.Close SaveChanges:=False

End Sub

Sub GapsFrequencyGapSize()

```

```

Dim ws As Worksheet
Dim wbNew As Workbook
Dim wsNew As Worksheet
Dim i As Long, j As Long, k As Long, l As Long
Dim lastRow As Long
Dim gapCount(1 To 3) As Long
Dim totalDataPoints As Long
Dim gapSizeSum(1 To 3) As Long
Dim gapSizeCount(1 To 3) As Long
Dim gapSizeMean(1 To 3) As Double
Dim gapSizeStdDev(1 To 3) As Double
Dim gapSizeVar(1 To 3) As Double

Set wbNew = Application.Workbooks.Add
Set wsNew = wbNew.Sheets(1)
k = 1

For Each ws In ThisWorkbook.Sheets

    lastRow = ws.Cells(ws.Rows.Count, "E").End(xlUp).Row

    'Reset counters for each sheet
    For i = 1 To 3
        gapCount(i) = 0
        gapSizeSum(i) = 0
        gapSizeCount(i) = 0
    Next i

    'Calculate gap frequency and gap size distribution
    For i = 1 To lastRow
        For j = 1 To 3
            If ws.Cells(i, j + 4).Value = 1 Then
                gapCount(j) = gapCount(j) + 1
                l = i
                Do While ws.Cells(l, j + 4).Value = 1 And l <= lastRow
                    gapSizeCount(j) = gapSizeCount(j) + 1
                    l = l + 1
                Loop
                gapSizeSum(j) = gapSizeSum(j) + gapSizeCount(j)
                gapSizeCount(j) = 0
            End If
        Next j
    Next i
End For

```

```

        End If
    Next j
Next i

'Calculate mean and standard deviation of gap sizes
For i = 1 To 3
    If gapCount(i) <> 0 Then
        gapSizeMean(i) = Cdbl(gapSizeSum(i)) / Cdbl(gapCount(i))
    Else
        gapSizeMean(i) = 0
    End If
    For j = 1 To lastRow
        If ws.Cells(j, i + 4).Value = 1 Then
            gapSizeCount(i) = gapSizeCount(i) + 1
        Else
            If gapCount(i) <> 0 Then
                gapSizeVar(i) = gapSizeVar(i) + (gapSizeCount(i) - gapSizeMean(i)) ^ 2
            End If
            gapSizeCount(i) = 0
        End If
    Next j
    If gapCount(i) <> 0 Then
        gapSizeStdDev(i) = Sqr(gapSizeVar(i) / gapCount(i))
    Else
        gapSizeStdDev(i) = 0
    End If
Next i

'Store results in the sheet and export to a new workbook
For i = 1 To 3
    ws.Cells(5, i + 7).Value = gapCount(i) / lastRow
    ws.Cells(7, i + 7).Value = gapSizeMean(i)
    ws.Cells(8, i + 7).Value = gapSizeStdDev(i)
    wsNew.Cells(k, i * 3 - 2).Value = ws.Cells(5, i + 7).Value
    wsNew.Cells(k, i * 3 - 1).Value = ws.Cells(7, i + 7).Value
    wsNew.Cells(k, i * 3).Value = ws.Cells(8, i + 7).Value
Next i
k = k + 1

Next ws

```

```
'Save the new workbook  
wbNew.SaveAs "C:\% your path% \GapsFrequency&GapSize_New.xlsx"  
wbNew.Close SaveChanges:=False
```

```
End Sub
```





## Chapter 4 Conclusion and Future Directions

The ExM has been rapidly evolving in the fast few years with over 600 experimental papers and preprints to date. There are many exciting future directions to explore or that have been explored, but still require further investigation.

For subExM, it would be interesting to explore whether anchoring and gelation can be conducted at even lower temperatures, enabling the capture of more dynamic processes with ExM. In addition, since DMAA has self-branching capabilities and allows for a higher expansion factor in a single shot, as demonstrated in X10 ExM<sup>30</sup>, subExM could be used to reveal more intricate details of cellular structures and interactions. In current subExM, we have only demonstrated subExM in cultured cells, so another direction would be to apply subExM to tissues, thereby broadening the applicability of this technique.

Regarding the general future directions of ExM, one such direction is combining ExM with super-resolution microscopy to achieve even higher resolution. This has been highlighted in several recent reports<sup>50,59,90,92,134,199–201</sup>, physical magnification has been combined with patterned illumination or single-molecule localization to achieve imaging resolution beyond optical super-resolution imaging. Another direction is to develop gel recipes that enable the expansion of the gel beyond 20-fold, either through iterative expansion or, preferably, in a single shot in cells and tissues. One example has expanded immunostained microtubules in cultured cells to 53x in three expansion rounds using iExM.<sup>7</sup> However, the imaging resolution of such >20x ExM protocols has not been validated and will be limited by spatial errors from two sources: the size of the labels and the spatial errors from the hydrogel synthesis and expansion process. Since the original polyacrylamide/polyacrylate-based ExM hydrogels, synthesized via radical polymerization, are known to have local structural defects and inhomogeneities that can amount to 15-25 nm variations in local polymer spacings<sup>29</sup> and in recent examples, such polyacrylamide/polyacrylate-based ExM hydrogel led to a median spatial error of ~14 nm for localizing the viral envelope layer of herpes simplex virus type 1 (HSV-1)<sup>35</sup>, and a standard deviation of ~16 nm for localizing fluorescent sites on artificial DNA structures<sup>202</sup>. Therefore, it would be interesting to explore the way to reduce the spatial error by using more homogeneous hydrogel systems, such as the recently reported new ExM hydrogel synthesized using monomers that have a tetrahedral geometry and a non-radical polymerization mechanism. In fact, these new ExM hydrogels, or so called tetra-gels<sup>35</sup>, showed reduced spatial errors compared to the original

polyacrylamide/polyacrylate-based ExM hydrogels: HSV-1 expanded via tetra-gel-based ExM protocol resulted in ~9 nm median spatial error for localizing the viral envelope layer<sup>35</sup>, and the standard deviation of localizing fluorescent site on an artificial DNA structure was reduced to below 5 nm<sup>202</sup>. In addition, new forms of ExM to visualize lipids, sugars, and small molecules are needed to image biomolecules other than proteins and RNAs with ExM. The key of developing these new forms of ExM is to develop ExM-compatible custom reagents to label biomolecules other than protein and RNA<sup>10,21</sup>, or via integrating existing biomolecule labeling reagents into existing ExM workflows<sup>13</sup>. For example, umExM has been introduced as a method for labeling and imaging lipids<sup>203</sup>, while click-ExM was developed for expansion microscopy of biomolecules tagged with click chemistry groups.<sup>10</sup> Additionally, FLARE (fluorescent labeling of abundant reactive entities) was created to stain expanded samples using fluorophore-conjugated N-Hydroxysuccinimide ester, which labels amines in proteins, fluorophore-conjugated hydrazides for staining oxidized carbohydrates, and DNA stains such as Hoechst or SYBR Green. Finally, integrating these new ExM forms with multiplexed imaging technologies, such as DNA barcoding, will enable simultaneous visualization of multiple types of biomolecules in a single biological specimen. Exploring the combination of multiple ExM methods to visualize various types of biomolecules with nanoscale resolution in a single expanded biological specimen could also be a promising direction. A method capable of imaging proteins, RNAs, DNAs, lipids, and small molecules will provide a multitude of spatial information of biomolecules and reveal their spatial relationships, which has broad biological applications. For instance, both LabelX and AcX are used in ExSeq of mouse brain tissues to read out the RNA content in the spatial context mapped by yellow fluorescent protein-labeled neurons.<sup>19</sup> In a recent example, LabelX and AcX are used in a method called dual-ExM to enable imaging of immunostained proteins and FISH probe-labeled mRNA in expanded cultured cells and mouse brain slices.<sup>204</sup> As another example, DNA fluorescent in situ hybridization was used together with immunostaining to visualize both proteins and chromosome sites in expanded human clinical specimens.<sup>32</sup> Finally, an epoxide-based anchor called GMA has been reported to enable ExM visualization of multiple types of biomolecules with a single biomolecule anchoring reagents and a unified ExM protocol called uniExM.<sup>15</sup> Combination of such multi-model ExM imaging protocols with high-expansion-factor methods such as iExM offers the possibility of imaging different kinds of biomolecules with very high imaging resolution.

The directions outlined above are worth further exploration to develop an ideal ExM protocol that can map all biomolecules, including proteins, RNAs, DNAs, lipids, and small molecules,

with molecular resolution. Such a comprehensive molecular picture could lay the foundation for deciphering interactions between different biomolecules in situ, thereby systematically studying a wide range of biological chemistry problems at the molecular scale.



## References

1. Chen, F., Tillberg, P. W. & Boyden, E. S. Expansion microscopy. *Science* **347**, 543–548 (2015).
2. Huang, B., Bates, M. & Zhuang, X. Super-Resolution Fluorescence Microscopy. *Annu. Rev. Biochem.* **78**, 993–1016 (2009).
3. Sigal, Y. M., Zhou, R. & Zhuang, X. Visualizing and discovering cellular structures with super-resolution microscopy. *Science* **361**, 880–887 (2018).
4. Tillberg, P. W. *et al.* Protein-retention expansion microscopy of cells and tissues labeled using standard fluorescent proteins and antibodies. *Nat. Biotechnol.* **34**, 987–992 (2016).
5. Ku, T. *et al.* Multiplexed and scalable super-resolution imaging of three-dimensional protein localization in size-adjustable tissues. *Nat. Biotechnol.* **34**, 973–981 (2016).
6. Chozinski, T. J. *et al.* Expansion microscopy with conventional antibodies and fluorescent proteins. *Nat. Methods* **13**, 485–488 (2016).
7. Chang, J.-B. *et al.* Iterative expansion microscopy. *Nat. Methods* **14**, 593–599 (2017).
8. Gambarotto, D. *et al.* Imaging cellular ultrastructures using expansion microscopy (U-ExM). *Nat. Methods* **16**, 71–74 (2019).
9. Sarkar, D. *et al.* Expansion Revealing: Decrowding Proteins to Unmask Invisible Brain Nanostructures. *bioRxiv* 2020.08.29.273540-2020.08.29.273540 (2020) doi:10.1101/2020.08.29.273540.
10. Sun, D. *et al.* Click-ExM enables expansion microscopy for all biomolecules. *Nat. Methods* **18**, 107–113 (2021).
11. Wen, G. *et al.* Evaluation of Direct Grafting Strategies via Trivalent Anchoring for Enabling Lipid Membrane and Cytoskeleton Staining in Expansion Microscopy. *ACS Nano* acsnano.9b09259 (2020) doi:10.1021/acsnano.9b09259.
12. Shi, X. *et al.* Label-retention expansion microscopy. *J. Cell Biol.* **220**, (2021).
13. Mao, C. *et al.* Feature-rich covalent stains for super-resolution and cleared tissue fluorescence microscopy. *Sci. Adv.* **6**, eaba4542–eaba4542 (2020).
14. Damstra, H. G. J. *et al.* Visualizing cellular and tissue ultrastructure using Ten-fold Robust Expansion Microscopy (TReX). *bioRxiv* 2021.02.03.428837-2021.02.03.428837 (2021) doi:10.1101/2021.02.03.428837.
15. Cui, Y. *et al.* A Multifunctional Anchor for Multimodal Expansion Microscopy. *bioRxiv* 2022.06.19.496699 (2022) doi:10.1101/2022.06.19.496699.
16. Chen, F. *et al.* Nanoscale imaging of RNA with expansion microscopy. *Nat. Methods* **13**, 679–684 (2016).
17. Tsanov, N. *et al.* smiFISH and FISH-quant – a flexible single RNA detection approach with super-resolution capability. *Nucleic Acids Res.* **44**, e165–e165 (2016).
18. Wen, G. *et al.* A Universal Labeling Strategy for Nucleic Acids in Expansion Microscopy. *J. Am. Chem. Soc.* (2021) doi:10.1021/jacs.1c05931.
19. Alon, S. *et al.* Expansion sequencing: Spatially precise in situ transcriptomics in intact biological systems. *Science* **371**, eaax2656 (2021).
20. Wang, Y. *et al.* EASI-FISH for thick tissue defines lateral hypothalamus spatio-molecular organization. *Cell* **184**, 6361-6377.e24 (2021).
21. Karagiannis, E. D. *et al.* Expansion Microscopy of Lipid Membranes. *bioRxiv* 829903 (2019) doi:10.1101/829903.

22. Götz, R. *et al.* Nanoscale imaging of bacterial infections by sphingolipid expansion microscopy. *Nat. Commun.* **11**, 6173 (2020).
23. Wassie, A. T., Zhao, Y. & Boyden, E. S. Expansion microscopy: principles and uses in biological research. *Nat. Methods* **16**, 33–41 (2019).
24. Tillberg, P. W. & Chen, F. Expansion Microscopy: Scalable and Convenient Super-Resolution Microscopy. *Annu. Rev. Cell Dev. Biol.* **35**, 683–701 (2019).
25. Klimas, A. & Zhao, Y. Expansion Microscopy: Toward Nanoscale Imaging of a Diverse Range of Biomolecules. *ACS Nano* **14**, 7689–7695 (2020).
26. Wang, W., Chan, Y. H., Kwon, S., Tandukar, J. & Gao, R. Nanoscale fluorescence imaging of biological ultrastructure via molecular anchoring and physical expansion. *Nano Converg.* **9**, 30 (2022).
27. Tanaka, T., Sun, S.-T., Nishio, I., Swislow, G. & Shah, A. Phase transitions in ionic gels. *Ferroelectrics* **30**, 97–97 (1980).
28. Hausen, P. & Dreyer, C. The Use of Polyacrylamide as an Embedding Medium for Immunohistochemical Studies of Embryonic Tissues. *Stain Technol.* **56**, 287–293 (1981).
29. Cohen, Y., Ramon, O., Kopelman, I. J. & Mizrahi, S. Characterization of inhomogeneous polyacrylamide hydrogels. *J. Polym. Sci. Part B Polym. Phys.* **30**, 1055–1067 (1992).
30. Truckenbrodt, S. *et al.* X10 expansion microscopy enables 25-nm resolution on conventional microscopes. *EMBO Rep.* **19**, e45836 (2018).
31. Park, H. *et al.* Scalable and Isotropic Expansion of Tissues with Simply Tunable Expansion Ratio. *Adv. Sci.* **6**, 1901673 (2019).
32. Zhao, Y. *et al.* Nanoscale imaging of clinical specimens using pathology-optimized expansion microscopy. *Nat. Biotechnol.* **35**, 757–764 (2017).
33. Freifeld, L. *et al.* Expansion microscopy of zebrafish for neuroscience and developmental biology studies. *Proc. Natl. Acad. Sci.* **114**, E10799–E10808 (2017).
34. Thevathasan, J. V. *et al.* Nuclear pores as versatile reference standards for quantitative superresolution microscopy. *Nat. Methods* **16**, 1045–1053 (2019).
35. Gao, R. *et al.* A highly homogeneous polymer composed of tetrahedron-like monomers for high-isotropy expansion microscopy. *Nat. Nanotechnol.* **16**, 698–707 (2021).
36. Asano, S. M. *et al.* Expansion Microscopy: Protocols for Imaging Proteins and RNA in Cells and Tissues. *Curr. Protoc. Cell Biol.* **80**, e56 (2018).
37. Lim, Y. *et al.* Mechanically resolved imaging of bacteria using expansion microscopy. *PLOS Biol.* **17**, e3000268 (2019).
38. Mascheroni, L. *et al.* Combining sample expansion and light sheet microscopy for the volumetric imaging of virus-infected cells with super-resolution. *Biomed. Opt. Express* **11**, 5032 (2020).
39. Gao, R. *et al.* Cortical column and whole-brain imaging with molecular contrast and nanoscale resolution. *Science* **363**, eaau8302 (2019).
40. Düring, D. N., Rocha, M. D., Dittrich, F., Gahr, M. & Hahnloser, R. H. R. Expansion Light Sheet Microscopy Resolves Subcellular Structures in Large Portions of the Songbird Brain. *Front. Neuroanat.* **13**, 2 (2019).
41. Glaser, A. K. *et al.* Multi-immersion open-top light-sheet microscope for high-throughput imaging of cleared tissues. *Nat. Commun.* **10**, 2781 (2019).
42. Bürgers, J. *et al.* Light-sheet fluorescence expansion microscopy: fast mapping of neural circuits at super resolution. *Neurophotonics* **6**, 15005 (2019).

43. Murakami, T. C. *et al.* A three-dimensional single-cell-resolution whole-brain atlas using CUBIC-X expansion microscopy and tissue clearing. *Nat. Neurosci.* **21**, 625–637 (2018).
44. Voleti, V. *et al.* Real-time volumetric microscopy of in vivo dynamics and large-scale samples with SCAPE 2.0. *Nat. Methods* **16**, 1054–1062 (2019).
45. Lin, R. *et al.* A hybridization-chain-reaction-based method for amplifying immunosignals. *Nat. Methods* **15**, 275–278 (2018).
46. Zhang, Y. S. *et al.* Hybrid Microscopy: Enabling Inexpensive High-Performance Imaging through Combined Physical and Optical Magnifications. *Sci. Rep.* **6**, 1–10 (2016).
47. Saka, S. K. *et al.* Immuno-SABER enables highly multiplexed and amplified protein imaging in tissues. *Nat. Biotechnol.* **37**, 1080–1090 (2019).
48. M'Saad, O. & Bewersdorf, J. Light microscopy of proteins in their ultrastructural context. *Nat. Commun.* **11**, 3850 (2020).
49. Shen, F. Y. *et al.* Light microscopy based approach for mapping connectivity with molecular specificity. *Nat. Commun.* **11**, 4632 (2020).
50. Zwettler, F. U. *et al.* Molecular resolution imaging by post-labeling expansion single-molecule localization microscopy (Ex-SMLM). *Nat. Commun.* **11**, 3388 (2020).
51. Park, J. *et al.* Epitope-preserving magnified analysis of proteome (eMAP). *Sci. Adv.* **7**, 1–14 (2021).
52. Valdes, P. A. *et al.* Decrowding Expansion Pathology: Unmasking Previously Invisible Nanostructures and Cells in Intact Human Brain Pathology Specimens. *bioRxiv* 2021.12.05.471271 (2021) doi:10.1101/2021.12.05.471271.
53. Schwarzkopf, M. *et al.* Hybridization chain reaction enables a unified approach to multiplexed, quantitative, high-resolution immunohistochemistry and in situ hybridization. *Development* **148**, 2021.06.02.446311 (2021).
54. Yu, C.-C. C. (Jay) *et al.* Expansion microscopy of *C. elegans*. *eLife* **9**, 1–78 (2020).
55. Kunz, T. C. *et al.* The Expandables: Cracking the Staphylococcal Cell Wall for Expansion Microscopy. *Front. Cell. Infect. Microbiol.* **0**, 128 (2021).
56. Cheng, S., Zhao, Y. & Department of Biological Sciences Pittsburgh, PA, USA, C. M. U. Nanoscale imaging of *E. coli* cells by expansion microscopy. *Discoveries* **7**, e98 (2019).
57. Rumyantseva, N. A., Vedyaykin, A. D., Vishnyakov, I. E. & Khodorkovskii, M. A. Visualization of the intracellular structures of bacteria using expansion microscopy. *J. Phys. Conf. Ser.* **1697**, 12048 (2020).
58. Kunz, T. C., Götz, R., Sauer, M. & Rudel, T. Detection of Chlamydia Developmental Forms and Secreted Effectors by Expansion Microscopy. *Front. Cell. Infect. Microbiol.* **9**, 276 (2019).
59. Cahoon, C. K. *et al.* Superresolution expansion microscopy reveals the three-dimensional organization of the *Drosophila* synaptonemal complex. *Proc. Natl. Acad. Sci.* **114**, E6857–E6866 (2017).
60. Mosca, T. J., Luginbuhl, D. J., Wang, I. E. & Luo, L. Presynaptic LRP4 promotes synapse number and function of excitatory CNS neurons. *eLife* **6**, e27347 (2017).
61. Jiang, N. *et al.* Superresolution imaging of *Drosophila* tissues using expansion microscopy. *Mol. Biol. Cell* **29**, 1413–1421 (2018).
62. Sim, J. *et al.* Nanoscale resolution imaging of the whole mouse embryos and larval zebrafish using expansion microscopy. *bioRxiv* 2021.05.18.443629 (2022).
63. Gambarotto, D. *et al.* Ultrastructure expansion microscopy (U-ExM). *Methods Cell Biol.* **161**, 57–81 (2021).

64. Laporte, M. H., Klena, N., Hamel, V. & Guichard, P. Visualizing the native cellular organization by coupling cryofixation with expansion microscopy (Cryo-ExM). *Nat. Methods* **19**, 216–222 (2022).
65. Klimas, A. *et al.* Nanoscale Imaging of Biomolecules Using Molecule Anchorable Gel-enabled Nanoscale In-situ Fluorescence Microscopy. *Microsc. Microanal.* **28**, 1568–1569 (2022).
66. Cipriano, B. H. *et al.* Superabsorbent Hydrogels That Are Robust and Highly Stretchable. *Macromolecules* **47**, 4445–4452 (2014).
67. Truckenbrodt, S., Sommer, C., Rizzoli, S. O. & Danzl, J. G. A practical guide to optimization in X10 expansion microscopy. *Nat. Protoc.* **14**, 832–863 (2019).
68. Saad, O. M. *et al.* All-optical visualization of specific molecules in the ultrastructural context of brain tissue. 1–52 (2022).
69. Wang, G., Moffitt, J. R. & Zhuang, X. Multiplexed imaging of high-density libraries of RNAs with MERFISH and expansion microscopy. *Sci. Rep.* **8**, 4847 (2018).
70. Coté, A. *et al.* The spatial distributions of pre-mRNAs suggest post-transcriptional splicing of specific introns within endogenous genes. *bioRxiv* 2020.04.06.028092-2020.04.06.028092 (2020) doi:10.1101/2020.04.06.028092.
71. Hafner, A.-S. S., Donlin-Asp, P. G., Leitch, B., Herzog, E. & Schuman, E. M. Local protein synthesis is a ubiquitous feature of neuronal pre- and postsynaptic compartments. *Science* **364**, eaau3644 (2019).
72. Xia, C., Fan, J., Emanuel, G., Hao, J. & Zhuang, X. Spatial transcriptome profiling by MERFISH reveals subcellular RNA compartmentalization and cell cycle-dependent gene expression. *Proc. Natl. Acad. Sci.* **116**, 19490–19499 (2019).
73. Suofu, Y. *et al.* Dual role of mitochondria in producing melatonin and driving GPCR signaling to block cytochrome c release. *Proc. Natl. Acad. Sci.* **114**, E7997–E8006 (2017).
74. Kunz, T. C., Götz, R., Gao, S., Sauer, M. & Kozjak-Pavlovic, V. Using Expansion Microscopy to Visualize and Characterize the Morphology of Mitochondrial Cristae. *Front. Cell Dev. Biol.* **8**, 1–10 (2020).
75. Bahri, H. *et al.* TMEM70 forms oligomeric scaffolds within mitochondrial cristae promoting in situ assembly of mammalian ATP synthase proton channel. *Biochim. Biophys. Acta BBA - Mol. Cell Res.* **1868**, 118942 (2021).
76. Fecher, C. *et al.* Cell-type-specific profiling of brain mitochondria reveals functional and molecular diversity. *Nat. Neurosci.* **22**, 1731–1742 (2019).
77. Srinivas, U. S. *et al.* PLK1 inhibition selectively kills ARID1A deficient cells through uncoupling of oxygen consumption from ATP production. *bioRxiv* 2021.06.01.446664-2021.06.01.446664 (2021) doi:10.1101/2021.06.01.446664.
78. Lindhout, F. W. *et al.* VAP-SCRN1 interaction regulates dynamic endoplasmic reticulum remodeling and presynaptic function. *EMBO J.* **38**, 1–17 (2019).
79. Dobbelaere, J. *et al.* Cep97 Is Required For Centriole Structural Integrity And Cilia Formation In Drosophila. *Curr. Biol.* **30**, 3045-3056.e7 (2019).
80. Steib, E. *et al.* Wdr90 is a centriolar microtubule wall protein important for centriole architecture integrity. *eLife* **9**, 1–28 (2020).
81. Lüders, J. *et al.* Sub-centrosomal mapping identifies augmin- $\gamma$ TuRC as part of a centriole-stabilizing scaffold. *bioRxiv* **2507**, 1–9 (2020).
82. Balestra, F. R. *et al.* Trim37 prevents formation of centriolar protein assemblies by regulating centrin. *eLife* **10**, 1–76 (2021).



83. Kong, D. *et al.* Prolonged mitosis results in structurally aberrant and over-elongated centrioles. *J. Cell Biol.* **219**, (2020).
84. SAHABANDU, N. *et al.* Expansion microscopy for the analysis of centrioles and cilia. *J. Microsc.* **276**, 145–159 (2019).
85. Decarreau, J. *et al.* The tetrameric kinesin Kif25 suppresses pre-mitotic centrosome separation to establish proper spindle orientation. *Nat. Cell Biol.* **19**, 384–390 (2017).
86. Guennec, M. Le *et al.* A helical inner scaffold provides a structural basis for centriole cohesion. *Sci. Adv.* **6**, eaaz4137–eaaz4137 (2020).
87. A, W. Expansion microscopy on *Drosophila* spermatocyte centrioles. *Methods Cell Biol.* **161**, 217–245 (2021).
88. Pierrick Le Borgne<sup>1</sup>, Marine H el ene Laporte<sup>2</sup>, Logan Greibill<sup>1</sup>, Michel Lemullois<sup>1</sup>, Mebarek Temagout<sup>3</sup>, Olivier Rosnet<sup>4</sup>, Maeva Le Guennec<sup>2</sup>, Laurent Lignieres<sup>5</sup>, Guillaume Chevreux<sup>5</sup>, France Koll<sup>1</sup>, Virginie Hamel<sup>2</sup>, Paul Guichard<sup>2</sup>, A.-M. T. The ternary complex CEP90, FOPNL and OFD1 specifies the future location of centriolar distal appendages, and promotes their assembly. *bioRxiv* **53**, 6 (2021).
89. Prasai, A. *et al.* The BBSome assembly is spatially controlled by BBS1 and BBS4 in human cells. *J. Biol. Chem.* **295**, 14279–14290 (2020).
90. Wang, Y. *et al.* Combined expansion microscopy with structured illumination microscopy for analyzing protein complexes. *Nat. Protoc.* **13**, 1869–1895 (2018).
91. Zwettler, F. U. *et al.* Tracking down the molecular architecture of the synaptonemal complex by expansion microscopy. *Nat. Commun.* **11**, 3222 (2020).
92. Xu, H. *et al.* Molecular organization of mammalian meiotic chromosome axis revealed by expansion STORM microscopy. *Proc. Natl. Acad. Sci.* **116**, 18423–18428 (2019).
93. Sacristan, C. *et al.* Dynamic kinetochore size regulation promotes microtubule capture and chromosome biorientation in mitosis. *Nat. Cell Biol.* **20**, 800–810 (2018).
94. So, C. *et al.* A liquid-like spindle domain promotes acentrosomal spindle assembly in mammalian oocytes. *Science* **364**, eaat9557 (2019).
95. Vukušić, K., Buđa, R., Ponjavić, I., Risteski, P. & Tolić, I. M. Chromosome segregation is driven by joint microtubule sliding action of kinesins KIF4A and EG5. *bioRxiv* 863381 (2019) doi:10.1101/863381.
96. Simon, C. S. *et al.* An extended DNA-free intranuclear compartment organizes centrosomal microtubules in *Plasmodium falciparum*. *bioRxiv* 2021.03.12.435157-2021.03.12.435157 (2021) doi:10.1101/2021.03.12.435157.
97. Hooikaas, P. J. *et al.* Kinesin-4 KIF21B limits microtubule growth to allow rapid centrosome polarization in T cells. *eLife* **9**, 2020.08.28.271643-2020.08.28.271643 (2020).
98. Park, C. E. *et al.* Super-Resolution Three-Dimensional Imaging of Actin Filaments in Cultured Cells and the Brain via Expansion Microscopy. *ACS Nano* **14**, 14999–15010 (2020).
99. Yan, C. *et al.* Microtubule Acetylation Is Required for Mechanosensation in *Drosophila*. *Cell Rep.* **25**, 1051-1065.e6 (2018).
100. Pothapragada, S. P., Gupta, P., Mukherjee, S. & Das, T. Matrix mechanics regulates epithelial defence against cancer by tuning dynamic localization of filamin. (2020) doi:10.21203/rs.3.rs-93643/v1.
101. Katrukha, E. A., Jurriens, D., Pastene, D. S. & Kapitein, L. C. Quantitative mapping of dense microtubule arrays in mammalian neurons. *bioRxiv* 2021.02.26.432992-2021.02.26.432992 (2021) doi:10.1101/2021.02.26.432992.

102. Gros, O. J., Damstra, H. G. J., Kapitein, L. C., Akhmanova, A. & Berger, F. Dynein self-organizes while translocating the centrosome in T-cells. *Mol. Biol. Cell* **32**, 855–868 (2021).
103. Garlick, E., Faulkner, E. L., Briddon, S. J. & Thomas, S. G. Simple methods for quantifying super-resolved cortical actin. *bioRxiv* 2021.05.26.445864-2021.05.26.445864 (2021) doi:10.1101/2021.05.26.445864.
104. Unnikannan, C. P., Reuveny, A., Grunberg, D. T. & Volk, T. *Mechanosensitive Recruitment of BAF to the Nuclear Membrane Inhibits Nuclear E2F1 and Yap Levels*. *bioRxiv* vol. 1 (2019).
105. Faulkner, E. L. *et al.* Imaging Nanoscale Nuclear Structures with Expansion Microscopy. *bioRxiv* 2021.05.04.442164-2021.05.04.442164 (2021) doi:10.1101/2021.05.04.442164.
106. Woodworth, M. A. *et al.* Multiplexed single-cell profiling of chromatin states at genomic loci by expansion microscopy. *Nucleic Acids Res.* (2021) doi:10.1093/NAR/GKAB423.
107. Marongiu, R., Le Gratiet, A., Pesce, L., Bianchini, P. & Diaspro, A. ExCIDS: a combined approach coupling Expansion Microscopy (ExM) and Circular Intensity Differential Scattering (CIDS) for chromatin-DNA imaging. *OSA Contin.* **3**, 1770 (2020).
108. Cirillo, L. *et al.* UBAP2L Forms Distinct Cores that Act in Nucleating Stress Granules Upstream of G3BP1. *Curr. Biol.* **30**, 698-707.e6 (2020).
109. Do, T. Q. T. *et al.* A Nuclear Stress Pathway that Parallels Cytoplasmic Stress Granule Formation. *iScience* **23**, 101664 (2020).
110. Alderson, T. R. *et al.* Dysregulated interactions triggered by a neuropathy-causing mutation in the IPV motif of HSP27. *bioRxiv* 708180 (2019) doi:10.1101/708180.
111. Fan, J.-B. *et al.* Type I Interferon Regulates a Coordinated Gene Network to Enhance Cytotoxic T Cell-Mediated Tumor Killing. *Cancer Discov.* **10**, 382–393 (2020).
112. Shurer, C. R. *et al.* Physical Principles of Membrane Shape Regulation by the Glycocalyx. *Cell* **177**, 1757-1770.e21 (2019).
113. Zhao, X. *et al.* Polarized endosome dynamics engage cytoplasmic Par-3 that recruits dynein during asymmetric cell division. *Sci. Adv.* **7**, eabg1244–eabg1244 (2021).
114. Jung, Y., Wen, L., Altman, A. & Ley, K. CD45 pre-exclusion from the tips of T cell microvilli prior to antigen recognition. *Nat. Commun.* **12**, 3872 (2021).
115. Kumar, A. *et al.* Influenza virus exploits tunneling nanotubes for cell-to-cell spread. *Sci. Rep.* **7**, 40360 (2017).
116. Heil, H. S. *et al.* Mapping densely distributed membrane receptors in blood platelets with expansion microscopy. *bioRxiv* 2021.02.16.431449-2021.02.16.431449 (2021) doi:10.1101/2021.02.16.431449.
117. Chozinski, T. J. *et al.* Volumetric, Nanoscale Optical Imaging of Mouse and Human Kidney via Expansion Microscopy. *Sci. Rep.* **8**, 10396 (2018).
118. Bucur, O. & Zhao, Y. Nanoscale Imaging of Kidney Glomeruli Using Expansion Pathology. *Front. Med.* **0**, 322 (2018).
119. Alvarez-Castelao, B. *et al.* Cell-type-specific metabolic labeling of nascent proteomes in vivo. *Nat. Biotechnol.* **35**, 1196–1201 (2017).
120. Kaverina, N. V *et al.* Dual lineage tracing shows that glomerular parietal epithelial cells can transdifferentiate toward the adult podocyte fate. *Kidney Int.* **96**, 597–611 (2019).
121. Unnersjö-Jess, D. *et al.* Confocal super-resolution imaging of the glomerular filtration barrier enabled by tissue expansion. *Kidney Int.* **93**, 1008–1013 (2018).

122. Wunderlich, L. C. S. *et al.* Superresolving the kidney—a practical comparison of fluorescence nanoscopy of the glomerular filtration barrier. *Anal. Bioanal. Chem.* **413**, 1203–1214 (2021).
123. Wang, Q., Cao, J. & Xu, H. 3D imaging of cellular features in kidney glomeruli using expansion microscopy and fluorescent covalent stains. *J. Phys. Conf. Ser.* **1865**, 022063 (2021).
124. Möller-Kerutt, A. *et al.* Crumbs2 Is an Essential Slit Diaphragm Protein of the Renal Filtration Barrier. *J. Am. Soc. Nephrol.* **32**, 1053–1070 (2021).
125. Kao, P. & Nodine, M. D. Transcriptional Activation of Arabidopsis Zygotes Is Required for Initial Cell Divisions. *Sci. Rep.* **9**, 17159 (2019).
126. Papareddy, R. K. *et al.* Chromatin regulates expression of small RNAs to help maintain transposon methylome homeostasis in Arabidopsis. *Genome Biol.* **21**, 251 (2020).
127. Edwards, S. J. *et al.* High-Resolution Imaging of Tumor Spheroids and Organoids Enabled by Expansion Microscopy. *Front. Mol. Biosci.* **0**, 208 (2020).
128. Scherer, K. M. *et al.* A fluorescent reporter system enables spatiotemporal analysis of host cell modification during herpes simplex virus-1 replication. *J. Biol. Chem.* **296**, 100236 (2021).
129. Aho *et al.* Quantitative Microscopy Reveals Stepwise Alteration of Chromatin Structure during Herpesvirus Infection. *Viruses* **11**, 935 (2019).
130. Goonawardane, N., Yin, C. & Harris, M. *A Pivotal Role of Serine 225 Phosphorylation in the Function of Hepatitis C Virus NS5A Revealed with the Application of a Phosphopeptide Antiserum and Super-Resolution Microscopy.* *bioRxiv* (2018) doi:10.1101/387407.
131. Rozario, A. M. *et al.* ‘Live and Large’: Super-Resolution Optical Fluctuation Imaging (SOFI) and Expansion Microscopy (ExM) of Microtubule Remodelling by Rabies Virus P Protein. *Aust. J. Chem.* **73**, 686–692 (2020).
132. Pavlou, G. *et al.* Coupling Polar Adhesion with Traction, Spring, and Torque Forces Allows High-Speed Helical Migration of the Protozoan Parasite Toxoplasma. *ACS Nano* **14**, 7121–7139 (2020).
133. Tosetti, N. *et al.* Essential function of the alveolin network in the subpellicular microtubules and conoid assembly in *Toxoplasma gondii*. *eLife* **9**, 1–22 (2020).
134. Halpern, A. R., Alas, G. C. M., Chozinski, T. J., Paredez, A. R. & Vaughan, J. C. Hybrid Structured Illumination Expansion Microscopy Reveals Microbial Cytoskeleton Organization. *ACS Nano* **11**, 12677–12686 (2017).
135. Hardin, W. R. *et al.* The *Giardia* lamellipodium-like ventrolateral flange supports attachment and rapid cytokinesis. *bioRxiv* 2021.01.31.429041-2021.01.31.429041 (2021) doi:10.1101/2021.01.31.429041.
136. Kalichava, A. & Ochsenteiter, T. Ultrastructure Expansion Microscopy in *Trypanosoma brucei*. *bioRxiv* 2021.04.20.440568-2021.04.20.440568 (2021) doi:10.1101/2021.04.20.440568.
137. Gorilak, P., Pružincová, M., Vachova, H., Olšinová, M. & Varga, V. Expansion microscopy facilitates quantitative super-resolution studies of cytoskeletal structures in kinetoplastid parasites. *bioRxiv* 2021.04.20.440601 (2021) doi:10.1101/2021.04.20.440601.
138. Isch, C. *et al.* Structural and functional studies of the first tripartite protein complex at the *Trypanosoma brucei* flagellar pocket collar. *bioRxiv* 2021.01.26.428227-2021.01.26.428227 (2021) doi:10.1101/2021.01.26.428227.

139. Bertiaux, E. *et al.* Expansion microscopy provides new insights into the cytoskeleton of malaria parasites including the conservation of a conoid. *PLOS Biol.* **19**, e3001020–e3001020 (2021).
140. Amodeo, S. *et al.* Characterization of the novel mitochondrial genome segregation factor TAP110 in *Trypanosoma brucei*. *J. Cell Sci.* **134**, (2021).
141. Hyun, S. *et al.* Proline Hinged Amphipathic  $\alpha$ -Helical Peptide Sensitizes Gram-Negative Bacteria to Various Gram-Positive Antibiotics. *J. Med. Chem.* **63**, 14937–14950 (2020).
142. Chen, L. *et al.* Applications of Super Resolution Expansion Microscopy in Yeast. *Front. Phys.* **0**, 136 (2021).
143. Götz, R. *et al.* Expansion Microscopy for Cell Biology Analysis in Fungi. *Front. Microbiol.* **11**, 574 (2020).
144. Grafe, M., Hofmann, P., Batsios, P., Meyer, I. & Gräf, R. In Vivo Assembly of a Dictyostelium Lamin Mutant Induced by Light, Mechanical Stress, and pH. *Cells* **9**, 1834 (2020).
145. Gärtig, P.-A. *et al.* Motor circuit function is stabilized during postembryonic growth by anterograde trans-synaptic Jelly Belly - Anaplastic Lymphoma Kinase signaling. *bioRxiv* 841106 (2019) doi:10.1101/841106.
146. Kohara, K. *et al.* BATTLE: Genetically Engineered Strategies for Split-Tunable Allocation of Multiple Transgenes in the Nervous System. *iScience* **23**, 101248 (2020).
147. Inoue, A., Kobayashi, T., Hirai, H., Kanaya, N. & Kohara, K. Protocol for BATTLE-1EX: A High-Resolution Imaging Method to Visualize Whole Synaptic Structures and their Components in the Nervous System. *STAR Protoc.* **1**, 100166 (2020).
148. Lee, K.-S. S., Vandemark, K., Mezey, D., Shultz, N. & Fitzpatrick, D. Functional Synaptic Architecture of Callosal Inputs in Mouse Primary Visual Cortex. *Neuron* **101**, 421–428.e5 (2019).
149. Herde, M. K. *et al.* Local Efficacy of Glutamate Uptake Decreases with Synapse Size. *Cell Rep.* **32**, 108182 (2020).
150. Comer, A. L. *et al.* Increased Expression of Schizophrenia-Associated Gene C4 Leads to Hypoconnectivity of Prefrontal Cortex and Reduced Social Interaction. *PLOS Biology* vol. 18 (2020).
151. Gallagher, B. & Zhao, Y. Nanoscale Imaging of Synaptic Connections with Expansion Microscopy. *Discoveries* **7**, e101 (2019).
152. Wang, L. *et al.* Different dendritic domains of the gnRH neuron underlie the pulse and surge modes of gnRH secretion in female mice. *eLife* **9**, 1–19 (2020).
153. Verstraelen, P. *et al.* Systematic Quantification of Synapses in Primary Neuronal Culture. *iScience* **23**, 101542 (2020).
154. Burger, C. A. *et al.* Lkb1 coordinates neurite remodeling to drive synapse layer emergence in the outer retina. *eLife* **9**, 1–27 (2020).
155. Hsieh, C. *et al.* Persistent increases of PKM $\zeta$  in memory-activated neurons trace LTP maintenance during spatial long-term memory storage. *bioRxiv* 2020.02.05.936146–2020.02.05.936146 (2021) doi:10.1101/2020.02.05.936146.
156. Ishola, A. O., Imam, A. & Ajao, M. S. Datumetine exposure alters hippocampal neurotransmitters system in C57BL/6 mice. *Drug Chem. Toxicol.* (2020) doi:10.1080/01480545.2020.1776315.
157. Burger, C. A. *et al.* LKB1 and AMPK instruct cone nuclear position to modify visual function. *Cell Rep.* **34**, 108698 (2021).

158. Mondo, E. *et al.* A Developmental Analysis of Juxtavascular Microglia Dynamics and Interactions with the Vasculature. *J. Neurosci.* **40**, 6503–6521 (2020).
159. McCauley, J. P. *et al.* Circadian Modulation of Neurons and Astrocytes Controls Synaptic Plasticity in Hippocampal Area CA1. *Cell Reports* vol. 33 (2020).
160. Campbell, L. A., Pannoni, K. E., Savory, N. A., Lal, D. & Farris, S. Protein-retention expansion microscopy for visualizing subcellular organelles in fixed brain tissue. *J. Neurosci. Methods* **361**, 109285 (2021).
161. Deshpande, T. *et al.* Subcellular reorganization and altered phosphorylation of the astrocytic gap junction protein connexin43 in human and experimental temporal lobe epilepsy. *Glia* **65**, 1809–1820 (2017).
162. Menon, K. P., Kulkarni, V., Takemura, S., Anaya, M. & Zinn, K. Interactions between Dpr11 and DIP- $\gamma$  control selection of amacrine neurons in *Drosophila* color vision circuits. *eLife* **8**, e48935 (2019).
163. Dantzler, H. A., Matott, M. P., Martinez, D. & Kline, D. D. Hydrogen peroxide inhibits neurons in the paraventricular nucleus of the hypothalamus via potassium channel activation. *Am. J. Physiol.-Regul. Integr. Comp. Physiol.* **317**, R121–R133 (2019).
164. Koppers, M. *et al.* Receptor-specific interactome as a hub for rapid cue-induced selective translation in axons. *eLife* **8**, e48718 (2019).
165. Weish, P. *et al.* Super-resolution microscopy informs on the molecular architecture of alpha-synuclein inclusions in model systems and in the human brain. *bioRxiv* 2021.04.25.441304-2021.04.25.441304 (2021) doi:10.1101/2021.04.25.441304.
166. Liu, X. *et al.* Highly redundant neuropeptide volume co-transmission underlying episodic activation of the gnRH neuron dendron. *eLife* **10**, 1–21 (2021).
167. Guo, F., Holla, M., Díaz, M. M. & Rosbash, M. A Circadian Output Circuit Controls Sleep-Wake Arousal in *Drosophila*. *Neuron* **100**, 624-635.e4 (2018).
168. Schlichting, M. *et al.* Light-Mediated Circuit Switching in the *Drosophila* Neuronal Clock Network. *Curr. Biol.* **29**, 3266-3276.e3 (2019).
169. Menon, K. P., Kulkarni, V., Shin-Ya, T., Anaya, M. & Zinn, K. Interactions between dpr11 and dip-y control election of amacrine neurons in *drosophila* color ision circuits. *eLife* **8**, (2019).
170. Jiang, N. *et al.* A conserved morphogenetic mechanism for epidermal ensheathment of nociceptive sensory neurites. *eLife* **8**, e42455 (2019).
171. Llorens-Bobadilla, E. *et al.* A latent lineage potential in resident neural stem cells enables spinal cord repair. *Science* **370**, (2020).
172. Sim, J. *et al.* Whole-ExM: Expansion microscopy imaging of all anatomical structures of whole larval zebrafish. *bioRxiv* 2021.05.18.443629-2021.05.18.443629 (2021) doi:10.1101/2021.05.18.443629.
173. Philips, R. M. & R. » How big is the “average” protein? <http://book.bionumbers.org/how-big-is-the-average-protein/>.
174. M'Saad, O. & Bewersdorf, J. Light microscopy of proteins in their ultrastructural context. *Nat. Commun.* **11**, 3850 (2020).
175. Kiernan, J. A. Formaldehyde, Formalin, Paraformaldehyde And Glutaraldehyde: What They Are And What They Do. *Microsc. Today* **8**, 8–13 (2000).
176. Sabatini, D. D., Bensch, K. & Barnett, R. J. The Preservation of Cellular Ultrastructure and Enzymatic Activity by Aldehyde Fixation. *J. Cell Biol.* **17**, 19–58 (1963).
177. Chang, J.-B. *et al.* Iterative expansion microscopy. *Nat. Methods* **14**, 593–599 (2017).

178. Tillberg, P. W. Expansion Microscopy: Improving Imaging Through Uniform Tissue Expansion. (2016).
179. Gherezghier, T. B., Ming, X., Villalta, P. W., Campbell, C. & Tretyakova, N. Y. 1,2,3,4-Diepoxybutane-Induced DNA–Protein Cross-Linking in Human Fibrosarcoma (HT1080) Cells. *J. Proteome Res.* **12**, 2151–2164 (2013).
180. Halpern, A. R., Howard, M. D. & Vaughan, J. C. Point by Point: An Introductory Guide to Sample Preparation for Single-Molecule, Super-Resolution Fluorescence Microscopy. *Curr. Protoc. Chem. Biol.* **7**, 103–120 (2015).
181. Hoffman, E. A., Frey, B. L., Smith, L. M. & Auble, D. T. Formaldehyde Crosslinking: A Tool for the Study of Chromatin Complexes. *J. Biol. Chem.* **290**, 26404–26411 (2015).
182. Sarkar, D. *et al.* Expansion Revealing: Decrowding Proteins to Unmask Invisible Brain Nanostructures. 2020.08.29.273540 Preprint at <https://doi.org/10.1101/2020.08.29.273540> (2020).
183. Tillberg, P. W. *et al.* Protein-retention expansion microscopy of cells and tissues labeled using standard fluorescent proteins and antibodies. *Nat. Biotechnol.* **34**, 987–992 (2016).
184. Gambarotto, D. *et al.* Imaging cellular ultrastructures using expansion microscopy (U-ExM). *Nat. Methods* **16**, 71–74 (2019).
185. Hamel, V. & Guichard, P. Chapter 14 - Improving the resolution of fluorescence nanoscopy using post-expansion labeling microscopy. in *Methods in Cell Biology* vol. 161 297–315 (Elsevier, 2021).
186. Zhang, C., Kang, J. S., Asano, S. M., Gao, R. & Boyden, E. S. Expansion Microscopy for Beginners: Visualizing Microtubules in Expanded Cultured HeLa Cells. *Curr. Protoc. Neurosci.* **92**, e96 (2020).
187. Cohen, Y., Ramon, O., Kopelman, I. J. & Mizrahi, S. Characterization of inhomogeneous polyacrylamide hydrogels. *J. Polym. Sci. Part B Polym. Phys.* **30**, 1055–1067 (1992).
188. Sarkar, D. *et al.* Revealing nanostructures in brain tissue via protein decrowding by iterative expansion microscopy. *Nat. Biomed. Eng.* 1–17 (2022) doi:10.1038/s41551-022-00912-3.
189. Hayat. *Basic Techniques for Transmission Electron Microscopy*. (Elsevier, 1986).
190. Bélanger, S. *et al.* A versatile enhanced freeze-substitution protocol for volume electron microscopy. *Front. Cell Dev. Biol.* **10**, (2022).
191. Humbel, B. & Müller, M. Freeze Substitution and Low Temperature Embedding. *Scan. Electron Microsc.* **4**, (1985).
192. Laporte, M. H., Klena, N., Hamel, V. & Guichard, P. Visualizing the native cellular organization by coupling cryofixation with expansion microscopy (Cryo-ExM). *Nat. Methods* 1–7 (2022) doi:10.1038/s41592-021-01356-4.
193. Ku, T. *et al.* Multiplexed and scalable super-resolution imaging of three-dimensional protein localization in size-adjustable tissues. *Nat. Biotechnol.* 2016 349 **34**, 973–981 (2016).
194. Asano, S. M. *et al.* Expansion Microscopy: Protocols for Imaging Proteins and RNA in Cells and Tissues. *Curr. Protoc. Cell Biol.* **80**, (2018).
195. Valdes, P. A. *et al.* Improved immunostaining of nanostructures and cells in human brain specimens through expansion-mediated protein decrowding. *Sci. Transl. Med.* **16**, eabo0049 (2024).
196. Zwettler, F. U. *et al.* Molecular resolution imaging by post-labeling expansion single-molecule localization microscopy (Ex-SMLM). *Nat. Commun.* **11**, 3388 (2020).

197. Damstra, H. G. J. *et al.* GelMap: intrinsic calibration and deformation mapping for expansion microscopy. *Nat. Methods* **20**, 1573–1580 (2023).
198. Schindelin, J. *et al.* Fiji: an open-source platform for biological-image analysis. *Nat. Methods* **9**, 676–682 (2012).
199. Mahecic, D. *et al.* Homogeneous multifocal excitation for high-throughput super-resolution imaging. *Nat. Methods* **17**, 726–733 (2020).
200. Gao, M. *et al.* Expansion Stimulated Emission Depletion Microscopy (ExSTED). *ACS Nano* **12**, 4178–4185 (2018).
201. Kim, D., Kim, T., Lee, J. & Shim, S. Amplified Expansion Stimulated Emission Depletion Microscopy. *ChemBioChem* **20**, 1260–1265 (2019).
202. Lee, H., Yu, C. C., Boyden, E. S., Zhuang, X. & Kosuri, P. Tetra-gel enables superior accuracy in combined super-resolution imaging and expansion microscopy. *Sci. Rep.* **11**, 1–7 (2021).
203. Shin, T. W. *et al.* Dense, Continuous Membrane Labeling and Expansion Microscopy Visualization of Ultrastructure in Tissues. 2024.03.07.583776 Preprint at <https://doi.org/10.1101/2024.03.07.583776> (2024).
204. Cho, I. & Chang, J.-B. Simultaneous expansion microscopy imaging of proteins and mRNAs via dual-ExM. *Sci. Rep.* **12**, 3360 (2022).